NASA SP–20

NUCLEAR ROCKET PROPULSION

NATIONAL AERONAUTICS AND SPACE ADMINISTRATION • Washington, D.C.
December 1962 • Office of Scientific and Technical Information

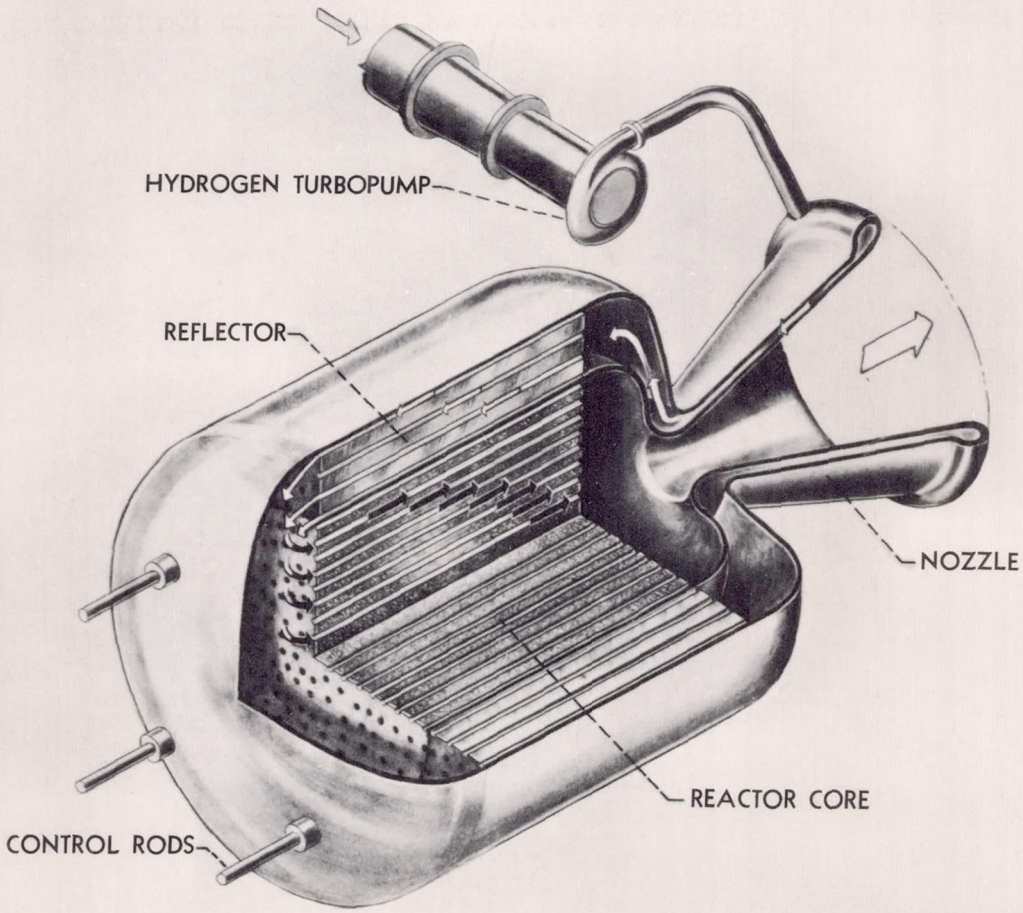

Foreword

The NASA-University Conference on the Science and Technology of Space Exploration, conducted in Chicago on November 1–3, 1962, was held "to provide an authoritative and up-to-date review of aeronautical and space science technology."

The scientific papers delivered at the conference were grouped for presentation by topics and are, in effect, 1962 state-of-the-art summaries. Accordingly, NASA has published under separate covers sixteen groups of conference papers to make them conveniently available to those interested in specific fields. This series (NASA SP–13 to NASA SP–28) is listed by title and price on the back cover.

All papers presented at the conference have also been published in a two-volume *Proceedings* (NASA SP–11) available from the Superintendent of Documents for $2.50 and $3.00, respectively. Those papers presented herein originally appeared on pages 61 to 122 of Volume 2 of NASA SP–11.

For sale by the Superintendent of Documents, U.S. Government Printing Office
Washington 25, D.C. — Price 45 cents

Contents

Introduction

By David S. Gabriel

DAVID S. GABRIEL, *Chief of the Advanced Development and Evaluation Division of the NASA Lewis Research Center, received his B.S. degree in Mechanical Engineering from the University of Akron in 1943, and did graduate work in Aeronautical Engineering at Case Institute of Technology.*

He has participated in directing research on turbines and rotating machinery, turbojets, ramjets, chemical rockets, and nuclear rockets and power conversion systems. He is a member of the Institute of the Aerospace Sciences and the New York Academy of Science.

The nuclear rocket engine is believed by many to be the most important space powerplant for the near future. Some of the reasons for this belief are illustrated by figure 1.

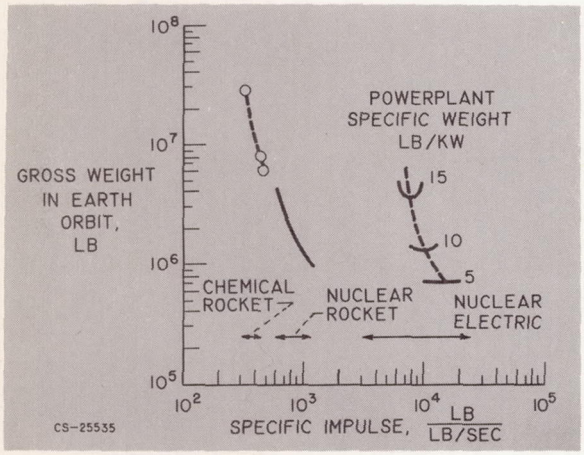

FIGURE 1.—Manned Mars mission with a seven-man crew and two-man surface exploration. Round-trip time, 420 days.

In figure 1 are shown the vehicle requirements for a seven-man trip to Mars in a little over 1 year flight time for three types of spaceships: chemically propelled, nuclear-rocket propelled, and nuclear-electric propelled. The ordinate is the weight of the vehicles in the Earth orbit (300 miles) required for the mission. About 25 times as much weight is required on the ground to boost these vehicles into orbit. The specific-impulse range for chemical rockets is from 300 to 450 and for nuclear rockets, from 700 to 1000 seconds. Electric propulsion provides much greater impulse, but, although not shown here, at a considerable sacrifice in ratio of thrust to weight. It is apparent that a rather fantastic reduction in launch weight is possible with nuclear rockets compared with chemical rockets. Because, for nuclear-electric systems, it is not now known how light these systems can be built, three curves are shown for various system weights. From current information, 5 pounds per kilowatt is extremely light and probably will not be achieved without some unforeseen breakthrough. The more likely range is 10 to 15 pounds per kilowatt. These results are, of course, highly dependent on the particular mission. A different one would give a different answer. At least for this type of highly energetic short-time trip, typical of many of great interest to us, nuclear rockets and nuclear electric systems are highly competitive, and neither is clearly superior to the other. Further, it is evident that even if very lightweight electrical systems are developed, the gains to be expected are

not spectacular. For very-long-term missions such as a trip to Pluto, the electric rocket is comparatively better. The nuclear rocket is, therefore, clearly a superior powerplant to the chemical rocket and at least competitive with nuclear electric systems for many future missions. For these reasons, a great urgency is felt for nuclear-rocket development.

Nuclear rockets require high-flow, high-pressure turbopumps, exhaust systems capable of withstanding heat loads in excess of any present system, and specialized instruments for the measurement of not only pressure, temperature, and flow, but also of nuclear environment. The design and development of reactors with impulses in the range previously mentioned introduce the requirement of very high power density in order to keep weight within reason. This necessity aggravates the usual problems in both nucleonics and heat transfer and, in turn, introduces the problem of maximum material temperature of the order of 4000° to 6000° F and minimum hydrogen temperatures around −400° F. Structures and materials must survive extreme environments. The control of the reactor and its associated systems is a very difficult problem, particularly in off-design conditions. The mating of the reactor to the vehicle creates interaction problems. Overlying all these problem areas are the difficulties caused by a high-nuclear-radiation environment.

Not all of these areas will be discussed in the following four papers, however. These papers are concerned primarily with the problems of nucleonics, heat transfer, control, and overall performance.

Advanced Concepts for Nuclear Rocket Propulsion

By Frank E. Rom and Robert G. Ragsdale

FRANK E. ROM, *Chief of the Nuclear Propulsion Concepts Branch of the NASA Lewis Research Center, attended Cornell University where he received his B.S. and M.S. degrees in Mechanical Engineering in 1946 and 1948, respectively. Mr. Rom has been active in research on nuclear propulsion systems for aircraft and rockets. He is the chairman of the Nuclear Propulsion Committee of the American Rocket Society and a member of the Nuclear Applications Panel of the Institute of Aerospace Sciences.*

ROBERT G. RAGSDALE, *Aerospace Scientist in heat-transfer research at the NASA Lewis Research Center, is currently working on experimental tests of hydrodynamic mixing, radiation heat transfer, and system evaluation of a coaxial flow gaseous nuclear rocket. He received his B.S. and M.S. degrees in Chemical Engineering from Purdue University in 1950 and 1951, respectively.*

INTRODUCTION

The use of the nuclear rocket offers about a tenfold reduction in interplanetary spacecraft weight when compared with chemical rockets (refs. 1, 2, 3, and 4). With such a great potential gain in view, the nation is currently developing the first flyable nuclear-rocket engine. The reactor for this engine is composed of high-temperature materials that serve to heat the hydrogen propellant. A schematic drawing of a solid-core heat-transfer-type nuclear rocket showing the principle of the nuclear-rocket engine is shown in figure 42–1. The fission energy is liberated within solid materials of which the reactor core is composed. This heat is then transferred from the solid-core materials to hydrogen as it flows through the heat-transfer passages. The hydrogen is stored in a propellant tank and then is pumped through the nozzle walls for cooling purposes. It is also passed through the reflector regions and any other parts that require cooling. On leaving the reflector, the hydrogen flows through the passages of the reactor core where it is heated to as high a temperature as the core materials will stand. The high-temperature hydrogen is then exhausted through a convergent-divergent nozzle to produce thrust.

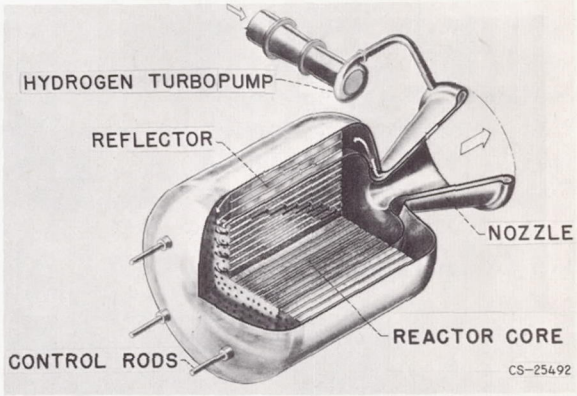

FIGURE 42–1.—Solid-core heat-transfer-type nuclear rocket.

Since nuclear rockets eject mass to produce thrust, the only reason for considering nuclear systems for rocket propulsion is that they have the potential for producing a higher specific impulse than chemical rockets.

The specific impulse that may be attained by nuclear rockets is shown in figure 42–2, where specific impulse is plotted as a function of hydrogen temperature. For reference purposes, the specific impulse of advanced hydrogen-oxygen rockets such as those that will power the Centaur and the upper stages of the Saturn C–5 is over 400 pounds per pound per second. The temperature capability of the materials of which the nuclear reactor is constructed will limit hydrogen temperatures to less than 6000° F or specific impulses of about 1000 pounds per pound per second. This limit is determined by the strength of reactor-core materials operating at temperatures approaching their melting points. Beyond this limit, reactors in which the fissionable material is in the gaseous form and heats hydrogen by direct contact or by thermal radiation must be envisioned. In this case, specific impulses up to 3000 pounds per pound per second may be possible.

There is considerable interest in specific impulses greater than 1000 pounds per pound per second, even though a tenfold advantage in spacecraft weight has been obtained over chemical systems at that value. Further increases in specific impulse will, of course, produce greater weight savings. Perhaps it may be more important to take advantage of the greater flexibility in performing interplanetary missions that higher specific impulse can give. For example, the use of solid-core nuclear rockets limits the departure time for a 460-day round trip to Venus to about 1 month every 2 years.

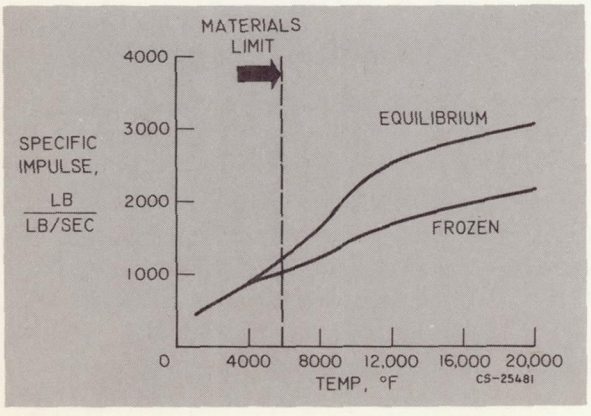

FIGURE 42–2.—Specific impulse of hydrogen as a function of temperature.

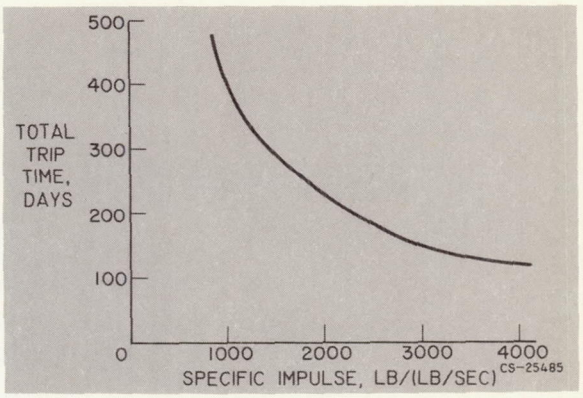

FIGURE 42–3.—Effect of specific impulse on mission time.

For a specific impulse of 2000 pounds per pound per second, departures during about 8 months out of every 2 years would be possible. A further benefit of higher specific impulse is that it will permit much shorter trip times for a given spacecraft weight as illustrated in figure 42–3, which shows the total trip for a 7-man Venus mission as a function of specific impulse. The weight of the spacecraft that is launched from an Earth orbit is fixed at 1.7 million pounds. The data in this figure apply only for high-thrust systems; that is, where the thrust-to-weight ratio of the spacecraft is greater than 0.10. Lower thrust-to-weight ratios will increase the trip time appreciably. Materials-limited nuclear rockets can accomplish this mission in about 450 days. A gaseous-core nuclear rocket with a specific impulse of 3000 pounds per pound per second could accomplish this mission in one-third the time or about 150 days.

In the following discussion, both solid-core and gaseous-core advanced nuclear-rocket concepts are considered. In the case of the solid-core nuclear rocket, the chief problem is to achieve the highest hydrogen temperature within the limits of the melting points of the most refractory materials. For the gaseous-core reactor, the chief problems are associated with schemes whereby hydrogen is heated by gaseous fissionable material without excessive fuel loss and without melting down the walls that contain gases at temperatures far beyond the melting point of solids.

ADVANCED SOLID-CORE REACTORS

First, consider advanced "solid-core" nuclear-rocket concepts that heat hydrogen by contact with high-temperature solids. The main objective in this case is to find which of the materials or combinations of materials found in nature can be made to produce the highest operating temperature and, hence, the highest specific impulse. In addition, reactor concepts that have the greatest probability of being successfully developed into highly reliable powerplants in the most economical and efficient manner must be found. Finally, there is always an interest in achieving the smallest size and weight.

Reactor Types

Some of the reactor types considered for nuclear-rocket use are shown in figure 42–4, namely, homogeneous thermal, fast, and heterogeneous thermal. The advantages and disadvantages are given in table 42–I.

Homogeneous thermal reactor.—In this reactor, the fissionable material is intimately mixed with a neutron-moderating material. The heat of fission is thus liberated in the moderator and is removed by the hydrogen propellant that flows through an array of coolant passages, which can be visualized as holes passing from one end of the reactor to the other. The highest temperatures in the reactor occur in the moderator, hence, the name "hot moderator". In addition to being capable of slowing down neutrons, the moderator must also be capable of operating at high temperatures. Graphite and beryllium oxide are the only two materials that

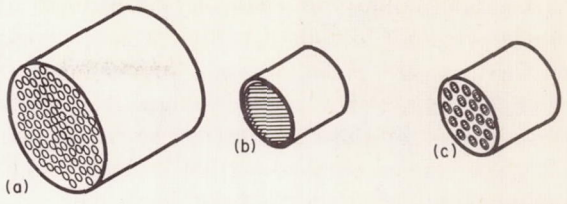

(a) Homogeneous thermal. (b) Fast. (c) Heterogeneous/thermal.

FIGURE 42–4.—Nuclear-rocket reactors.

can reasonably serve this dual function. Graphite has the poorer moderating properties of the two, and therefore its use leads to larger core dimensions and weight. On the other hand, beryllium oxide is limited to operating temperatures of at least 1000 degrees Fahrenheit less than that of graphite. Since specific impulse is of the utmost importance, graphite is really the only contender. The use of graphite, however, requires a protective coating on the heat-transfer passages to prevent chemical reaction with hydrogen.

Fast reactors.—This type of reactor is composed of all fuel-bearing material, schematically considered as an array of fueled plates for heat-transfer surfaces with no moderator. Fast reactors can be made very small (ref. 5) and can use the best available high-temperature fuel-bearing materials. The largest drawback stems from the fact that nuclearwise fast reactors are less efficient than moderated systems, and a great deal more fissionable material is required for criticality. This leads to more difficult materials problems, since the volume of

TABLE 42–I.—*Characteristics of Three Types of Nuclear-Rocket Reactors*

Reactor type	Homogeneous thermal (hot moderator)	Fast (no moderator)	Heterogeneous thermal (cooled moderator)
Moderating material	Graphite Beryllium oxide	None	Water Heavy water Beryllium Beryllium oxide Metallic hydrides
Fuel-bearing material	Coated graphite Beryllium oxide	Refractory metals (W, Mo) Carbides (ZrC, HfC, TaC)	Refractory metals (W^{184}, Mo) Coated graphite Carbides (ZrC)

672065 O–63—2

fissionable material must be about equal to the total volume of all other materials in the core. Unfortunately, since fissionable compounds are not very satisfactory as structural or heat-transfer materials, they must be contained within a refractory material such as tungsten, molybdenum, or the carbides of zirconium, hafnium, or tantalum. Development of satisfactory fuel elements that contain 50 volume percent of fissionable material without penalizing high-temperature performance is difficult. This major problem area of fast-reactor concepts requires a great deal of research on materials and techniques for achieving the high fuel loadings.

Heterogeneous thermal reactors.—In this reactor, the fissionable material is separated from the moderator and contained in a refractory fuel-bearing material that provides the heat-transfer surfaces. The moderator is independently cooled and, therefore, can be maintained at a lower temperature than the fuel elements. Relatively low-temperature operation permits consideration of such moderating materials as water, heavy water, beryllium, beryllium oxide, and metallic hydrides. The fuel-bearing material can be any of the best high-temperature materials such as tungsten, molybdenum, graphite, or low neutron absorbing ceramics such as zirconium carbide. Fuel loadings of 15 to 20 volume percent are sufficient. The heterogeneous reactor does involve the complication of requiring a cooling system for the moderator. In addition, the relatively cold moderator must be thermally insulated from the high-temperature fuel-element regions, and in the case of tungsten, it must be enriched in the tungsten 184 isotope (ref. 6). The homogeneous thermal and the fast reactors appear, at least in concept, to be the simplest since fuel-bearing material constitutes the entire core. The heterogeneous thermal reactor seems to have the greatest potential for producing the high specific impulse, since the relatively low fuel concentrations required are expected to permit the fuel bearing materials to operate nearer to their melting points.

Fuel-Element Materials

Table 42–II shows the properties of the most refractory materials available. Shown here are graphite, which sublimes at 7000° F, tungsten, the most refractory metal, which melts at 6170° F, and the most refractory ceramics which are the carbides of hafnium and tantalum, which melt at 7030°F and 7020° F, respectively. These materials can be utilized as fuel elements by adding a suitable uranium compound. Uranium dioxide, the most refractory of all uranium compounds (m.p. 5000° F, ref. 7) can be used with tungsten. Unfortunately in the case of hafnium and tantalum carbides, a solid solution forms with uranium carbide. Thus,

TABLE 42–II.—*Properties of Refractory Materials*

Material	Melting point, °F	Tensile strength at 5000° F, psi	Creep strength at 5000° F, psi [a]	Thermal conductivity, $\frac{(Btu)(in.)}{(ft^2)(hr)(°F)}$	Linear expansion coefficient, $\frac{10^{-6}\ in.}{(in.)(°F)}$	Modulus of elasticity, 10^6 lb/in.^{2}	Hydrogen reaction	Evaporation rate at 5000° F, mils/hr	Compatible fuel material	Other limits
Graphite	7000 (sublimes)	1000 to 6000	10 to 800	140 at 5000° F	2.75 up to 4000° F (ATJ).	1.4 to 2.0 at 4000° F	>2800° F	30	UC_2	UC_2 melts at 4535° F
Tungsten	6170	[b] 3000 to 7000	1000	920 at 5000° F	3.6	1 to 10	None	0.1	UO_2	----------
Hafnium carbide	7030	[c] 2500 at 4000° F	--------	260 to 310 at 4000° F	2.88 up to 4000° F	79	>4840° F	3	UC	----------
Tantalum carbide	7020	[c] 6000 at 4000° F	--------	275 at 4000° F	3.05 up to 4000° F	----------	>4630° F	0.6	UC	Loses carbon above 4000° F

[a] Creep rate, 10^{-5} inch per inch per minute.
[b] One-half of measured bend strength.
[c] For tensile test strain rate of 0.02 to 2.0 inch per inch per minute.

the melting point of a 50–50 mixture of 50 percent hafnium carbide and 50 percent uranium carbide is only about 5750° F compared with 7030° F, the melting point of hafnium carbide alone.

The tensile strength of graphite given for a temperature of 5000° F varies from 1000 to 6000 pounds per square inch depending on its grade and density (ref. 8). The tensile strength of tungsten varies from 3000 to 7000 pounds per square inch depending on the rate of applying the load (refs. 9 and 10). The highest temperature for which the strengths of the carbides have been measured is 4000° F. At this temperature, the tensile strength was assumed to be one-half of the measured strength in bending. The values for hafnium carbide and tantalum carbide at 4000° F are 2500 and 6000 pounds per square inch, respectively (refs. 11 and 12).

Since the fuel-element materials are subjected to loads for finite periods of time, creep strength is of great importance. The creep strengths are presented at 5000° for a creep rate of 10^{-5} inch per inch per minute, which corresponds to an elongation of about ½ percent in 10 hours. The creep-rate values for graphite depend on grain orientation, density, and grade and range from 10 to 800 pounds per square inch (ref. 13). Tungsten has a value of 1000 pounds per square inch (ref. 14).

Values of thermal conductivity vary from 140 Btu per hour per square foot per degrees Fahrenheit per inch for graphite (ref. 15) up to 920 for tungsten (ref. 16). The thermal conductivity of hafnium carbide was obtained from reference 12. The value for tantalum carbide was obtained from reference 17. The coefficients of linear expansion were obtained from references 16 and 17. The modulus of elasticity was obtained from references 16, 17, and 18. Further data on properties of refractory materials can be found in reference 11.

A strong hydrogen reaction with graphite begins at 2800° F (ref. 19); therefore, protective coatings are essential when graphite is used. Hydrogen does not react with tungsten, but hafnium and tantalum carbides do react at temperatures of 4840° and 4630° F, respectively (ref. 20).

The evaporation rate of graphite at 5000° F in a vacuum is 30 mils per hour (ref. 21). The use of sound coatings on graphite should reduce the evaporation rate to the rate of evaporation of the coating material. Because it is usually desirable to minimize coating thicknesses, low evaporation rates of suitable coating materials are of extreme importance: tungsten has the lowest rate at 0.1 mil per hour (ref. 22). Tantalum and hafnium carbides have intermediate rates (refs. 21 and 23).

Uranium carbide (UC_2) melts at 4535° F (ref. 24) and would be expected to affect adversely the properties of graphite fuel elements at higher temperatures. Tantalum carbide loses carbon above about 4000° F with the resultant formation of Ta_2C. The use of tantalum carbide would be limited to applications where relatively short life is adequate. The data presented in the table are for refractory materials with no uranium compounds added. Much less data are available for these materials when they contain fuel compounds. Supplying these data represents a major field for continued research.

On the basis of data presented in the table, tungsten may be expected to have the greatest potential for producing the highest specific impulse attainable by solid-core nuclear rockets. Whether or not this potential will be realized can only be determined by extensive experimental investigations.

Solid-Core Reactor Studies

A portion of the nuclear-rocket program at Lewis involves the study of advanced solid-core-reactor concepts and their problems. This work is aimed at pushing forward the technology of nuclear-rocket reactors and providing some degree of insurance for the nation's nuclear-rocket program. In developing a new engine based on a relatively advanced technology, success is not assured for any chosen approach to the problem. Within the limits of resources available, alternate or backup approaches must be undertaken. In a limited way, the program at Lewis on advanced solid-core nuclear rockets is such a backup effort, even though the main emphasis is on providing the technology for the development of the ultimate solid-core nuclear rocket.

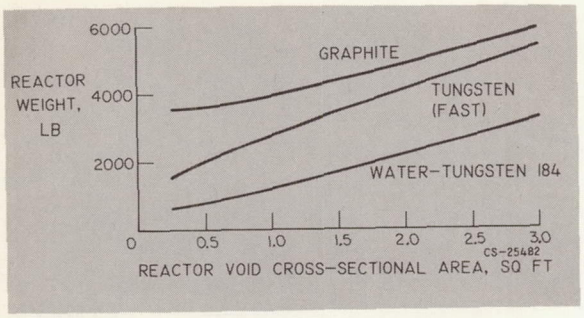

FIGURE 42–5.—Nuclear-rocket reactor weight as a function of reactor void cross-sectional area.

Reactor-weight comparison.—A study has been made of the three reactor types described earlier to help determine the selection of the most promising avenues of research. Figure 42–5 shows one of the results of this investigation. Reactor core plus reflector weight is plotted as a function of reactor void cross-sectional area. (A 1000 megawatt reactor requires about 1 sq ft of flow area.) The graphite reactor, which represents the best of the homogeneous-thermal type, is the heaviest. The fast-tungsten reactor, which assumes a 50–50 volume ratio of tungsten and uranium dioxide, is lighter than the graphite reactor. The lowest curve is the best that can be done with heterogeneous-reactor cores. Water was found to be the best of the moderators considered. Tungsten enriched in the tungsten 184 isotope was considered to have the best potential for high-temperature performance, because it has the desirable structural properties of metal and its use requires a lower percentage of uranium dioxide to be contained within the fuel-element material. It should be emphasized that the weight of the reactor is only one criterion for the selection of a reactor for nuclear rockets. The importance of high temperature materials has already been discussed. Consideration must also be given to the mechanical aspects of the core design. In other words, does a reactor design exist that is practical and can be developed in a reasonable fashion?

Reactor design problems.—Some typical reactor-core-design problems arising in advanced concept studies can be illustrated by using the tungsten–water-moderated reactor as an example. The reactor shown schematically in figure 42–6 consists of an aluminum tank of water with an array of aluminum tubes joining the end header plates. It is very similar in principle to the heat-transfer-reactor experiment number 1 (ref. 25), which was used to heat air for a turbojet powerplant, and the ML–1 reactor (refs. 26 and 27), which is used to heat gas for a mobile powerplant unit. The tubes provide space for fuel elements and flow passages for the hydrogen. First, the hydrogen passes through the regeneratively cooled nozzle, then through a water-to-hydrogen heat exchanger to remove the heat generated by neutron and gamma radiation and any other heat that may be absorbed by the water, then through the fuel elements located within the aluminum tubes. The heated hydrogen is then expanded through the nozzle to produce thrust. The sketch in the figure indicates how insulation is provided to reduce the heat transferred from the high temperature elements to the water. The fuel elements are supported by a continuous tungsten tube that runs the full length of the core. The space between this tube and the aluminum tank is filled with stagnant hydrogen. This is accomplished by venting the downstream end to the reactor exit region and sealing the upstream portion. A molybdenum radiation shield is also

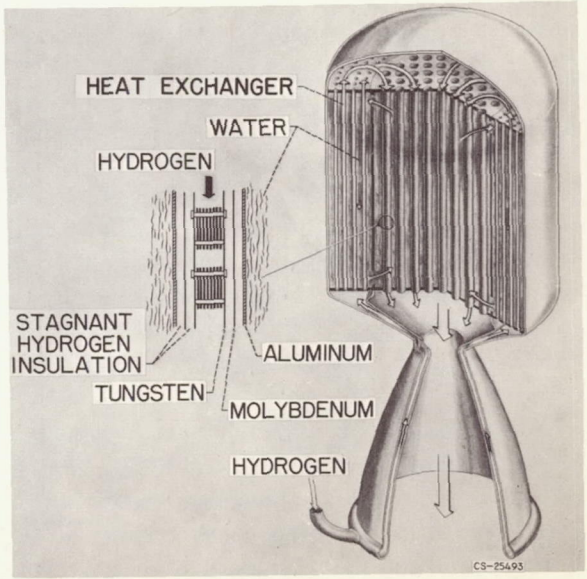

FIGURE 42–6.—Tungsten–water-moderated reactor concept.

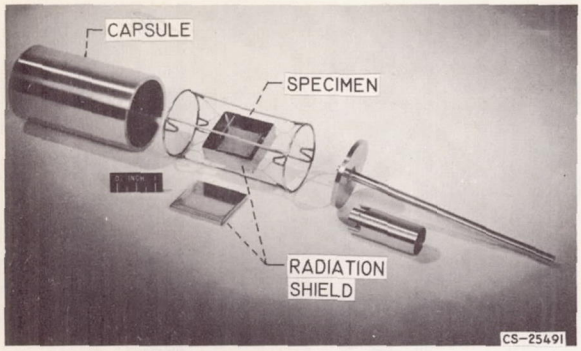

FIGURE 42–7.—In-pile capsule experiment.

shown. A hydrogen thickness of less than $\frac{1}{8}$ inch is sufficient to reduce the heat flow to less than 1 percent of the reactor power.

The most important problems of this or any other reactor concept employing tungsten are the fueled materials and the fuel-element structure. The question is can suitable fueled-tungsten material be made and can this material retain fissionable material such as uranium dioxide at temperatures of the order of 5000° F for periods of up to 10 hours with no loss or attack by hydrogen? Once a suitable material is obtained, a fuel-element structure that supplies the required heat-transfer surfaces and flow passages must be designed and evaluated. The fuel-element structure, indicated schematically by flat plates (fig. 42–6), must be capable of withstanding very high heat-transfer rates and large aerodynamic loads at high temperatures with a minimum of stress to avoid creep or distortion. The fuel element must be capable of withstanding severe thermal cycling loads corresponding (1) to reactor startups and shutdowns required for space missions, and particularly (2) for economical development of highly reliable powerplants, where a very large number of tests must be performed to demonstrate reliable operation.

Experimental investigations.—Experimental investigations are required to determine the performance limits of the fuel-element materials and proposed fuel-element structures because of the lack of fundamental data and understanding of the complex structures usually encountered. Analytical procedures are used as tools to correlate or extrapolate experimental data.

In-pile capsule tests (fig. 42–7) have been and are being conducted in materials-testing reactors to evaluate fueled materials. The test specimen shown is a fueled plate 1 inch square and about $\frac{1}{32}$ inch thick made by powder-metallurgy techniques. It contains fully-enriched uranium (235) dioxide. It is surrounded by a box of molybdenum that forms a radiation shield. Tungsten wires suspend the specimen and shield within the central region of the capsule. The heat generated by fissions is removed by radiation to the water-cooled capsule walls. After the capsule is sealed and evacuated, it is inserted into a test hole next to the testing reactor, where the specimen is heated by the fissioning uranium contained therein. Tests such as these are used to establish the ability of the fueled material to retain fissionable compounds at any desired temperature level. In addition, the effects of fuel burnup and radiation damage can be ascertained. This type of test can also be used to obtain rapid and inexpensive evaluation of a wide range of fueled materials to determine their potential and for research aimed at improving the properties of the materials considered.

These tests cannot determine the effect of flowing hydrogen, high heat-transfer rates or aerodynamic loads on fuel-element geometries. Such problems can be investigated by electrically heating sample fuel elements and subjecting them to the hydrogen flow rates and heat-transfer rates to be encountered in the reactor. Study of the effects of simultaneous

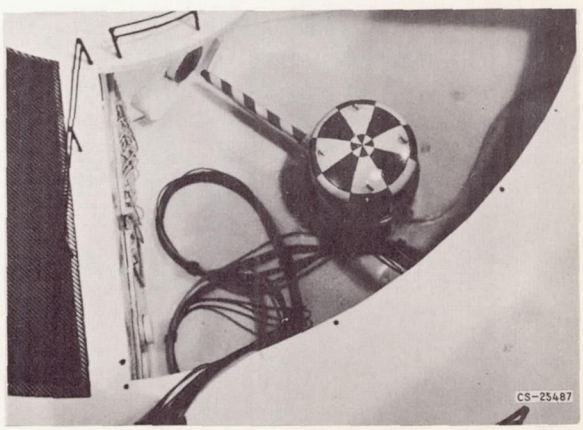

FIGURE 42–8.—Fuel-element-experiment facility in Plum Brook reactor.

fission heating and aerodynamic loads can be made during flow tests run on fuel elements that are placed within a testing reactor. Figure 42–8 shows a model of the NASA Plum Brook Reactor Facility with a fuel-element test loop about to be inserted into the core. The ends of the test holes, which are directly adjacent to the reactor, are shown as the flanged pipes. The test fuel element is located within the snout of the fuel-element test loop. The tank houses the pumps and heat exchangers necessary to flow the helium coolant. This loop, which is now under construction, is designed to operate with the test fuel element to produce 100 kilowatts of power.

GASEOUS-CORE REACTORS

The problems of attaining the ultimate performance of solid-core reactors basically limited by the melting temperature of solid materials have been discussed briefly. Now consider gaseous-reactor concepts, where the aim is to bypass the materials limit and to produce hydrogen temperatures of 10,000 to 20,000° F. with specific impulses up to 3000 pounds per pound per second. This is accomplished by maintaining nuclear fuel in the reactor as a gas rather than as a solid.

Basic Concept

The fundamental concept of a gas-core reactor is shown in figure 42–9. The nuclear fuel in gaseous form is contained in a reactor cavity that is externally moderated and reflected. The reactor is made critical by increasing the pressure of the fissionable gas. The heat generated by the fissioning gas can be used to heat hydrogen by direct mixing. The heated mixture is then ejected through a nozzle to produce thrust. The weight-flow ratio of fissionable material to hydrogen, of course, is limited by various considerations. For example, if the cost of the fissionable material is limited to the cost of hydrogen for an orbital launch interplanetary space mission, the fissionable-material flow would be about $\frac{1}{35}$ of the hydrogen mass flow (assuming that hydrogen placed in orbit costs $200 per pound, while fissionable material costs $7,000 per pound.) A less severe limit arises from the increase of propellant

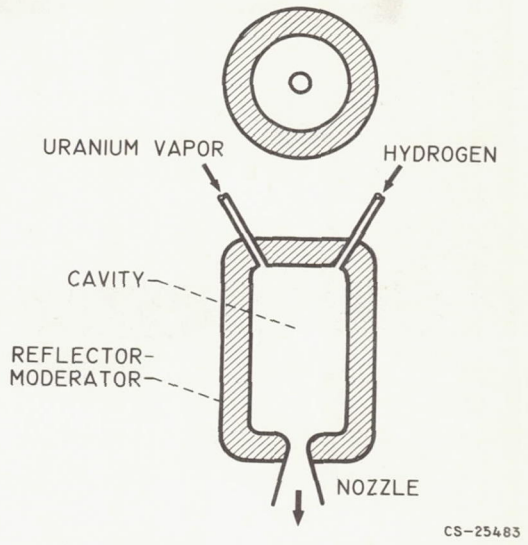

FIGURE 42–9.—Gaseous-cavity reactor.

average molecular weight; a 1-to-1 flow ratio would yield a specific impulse equal to 70 percent of that of pure hydrogen. For a ratio of 1 to 35 or less the effect on specific impulse is less than 3 percent. For a mass flow ratio of 1 to 35, the hydrogen pressure would be about 4000 times greater than the fissionable-material pressure because of the low molecular weight of hydrogen compared with that of uranium or plutonium. Under rather ideal conditions, the required partial pressure of fissionable material for criticality is of the order of 25 pounds per square inch (ref. 28). The total pressure in the cavity, therefore, would be of the order of 100,000 pounds per square inch!

Clearly some scheme is required to circumvent the pressure dilemma. If the uranium

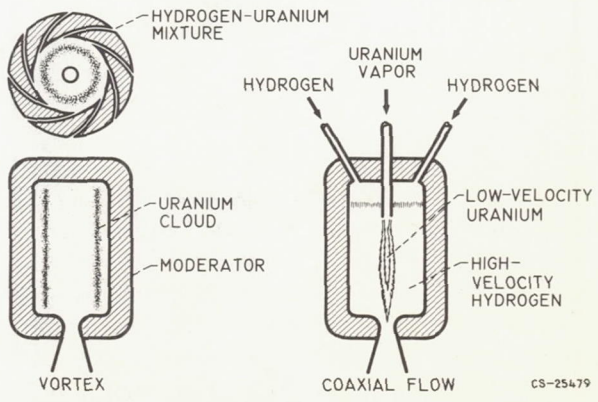

FIGURE 42–10.—Gaseous-cavity-reactor concepts.

could be caused to recirculate so that its residence time relative to the hydrogen would be increased by a factor of 100, the pressure level would be reduced by this ratio.

Figure 42–10 illustrates two gaseous-reactor concepts. The scheme on the left uses a vortex to increase the residence time of the uranium (refs. 29 and 30). A mixture of hydrogen and

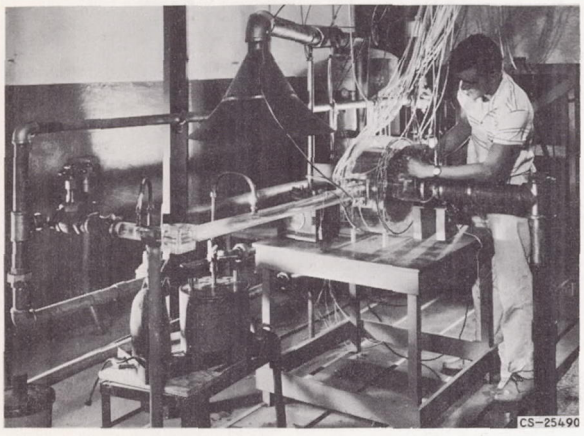

FIGURE 42–11.—Two-fluid vortex experiment.

uranium vapors is introduced tangentially into a cavity. The resultant centrifugal field set up will tend to throw the uranium atoms toward the walls, since they are heavy relative to the hydrogen. The radial-velocity component of the gas flowing through the reactor will try to drag the uranium with it. The hydrogen is heated as it diffuses through the resulting uranium cloud. If the flow rate is too high, the centrifugal forces on the uranium atoms will be overcome, and the uranium will be blown out. The limitation of this system appears to be the low flow rates that are permissible. In the scheme on the right, the uranium and hydrogen are introduced in separate streams in a coaxial fashion (ref. 31). The uranium must flow at a lower velocity than the hydrogen to maintain a reasonable uranium-to-hydrogen weight-flow ratio. Here the hydrogen is heated by thermal radiation from the fissioning uranium gas in the cavity center. In both reactor concepts, the hydrogen must contain a material to render it essentially opaque to radiation at temperatures below about 10,000° F. Above this temperature, hydrogen absorbs radiation by itself.

Other schemes have been proposed for gaseous reactors. Some utilize electromagnetic forces to increase the residence time of uranium (ref. 32), others use a multiple array of vortex tubes (ref. 29). Another scheme is called a "glo-plug" system (ref. 33), which, in principle, is similar to the coaxial-flow system except that a transparent hydrogen-cooled tube separates the uranium from the hydrogen. The problem of providing a transparent tube for the "glo-plug" system seems very formidable. The plasma-core concept requires very large magnetic-field strengths (ref 32).

The hydrodynamics of the gaseous-vortex reactor has received considerable attention (refs. 34, 35, and 36). A bromine-vapor–air experimental vortex system is shown in figure 42–11 (ref. 30). A bromine-air mixture is introduced tangentially into a transparent vortex chamber. The radial concentration profiles of bromine are measured by light-absorption techniques. Attempts to predict the observed data using one-dimensional analyses for two-component flow have not been too succesful (ref. 30). Recent investigations (refs. 35 and 36) suggest that the flow pattern in a vortex is much more complex compared with the models that have been used for analyses. Realistic analyses must consider the influences of turbulence and end-wall boundary-layer flow. A similar set of experiments run with a coxially flowing bromine-air system is shown in figure 42–12. In this case analysis agrees very well with experimental results for both laminar and turbulent situations. Typical data are shown in figure 42–13 for luminar- and turbulent-flow regimes.

The results of these hydrodynamics experiments are used to verify or check theoretical predictions that are used as a basis for determing performance of real gaseous reactors. Inasmuch as the gases in the real situation are quite different and the tests are isothermal, such experiments must be extended to other gases and heating must be provided to increase further the confidence in theoretical estimates.

Analytical investigations are being conducted for the coaxial system, where flow and radiation heat transfer are considered simultaneously (ref. 37). This analysis has predicted the effective absorptivity required to prevent melting

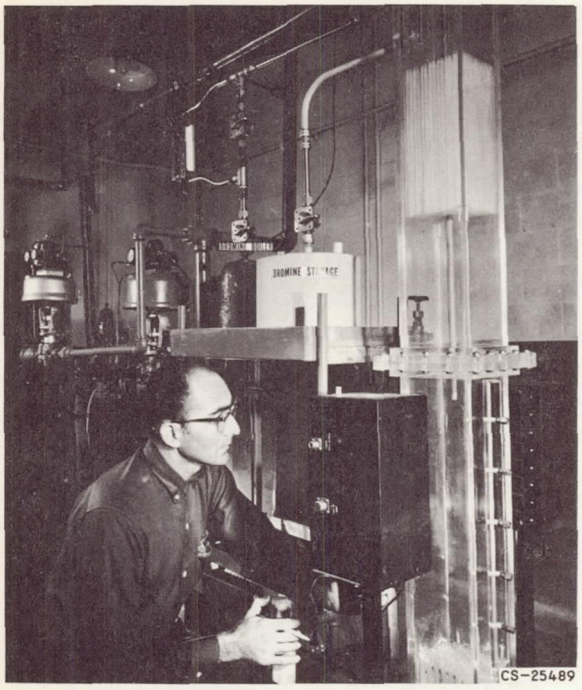

FIGURE 42–12.—Coaxial-flow experiment.

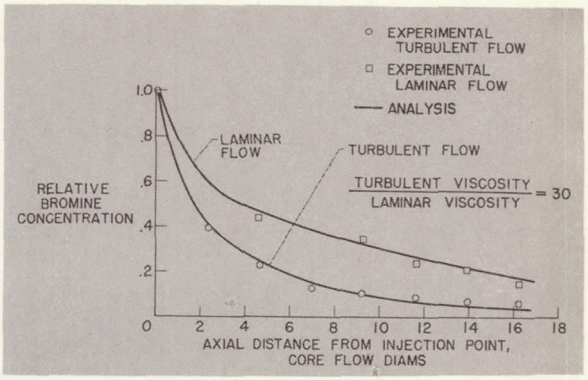

FIGURE 42–13.—Air-bromine coaxial-flow experimental data.

down the cavity walls. The use of seeding material such as graphite dust has been suggested to increase the thermal radiation absorption of the hydrogen, and some basic transmissivity measurements have been reported (ref. 38).

The results of reference 38 are summarized in figure 42–14. The conclusions indicate that the transmissivity of carbon-particle clouds is relatively independent of wavelength for 0.2 to 1.0 micron radiation and that the exponential dependency on concentration predicted by Beer's law exists. These data were all obtained at room temperature, however, and additional information at elevated temperatures and pressures including the chemical interaction with hydrogen is required. Currently, experiments are being conducted on the radiation absorption of seeded gases in flowing systems. Figure 42–15 shows the test apparatus used in these experiments. An arc about 2 feet long with a power of about 250 kilowatts is struck between the electrodes and is stabilized in a nitrogen vortex. The arc supplies a source of radiant thermal energy. Flowing coaxially in an annular region outside the arc tube is a stream of gas that can be seeded with dust particles. The energy transmitted through the gas with and without seeding is measured to determine the effect of seeding.

Very little work has been done or is under way in the area of criticality of gaseous reactors. The importance of this research stems from the fact that the operating pressure of gaseous-reactor concepts is directly determined by the critical-mass requirements of cavity reactors with unusual three-dimensional fuel distributions. These distributions arise from the hydrodynamics of fuel-separation schemes and nonuniform temperature distributions. Early work on criticality of cavity reactors has considered the case of uniform fuel distributions in spherical one-dimensional geometries (refs. 39, 40, and 41). This work has been extended at Lewis to two-dimensions where nonuniform radial fuel distribution has been considered (refs. 42 and 43).

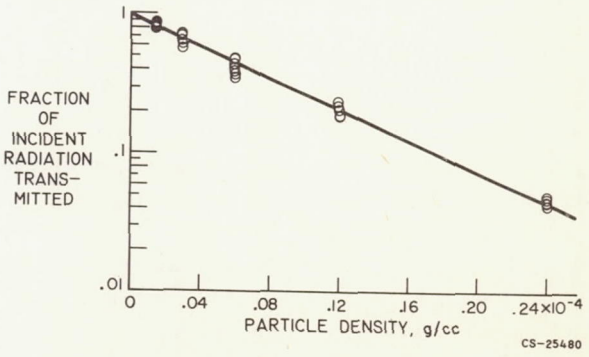

FIGURE 42–14.—Spectral transmissivities of carbon particles. Particle diameter, 0.15 micron; radiation wavelength, 0.2 to 1.0 micron; radiation path length, 10 centimeters.

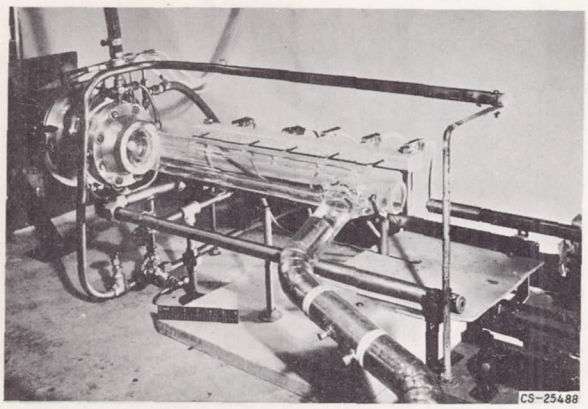

FIGURE 42–15.—Thermal-radiation-absorption experiment.

Because the potential performance of gaseous-nuclear rockets is far beyond that of advanced solid-core systems, the necessary research to determine feasibility should be vigorously pursued. The degree to which gaseous reactors can realistically attain their potential requires a great deal of work in the fundamental fields of gaseous radiant heat transfer, nucleonics, and hydrodynamics, and especially in their interaction.

CONCLUDING REMARKS

A limited amount of work is under way on the problems of both advanced solid-core and gaseous-core nuclear-rocket reactors. As the goals of our space program expand, the importance of nuclear rockets will become increasingly recognized. Therefore, the necessary technology needed to develop reliable nuclear rockets for manned interplanetary flight must be expanded as quickly as possible so that a solid foundation on which to base decisions to develop powerplants will exist. Most important among the things to be done in the study of solid-core reactors is the experimental evaluation of fueled materials and reactor concepts. In the study of gaseous reactors, the problems of hydrodynamics associated with increasing the residence time of the fuel, gaseous heat transfer by thermal radiation, and criticality of gaseous cores are the most pressing.

REFERENCES

1. HIMMEL, S. C., DUGAN, J. F., JR., LUIDENS, R. W., and WEBER, R. J.: A Study of Manned Nuclear-Rocket Missions to Mars. Paper 61–49, Inst. Aerospace Sci., Inc., 1961.
2. HIMMEL, S. C., DUGAN, J. F., JR., LUIDENS, R. W., and WEBER, R. J.: Nuclear-Rocket Vehicles for Mars and Venus Missions. Paper presented at ARS/ORNL Space-Nuclear Conf., Gatlinburg (Tenn.), May 1961.
3. JOHNSON, PAUL G., and ROM, FRANK E.: Perigee Propulsion for Orbital Launch of Nuclear Rockets. NASA TR R–140, 1962.
4. ROM, FRANK E., LIETZKE, ARMIN F., and JOHNSON, PAUL G.: Small Nuclear Rockets for Space Missions. Nucleonics, vol. 20, no. 11, 1962.
5. COOPER, RALPH S.: Fast Reactor Rocket Engines-Criticality. Nuclear Sci. and Eng., vol. 13, no. 4, Aug. 1962, pp. 355–365.
6. LEVIN, S. A., HATCH, D. C., and VON HALLE, E.: The Separation of Tungsten-184. Rep. KOA–865, Paper presented at ARS/ORNL Space-Nuclear Conf., Oak Ridge Gaseous Diffusion Plant, Union Carbide Nuclear Co.
7. WISNYI, L. G., and PIJANOWSKI, S. W.: The Thermal Stability of Uranium Dioxide. KAPL–1702, Knolls Atomic Power Lab., Nov. 1, 1957. (Available from Office Tech. Services, U.S. Dept. Commerce, Wash., D.C.)
8. Anon.: Tensile Strength—Graphite: Some Mechanical Properties of Graphite at Elevated Temperatures. Jour. App. Phys., vol. 22, no. 5, 1951, pp. 593–600.
9. Anon.: Tensile Strength—Tungsten: Memo. 157, Defense Metals Info. Center, Sept. 11, 1962, p. 20.
10. SIKORA, PAUL F., and HALL, ROBERT W.: Effect of Strain Rate on Mechanical Properties of Wrought Sintered Tungsten at Temperatures Above 2500° F. NASA TN D–1094, 1961.
11. BRADSHAW, WANDA D., and MATTHEWS, CLAYTON O.: Properties of Refractory Materials: Collected Data and References. LMSD–2466, Missile Systems Div., Lockheed Aircraft Corp., Jan. 15, 1959.

12. SANDERS, WILLIAM A., CREAGH, J. W. R., ZALABAK, C., and GANGLER, J. J.: Preliminary Investigation of the Fabrication and Properties of Hafnium Carbide. Paper presented at Tech. Conf. on High Temperature Materials, AIME, Apr. 26–27, 1961.
13. Graphite Creep Strength: Research and Development on Advanced Graphite Materials. TN 61–18, WADD, Apr. 1961.
14. GREEN, WALTER V.: Short-Time Creep-Rupture Behavior of Tungsten at 2250° to 2800° C. Trans. AIME, vol. 215, no. 6, Dec. 1959, pp. 1057–1060.
15. Materials Symposium, Sept. 13–15, 1961: ASD Tech. Rep. 61–322, p. 71.
16. BARTH, V. D.: Physical and Mechanical Properties of Tungsten and Tungsten-Base Alloys. DMIC Rep. 127, Defense Metals Info. Center, Battelle Memorial Inst., Mar. 15, 1960.
17. NEEL, D. S., and PEARS, C. D.: Southern Research Inst., Nov. 1960.
18. Investigation of Graphite Bodies. TR 59–706, WADC, Apr. 1960, p. 58.
19. MACMILLAN, DONALD P.: High Temperature Materials for Rocket Reactors. Nucleonics, vol. 19, no. 4, Apr. 1961.
20. MAY, CHARLES E., and HOEKSTRA, PAUL D.: Stability of Refractory Compounds in Hydrogen Between 4500° and 5000° F, and Their Compatibility with Tungsten. NASA TN D–844, 1961.
21. Anon.: Carbonization of Plastics and Refractory Materials Research, pt. 1. TR 60–646, WADD, Feb. 1961, p. 50.
22. DUSHMAN, S.: Vacuum Technique. John Wiley & Sons, Inc., 1949.
23. Anon.: Carbonization of Plastics and Refractory Materials Research. Fifth Quarterly Prog. Rep., General Electric Co., Mar. 30, 1960.
24. Anon.: Progress in the Development of Uranium Carbide-Type Fuel. BMI–1554, Battelle Memorial Inst., Nov. 17, 1961.
25. Anon.: Heat Transfer Reactor Experiment No. 1. APEX–904, Flight Prop. Lab. Dept., General Electric Co.
26. LISIN, A. V., and MONTGOMERY, H.: Application of the ML–1 Reactor to a Nuclear Rocket Experiment. Rep. AN–232, Aerojet General Nucleonics, Aug. 1960.
27. Anon.: Preliminary Hazards Summary Report for the ML–1 Nuclear Powerplant. Rep. IDO–28537, Aerojet General Nucleonics, Apr. 22, 1959.
28. ROM, FRANK E.: Advanced Reactor Concepts for Nuclear Propulsion Astronautics, vol. 4, no. 10, Oct. 1959, pp. 20–22; 46–50.
29. KERREBROCK, JACK L., and MEGHREBLIAN, ROBERT V.: Vortex Containment for the Gaseous-Fission Rocket. Tech. Release 34–205, Jet Prop. Lab., C.I.T., Sept. 1961.
30. RAGSDALE, ROBERT G.: NASA Research on the Hydrodynamics of the Gaseous Vortex Reactor. NASA TN D–288, 1960.
31. WEINSTEIN, HERBERT, and RAGSDALE, ROBERT G.: A Coaxial Flow Reactor—A Gaseous Nuclear-Rocket Concept. Preprint 1518–60, Am. Rocket Soc., Inc., 1960.
32. SPENCER, D. F.: Thermal and Criticality Analysis of the Plasma Core Reactor. Tech. Rep. 32–189, Jet Prop. Lab., C.I.T., Jan. 1962.
33. Anon.: A Summary of Douglas Research in Advanced Propulsion Systems. Rep. SM–41961, Douglas Aircraft Corp., June 1962.
34. ROSENZWEIG, MARTIN L., LEWELLEN, W. S., and KERREBROCK, JACK L.: The Feasibility of Turbulent Vortex Containment in the Gaseous Fission Rocket. Preprint 1516A–60, Am. Rocket Soc., Inc., 1960.
35. RAGSDALE, ROBERT G.: Applicability of Mixing Length Theory to a Turbulent Vortex System. NASA TN D–1051, 1961.
36. KENDALL, JAMES M., JR.: Experimental Study of a Compressible, Viscous Vortex. Tech. Rep. 32–290, Jet Prop. Lab., C.I.T., June 1962.
37. EINSTEIN, THOMAS H.: Radiant Heat Transfer to Absorbing Gases Enclosed in a Circular Pipe with Conduction, Gas Flow, and Internal Heat Generation. (NASA TR to be publ.)
38. LANZO, CHESTER D., and RAGSDALE, ROBERT G.: Experimental Determination of Spectral and Total Transmissivities of Clouds of Small Particles. NASA TN D–1405, 1962.
39. SAFONOV, G.: Externally Moderated Reactors. Vol. 12—Reactor Physics. Paper 625, Proc. Second United Nations Int. Conf. on Peaceful Uses of Atomic Energy (Geneva), 1958, pp. 705–718.
40. BELL, GEORGE I.: Calculations of the Critical Mass of UF_6 as a Gaseous Core with Reflectors of D_2O, Be, and C. LA–1874, Los Alamos Sci. Lab., Feb. 1955.

41. PAXTON, H. C., and ORNDOFF, J. D.: Group N–2. Prog. Rep. for Oct. 21–Nov. 20, 1960, Los Alamos Sci. Lab., 1960.
42. RAGSDALE, ROBERT G., and HYLAND, ROBERT E.: Some Nuclear Calculations of U^{235}–D_2O Gaseous-Core Cavity Reactors. NASA TN D–475, 1961.
43. HYLAND, ROBERT E., RAGSDALE, ROBERT G., and GUNN, EUGENE J.: Two-Dimensional Criticality Calculation of Gaseous-Core Cylindrical Cavity Reactors. NASA TN D–1575, 1962.

Nuclear Physics of Solid-Core Gas-Cooled Rocket Propulsion Reactors

By Donald Bogart and Edward Lantz

DONALD BOGART, *Chief of the Reactor Physics Branch, NASA Lewis Research Center, has specialized in the fields of thermodynamics, nuclear engineering and reactor physics. Mr. Bogart earned a B.S. degree in Mechanical Engineering from Cooper Union in 1943 and an M.S. degree in Mechanical Engineering from Case Institute of Technology in 1948. He is a member of the American Nuclear Society.*

EDWARD LANTZ, *Aerospace Scientist at the NASA Lewis Research Center, is presently working in the field of nuclear propulsion and power research. He attended Case Institute of Technology, where he received his B.S. degree in Physics in 1949. In 1960 he received his M.S. degree in Physics from Union College. He is a member of the American Nuclear Society, American Rocket Society and Sigma Xi.*

SUMMARY

The design of a nuclear-rocket reactor that will produce maximum propellant-gas temperature for limited core-material temperature requires successful integration of the mechanical, thermal, and nuclear aspects of a complex problem. The strong interaction of the three-dimensional heat generation with heat transfer to the propellant requires "tailoring" of reactor composition and geometry. The techniques used are zoning of uranium concentration, metering of gas flow through fuel-element cooling passages, core-moderator zoning, and judicious use of reflectors.

Control systems should encompass sufficient excess reactivity to start, shutdown, and restart a nuclear-rocket engine without introducing severe power distortions.

Herterogeneous moderated reactors that use tungsten, which exhibits neutron resonance absorption, require that fuel-element-moderator lattices be optimzied to produce maximum neutron multiplication.

INTRODUCTION

A considerable effort has been mobilized during the past few years for the development of a nuclear-rocket engine. The engine contains a solid-core reactor that directly heats a gaseous hydrogen propellant. During its operating life of a few hours, the reactor should be capable of power densities of about 2 megawatts per liter and produce hydrogen exit temperatures near 4500° R. At these operating conditions, construction and support of reactor fuel elements pose extremely difficult mechanical-design problems. The strength of materials becomes marginal at anticipated core-operating temperatures, but some strength is required to withstand the forces of the hydrogen flow without excessive creep.

If acceptable hydrogen temperatures are to be obtained for limited core-material temperatures, the mechanical, thermal, and nuclear design aspects of the reactor have to be thoroughly integrated.

Some aspects of reactor physics are presented that are exploited by the reactor designer to permit the use of available high-temperature materials to advantage. Techniques are discussed for adjusting heat-generation distributions in the core to obtain maximum possible

gas temperature. Required reactor excess reactivity and general methods for its control are briefly discussed. Finally, the problem of fuel-element-moderator-lattice optimization in heterogeneous tungsten reactors is presented. The objective of finding the best fuel-element spacings that produce maximum neutron multiplication is illustrated by calculations of tungsten-water lattices.

REACTOR CRITICALITY

The spectra of reactor criticality can be observed conveniently by the variation of critical mass of a reactor as a function of its size as various diluents are added to fissionable material. Such a variation is presented in figure 43–1 in which the critical mass in kilograms of uranium 235 is plotted against the radii of bare homogeneous spheres of fully enriched uranium containing several diluting materials. The critical condition implies a balance between neutrons produced by fission and neutrons lost by absorption and leakage.

The anchor point is the undiluted ball of uranium 235, which is about 8.5 centimeters in radius, that is critical with about 48 kilograms. This is a true fast reactor, since the neutron spectrum in the core is essentially that of the prompt fission neutron spectrum. Of course, in the rocket application, uranium metal, which melts at 2550° R, cannot be used; however, compounds such as uranium carbide or uranium oxide, which melt at temperatures of 4950° R and 5550° R, respectively, are desirable. Although these uranium compounds have poor structural properties, they may be incorporated with graphite or tungsten, which still have some structural strength as 5000° R is approached.

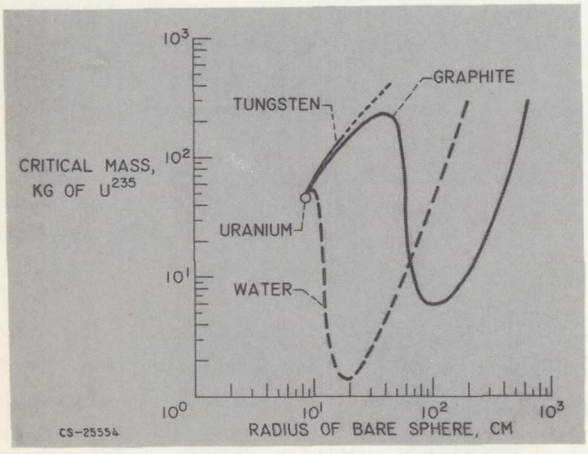

FIGURE 43.1.—Critical masses of homogeneous bare spheres of uranium 235 with diluents.

Refer to figure 43–1 and note that initial dilution of uranium with graphite causes the critical mass to increase at first. This is the result of the neutron spectrum shifting so as to increase nonproductive absorption in uranium. As more graphite is added, a point is reached where decreasing neutron leakage causes the critical mass to decrease, resulting in the peak reversal. Additional graphite now begins to act as a moderator, and the neutron spectrum approaches thermal equilibrium with the temperature of the carbon atoms; at thermal energies the neutrons see a large fission cross section and critical mass decreases to the low reversal point. Further addition of moderator causes the size and critical mass to increase, since the uranium atoms are already being used with maximum effectiveness and the additional moderator acts as a neutron poison.

The same characteristics are shown by the addition of water as the moderator, except that the unusually excellent slowing-down properties of hydrogen in water cause rapid neutron thermalization. The low reversal point of the thermal core shown in figure 43–1 is obtained at relatively small size and with small critical mass.

The criticality curve for natural tungsten as the diluent starts out similar to that for graphite, but since tungsten is ineffective as a moderator, the critical mass can be expected to increase as shown. The data of figure 43–1 were taken from a correlation of experimental and analytical criticality data presented in reference 1.

Of course, any real core must contain propellant-gas heating passages and be cylindrical instead of spherical. In addition, in a water-moderated core the high-temperature metallic fuel elements have to be thermally insulated from the water. If the metal is tungsten, it is desirable to use a mixture of separated tungsten isotopes that have low resonance capture for neutrons during the slowing-down process. This subject is discussed in detail later in connection with heterogeneous moderated cores.

Fast-spectrum reactors, characterized by the tungsten-diluent curve in figure 43–1, are sensitive to the introduction of gas passages; in particular, hydrogen gas introduces peculiar reactivity effects. Core-uranium loadings rise rapidly requiring fuel elements that contain much higher metallurgical uranium concentrations than those required for moderated systems; however, fast-spectrum reactors can use natural tungsten and other thermal neutron-absorptive materials that are less absorptive at high neutron energies.

HEAT-GENERATION DISTRIBUTIONS

Reference neutron-flux distributions φ in a schematic homogeneous cylindrical core are shown in figure 43–2. The core has axial cooling channels and may have thick or thin neutron reflectors on the sides and ends of the core. Slowing down and diffusion of neutrons to the boundaries result in a bare core taking on a radial flux of J_0 Bessel variation as shown. For a core with a side reflector, reflected neutrons contribute an added component near the radial core-reflector interface region. The axial flux takes on a cosine distribution in a bare core; an added component due to a thin front reflector is shown.

The heat released in every unit volume of the core is the product of the local neutron flux, uranium concentration, and fission cross section. This product integrated over all neutron energies provides a measure of the local heat-release rate. Since the neutron fluxes and flux

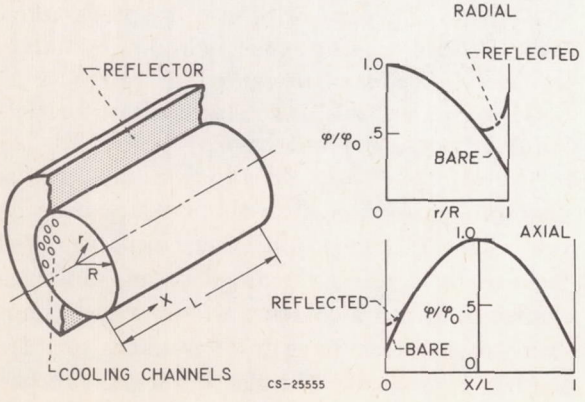

FIGURE 43–2.—Reference neutron fluxes in homogeneous cylindrical core.

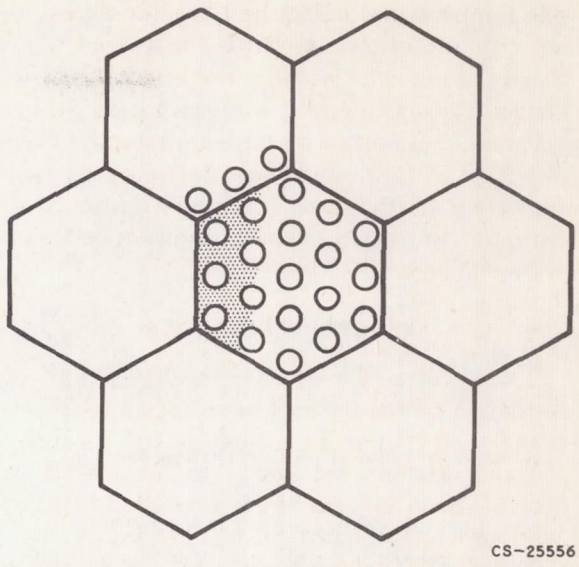

FIGURE 43–3.—Typical fuel-element array for homogeneous core.

spectra vary from unit volume to unit volume in the core, the heat-release rate varies in a unique three-dimensional way. What the reactor designer desires is for every unit volume of the core to be releasing as much heat as the materials will stand. These objectives require cylindrical reactors to have a radial heat-release rate that is uniform or flat, and an axial heat-release rate that heats up the propellant gas to the desired exit temperatures without exceeding limiting material temperatures and thermal stresses within the core.

The basic building blocks of the reactor are the fuel elements, which for a typical homogeneous honeycomb core look like the array shown in figure 43–3. All the fuel elements have some fixed uranium composition, and the generated heat is removed by thermal conduction to the many small cooling channels that axially pierce the element. In order to approach a flat radial heat generation with such elements, the uranium concentration may be altered from one element to another. Variation of the heat generation axially would require the elements to be segmented and each segment to have a different uranium composition. Gradients in heat generation across a given element can be accomodated by regulating the propellant mass flow through the individual cooling channels.

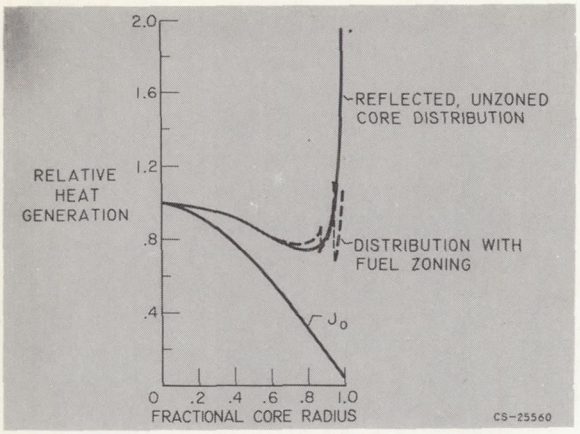

FIGURE 43–4.—Radial heat-generation distributions.

These methods of literally "tailoring" the heat-generation distributions in a cylindrical reactor are illustrated.

Radial Heat-Generation Distribution

The radial heat-generation distribution at the midplane of a homogeneous cylindrical graphite reactor using a berryllium side reflector is shown in figure 43–4. The beryllium reflector admirably produces a large thermal neutron flux that spills over from the reflector into the core. These thermal neutrons, which encounter a core loaded with uranium, produce sharp peaks in heat release, as shown by the upper solid curve in figure 43–4. The peak produced at the core-reflector interface is about twice that of the heat-release rate at the core center. This so-called "thermal spike" is intolerable and may be reduced by nonuniform radial distribution of fuel that would have to be continuously variable to produce a flat radial distribution.

A practical compromise is achieved by using several uranium concentrations in radial zones of the core. The results for three such zones are shown by the dashed curve of figure 43–4. Large heat-release variations are still present in short radial distances, but these can be accommodated by nonuniform propellant mass flow in the cooling holes that hopefully keep the maximum graphite temperatures within acceptable limits. This calls for solving a rather tricky problem of orificing gas flows through parallel passages with variable heat inputs and with a given overall pressure drop.

Of course, if there were no side reflector, the radial heat-generation distribution would be given a J_0 Bessel function shown as the bottom curve in figure 43–4. Its drooping character could never be compensated for by nonuniform uranium distribution. Without a side reflector, this resulting distribution severely penalizes the total power output of the reactor.

Axial Heat-Generation Distribution

The increase in propellant gas temperature as it passes through the core is proportional to the integral of the axial heat release. The fuel surface temperature at any axial position is higher than the gas temperature by a temperature difference that is directly proportional to the heat release at that point. The shape of the axial heat-generation curve is, therefore, an important factor in determining gas exit temperature for a maximum fuel temperature. It is here that reactor physics and heat transfer are very intimately related.

A typical axial heat-generation curve for a homogeneous core is shown in figure 43–5(a). This distribution is for a reactor with uniform axial uranium concentration and a thin front reflector. The axial heat generation is very closely a cosine function. The thin front reflector alters the cosine shape slightly. The curve for the propellant-gas temperature rises monatomically through the core. The cooling-

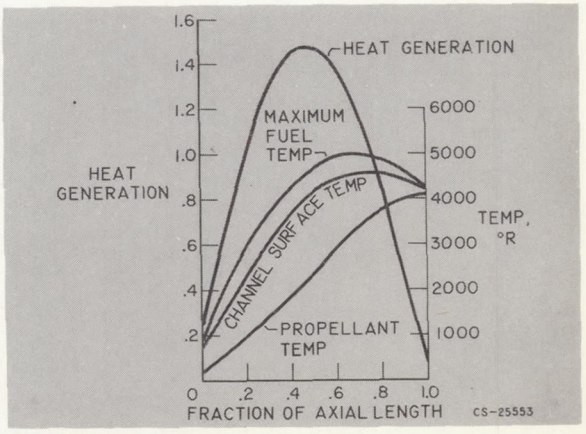

(a) Uniform core with top reflector.
FIGURE 43–5.—Axial distributions.

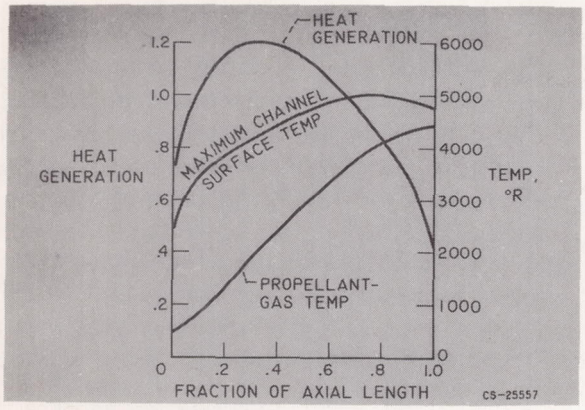

(b) Fuel-zoned core with top reflector.

FIGURE 43–5.—Concluded. Axial distributions.

channel-surface and maximum-fuel-temperature curves reach a peak well before the end of the cooling channel is reached. In this example, a gas exit temperature of about 4100° R is achieved with a maximum fuel-element temperature of 5000° R.

The axial situation shown in figure 43–5(a) is not the best but is the distribution that exists for reactors in which axial fuel zoning is not employed. An example of a better axial distribution is shown in figure 43–5(b), which employs segmented axial fuel elements. This particular core used a metallic fuel element made in small axial segments so that fuel may be axially zoned. In addition, a thicker front reflector has been employed. In this case, the axial heat-generation distribution is far from a cosine function; it reaches a peak in the front half of the core. Since the fuel element is metallic and has good thermal conductivity, the maximum-fuel and cooling-channel-surface temperatures are practically the same. In this case, a gas exit temperature of 4500° R is calculated for a maximum fuel temperature of 5000° R.

In summation, it has been shown that core designs to produce maximum gas temperature for a limited material temperature require zoning of uranium concentration, delicate metering of gas flow through fuel-element cooling passages, and judicious use of reflectors.

Proved neutron-diffusion and heat-transfer theories have provided good first approximations to core design problems. In conjunction with separate criticality and flow experiments, further design refinements may be built into the reactor; however, what cannot be answered by these approaches are the effects of interaction of the mechanical, thermal, and nuclear aspects as design conditions are approached. The question remains whether or not the core structure will hold up at the high temperatures under the combined thermal stresses resulting from nonuniform internal heat generation and other stresses resulting from the forces of the hydrogen flow.

REACTOR-CONTROL CONSIDERATIONS

The control system requirements for nuclear-rocket reactors are unique because of the short operating time (of the order of an hour), which results in small fuel burnup and fission product buildup. Therefore, provision for fuel burnup, which is the largest part of required excess reactivity in conventional power reactors, is unnecessary in the rocket reactor.

Reactivity is required to place the rocket reactor on fairly short startup periods and to compensate for the large rise in temperature which the liquid hydrogen and reactor must experience. In addition, positive shutdown requires that the control system ensure subcriticality by a safe margin. Finally, since it is desirable for the reactor to be restarted several times to execute its mission, some loss of fuel from the core must be anticipated and allowed for.

Most control devices introduce absorbers to compete with the fuel for neutrons. The best absorbers are materials with high capture cross section for thermalized neutrons such as boron, cadmium, or hafnium. As shown in figure 43–6, these absorptive materials can be placed in conventional push-pull control rods in the core of a thermal reactor or placed on one side of rotating control drums in the side reflector of thermal or intermediate spectrum reactors. The drums are shown in the figure at the halfway position.

In homogeneous cores, it is convenient to use rotating cylindrical control drums in the side reflector; however, both control rods and rotating drums introduce distortion in the local power generation. Consider the radial distri-

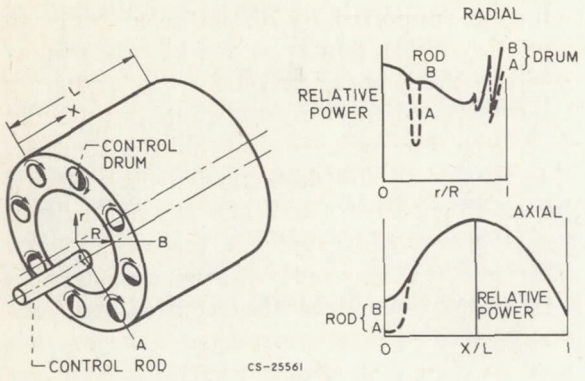

FIGURE 43–6.—Power distortion due to control devices.

butions along direction A, which passes through the rod and drum position, and direction B, which avoids the local flux perturbation. The rotating drums perturb the power distributions near the core-reflector interface by partial insertion of poison as shown in the radial distribution of figure 43–6. This introduces a scalloped circumferential power distribution that must be considered in the thermal design. In the same manner, the push-pull control rods depress the fluxes around the partly inserted rod in both the radial and axial directions, as shown in figure 43–6.

From an engineering viewpoint, the reflector control system is convenient in that the rotating drums are located in a cooled reflector; however, the reflector is a region of relatively low statistical importance and many large control drums are required. In a thermal core, the same control could be accomplished by smaller rods within the core but with attendant difficult cooling problems. For larger homogeneous cores, the side reflector becomes less important, and methods other than reflector control are necessary.

Control for heterogeneous reactors like the water-moderated core opens many new avenues of approach because of the accessibility of the moderator. For example, the use of liquid-poison passages or gas passages in the low-temperature water moderator of the core looks interesting. Such control techniques should be independent of the size of the core. Of course, several methods of control are usually possible for any reactor depending on the specific design.

HETEROGENEOUS MODERATED REACTORS

As mentioned earlier, in order to use the efficient water moderator, the high-temperature fuel elements have to be insulated and separated from the water. This results in a heterogeneous core arrangement that introduces peculiar reactor physics problems, which are discussed in connection with the tungsten-water-moderated core. The use of the most refractory metal, tungsten, in a moderated reactor introduces the problem of neutrons escaping resonance capture during slowing down.

The total cross section for natural tungsten in the slowing down energy region is shown in figure 43–7 (ref. 2). The four major isotopes, tungsten 182, 183, 184, and 186, exhibit large absorptive resonant cross sections in the region below a kilovolt. Tungsten 186 has an especially large resonance at about 20 electron volts, which is shown in the figure with a change of scale. The most abundant isotope, tungsten 184, is relatively free of absorptive resonances so that tungsten enriched in tungsten 184 is desirable. Fission neutrons born in the Mev energy region make collisions with water and must bypass this resonance region by spending most of the slowing down time in the water and not in the tungsten. The fraction of fission neutrons starting out that slow down past the resonance region is known as the resonance escape probability.

Shown in figure 43–8 is a representative heterogeneous core region consisting of an array of lattice cells of the high-temperature tungsten fuel elements in insulated water-

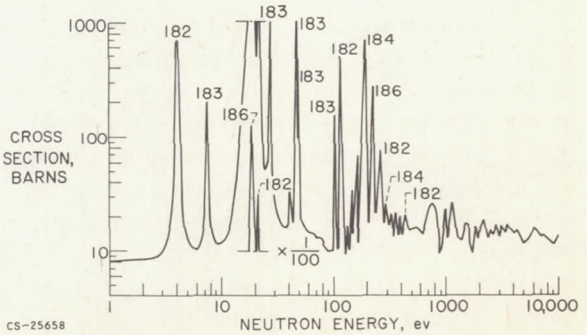

FIGURE 43–7.—Tungsten total cross section in slowing-down energy region.

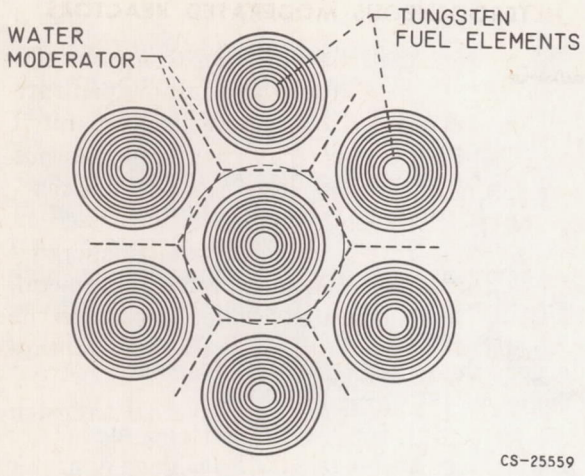

FIGURE 43–8.—Typical fuel-element array for heterogeneous core.

moderator regions. Tungsten enriched in the tungsten 184 isotope may be used to avoid excessive resonance capture while neutrons slow down in the water regions. The thermalized neutrons that have bypassed the resonance capture energies then diffuse into the individual fueled region from the water to produce the bulk of the fissions. For ease in calculation, the equivalent cylindrical cell shown in figure 43–8 is studied, and the flux variation in the lattice cell is determined.

The variation of the thermal-neutron flux in this individual cell is plotted against cell radius in figure 43–9. The separate fuel and water regions may be seen. This illustrative fuel element contains five concentric fueled tungsten cylinders supported by an unfueled tungsten tube. Hydrogen flow is guided by this support tube and tungsten center plug. The insulating spaces between the tungsten support tube and the moderator pressure tube have a thermal-radiation shield and stagnant hydrogen to keep the water container cool. The thermal neutron flux is seen to fall rapidly in the water region and through the successive fueled cylinders.

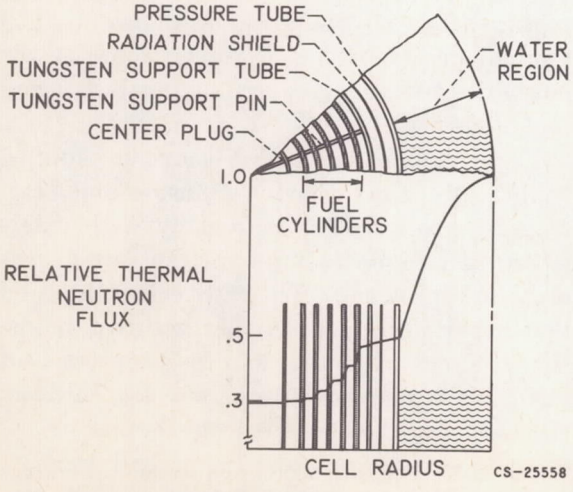

FIGURE 43–9.—Lattice cell of heterogeneous core.

In order to achieve the required exit gas temperature, a heat-generation tailoring job must be done. Because the metallic fuel elements are individual, the fuel loadings in the various fuel cylinders may be varied to permit each one to operate at its maximum temperature. The thermal design may be aided further by varying the heat-transfer spacings between fuel cylinders. Once again there appears the complex interplay between the nuclear, thermal, and mechanical aspects of the problem. Once an acceptable fuel-element configuration is determined, it is convenient for all the fuel elements of the core to be identical. Variations in gross radial heat generation from one fuel element to another can be tailored by small changes in moderator thickness called moderator zoning; however, it must be remembered that water captures thermal neutrons and too large a water thickness in the lattice will waste neutrons. Alternately, if the water thickness is too small, not enough neutrons will bypass the tungsten while slowing down and escape resonance capture.

The effects of resonance capture in tungsten enriched in varying degrees in the tungsten 184 isotope is shown in figure 43–10. Here the

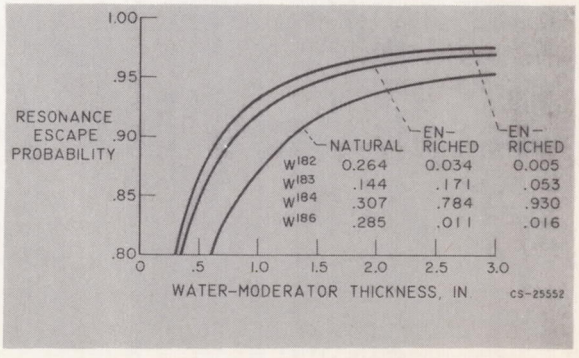

FIGURE 43–10.—Resonance capture in enriched tungsten for tungsten slabs 0.10 inch thick in water.

resonance escape probability is plotted against water thickness. Recall that the resonance escape probability is the fraction of fission neutrons starting to slow down that escape tungsten resonance absorption and become thermal neutrons. These results are for lattice cells containing tungsten slabs 0.100 inch thick based on analytical and experimental data presented in reference 3. The enrichment varies from natural tungsten that contains 30.7 percent tungsten 184 to separated isotopic mixtures containing 78.4 and 93.0 percent of tungsten 184.

It may be seen that resonance escape increases for larger water thicknesses. For any given water thickness, separation of tungsten 184 significantly increases the resonance escape probability. Enrichment in tungsten 184 also reduces the thermal-neutron absorption cross section and results in less competition with the uranium to improve the neutron multiplication factor of the lattice cell. The multiplication factor K is simply the number of neutrons produced by fission per neutron absorbed in the cell. Since resonance escape is increasing for larger water spacings because of better bypassing of resonances even though more thermal neutrons are wasted by absorption in water, an optimum neutron multiplication factor K exists for the fueled lattice cell; that is, there is some water thickness for a given fuel cell for which K is a maximum. The resultant multiplication factor for tungsten-fuel slab lattices containing 0.10 inch of natural or separated tungsten and a concentration of uranium 235 of about 10 percent by weight is shown in figure 43–11. It may be seen that K reaches a peak at 1.18 for natural tungsten, but for tungsten enriched in tungsten 184, K can be greater than 1.50. These peak values occur for water thickness between 0.5 and 1.0 inch.

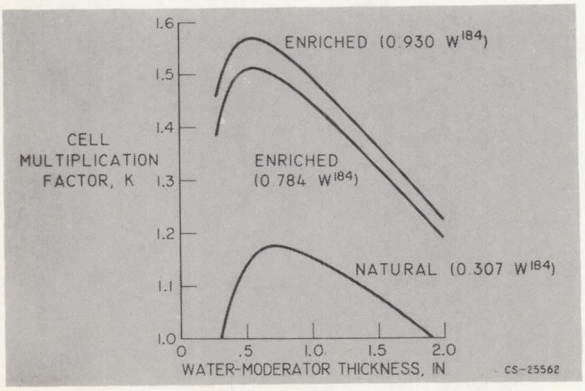

FIGURE 43–11.—Multiplication factor for tungsten fuel cell for tungsten slabs 0.10 inch thick in water.

Since the cell multiplication factor is a measure of the reactivity for an infinite number of these cells, the excess above unity must be used for neutrons to be lost by leakage from a finite critical reactor size. It follows that a natural tungsten reactor would have to be very much larger than an enriched tungsten reactor. Tungsten 184 enrichment further provides excess reactivity for use in fuel and moderator zoning that is so necessary to achieve desirable heat-generation distributions in any reactor.

CONCLUDING REMARKS

The strong interaction between the three-dimensional heat generation and heat transfer in nuclear-rocket reactors has been illustrated. It has been seen that both homogeneous and heterogeneous reactors must be tailored to approach maximum gas exit temperatures for a given maximum core material temperature. Techniques such as fine-scale fuel zoning and nonuniformly sized cooling passages in fuel elements are applied; on the gross scale, the use of reflectors and moderator zoning in the core are exploited.

A nuclear rocket control system must have a sufficient amount of controlled excess reactivity to start and maintain criticality throughout the required operating time and to restart the engine after it has been shut down. The thermal design of the core must consider the power distortions introduced by partly inserted control devices.

These design techniques may be applied analytically, since neutron-diffusion and heat-transfer processes are reasonably well understood, and digital computers can handle the elaborate problem. Separate criticality and flow experiments may further improve the design. Even with the known properties of materials at temperatures of interest, however, the basic question remains of whether or not a nuclear-rocket reactor design will perform satisfactorily as rated conditions are ap-

proached. The question remains because the complex interaction of the mechanical, thermal, and nuclear aspects of the design cannot be fully analyzed.

At the present time, the development of a nuclear-rocket reactor must telescope a large number of uncertainties into every hot-reactor experiment. A great deal more must be learned before nuclear-rocket reactors may be adequately and reliably designed.

REFERENCES

1. PAXTON, H. C.: Correlations of Experimental and Theoretical Critical Data. Rep. LAMS–2537, Los Alamos Sci. Lab., May 15, 1961.
2. HUGHES, D. J., and SCHWARTZ, R. B.: Neutron Cross Sections. Rep. BNL–325, Brookhaven Nat. Lab., July 1, 1958.
3. SCHNEIDER, HAROLD, LEVITT, LEO, and SROUB, KEVIN J.: A Monte Carlo Study of Resonance Escape Probability in Heterogeneous Slab Lattices Containing Resonant Absorbers and Scatterers. NASA TN D–1184, 1962.

Fluid-Flow and Heat-Transfer Problems in Nuclear Rockets

By Herman H. Ellerbrock, John N. B. Livingood, and David M. Straight

HERMAN H. ELLERBROCK, *Chief of the Nuclear Propulsion Branch of the NASA Lewis Research Center, has specialized in research on heat transfer and propulsion. He joined the NACA staff, NASA's predecessor, in 1930. Mr. Ellerbrock received his B.S. degree in Mechanical Engineering from Johns Hopkins and his M.S. degree from Case Institute of Technology. He is an Associate Member of the Institute of the Aerospace Sciences, a Senior Member of the American Rocket Society, and a member of the New York Academy of Sciences and Sigma Xi.*

DR. JOHN N. B. LIVINGOOD, *currently working on nuclear rocket heat-transfer and flow problems, has been a member of the NASA Lewis Research Center staff for 16 years. He is a member of the American Mathematical Society and Phi Beta Kappa and is listed in American Men of Science and Who's Who in World Aviation. He received his A.B. degree from Gettysburg College and his A.M. and Ph. D. degrees from the University of Pennsylvania.*

DAVID M. STRAIGHT, *Aerospace Scientist at the NASA Lewis Research Center, is presently working in nuclear propulsion and power system research. In his 19-year career at Lewis, he has worked in research on fuel-feed systems, turbojet and rocket ignition and starting, rocket combustion, and flow dynamics of cryogenic systems. Mr. Straight holds a B.S. degree in Mechanical Engineering from Northeastern University and is an Associate Fellow of the Institute of the Aerospace Sciences.*

INTRODUCTION

Deep-space probes and interplanetary travel require the successful development of the nuclear rocket. The use of nuclear rockets will permit such missions with lower takeoff weight and in shorter time than would be required if only chemical rockets were used. For these reasons, numerous scientists and engineers are actively engaged in a search for solutions to the many problems connected with the successful development of the nuclear rocket. This discussion is restricted to some of the typical heat-transfer and flow problems encountered in the development of the nozzle and the nuclear reactor and of progress being made in attempts to solve these problems.

The solutions to numerous reactor-core problems must be known before a successful nuclear rocket can be developed. For cores consisting of fuel modules with solid fuel elements, an accurate knowledge of the module temperature gradients is important. These values depend on the material, the type of passage configuration, passage size, etc. Some typical fuel-module temperatures for a given configuration, with allowance for different void fractions (or passage sizes), are presented herein. The effects of modifying the fuel distribution are also included. With a knowledge of fuel-module temperature gradients, core stresses can be calculated in order to determine whether the core is mechanically satisfactory. The state of the

art of calculating these stresses is briefly discussed.

Another important core problem is encountered during reactor cool down. The amount of cooling required to overcome the afterheat may be so low that laminar flow exists and conditions become favorable for the well-known "flow excursion" or "static instability" to occur. A discussion of this problem is included.

For safe operation of the reactor, it is desirable to have the hydrogen propellant enter the reactor core in the gaseous phase. Since the hydrogen is stored in the liquid phase in the storage tank, the hydrogen must pass through the two-phase state somewhere in the system during reactor startup. For chemical rockets, in which startup times are of the order of 1 to 2 seconds, no problem is encountered; for nuclear rockets, in which startup times may be of the order of 20 to 30 seconds, serious problems may be caused by the two-phase flow. In addition, any flow or pressure instabilities or maldistributions of the hydrogen can cause local hot spots in the core and create problems for the control system that regulates the coolant flow, the pressure, and the reactor power of the engine system.

Since current two-phase hydrogen heat-transfer and flow knowledge is inadequate for nozzle and reactor design, an experimental program is in progress at the Lewis Research Center to augment the existing information. A résumé of the present state of knowledge, a description of experimental apparatus being used to augment fluid-flow and heat-transfer knowledge for the reactor, and presentation of some results of tests will be given. Single heated tubes (steady state), single unheated tubes (transient), nozzle sectors, and simulated reflector pieces with parallel unlike passages are all included in the Lewis program. Moreover, the test sections are of sufficient length that the gaseous phase of the hydrogen is achieved within the tube and experimental data for gaseous hydrogen are also included.

Since a typical reflector contains numerous different size coolant passages, the problems of flow maldistribution and detrimental pressure oscillations must also be investigated and solved. Oscillatory-flow data for hydrogen flow through the unheated and the heated tubes and frames from motion pictures of flow distribution for the multiple-hole reflector pieces are presented; a discussion of current knowledge on these subjects is included. Information obtained from these investigations should also apply to the nozzle.

Current plans indicate the nuclear reactor will probably be started in or near an Earth orbit. As a consequence, the effects of low or zero gravity on flow and heat transfer must be known. A brief discussion of the problem is presented.

Current nozzle design procedures involve the specification of a wall temperature. The gas-side heat-transfer coefficient is then estimated, and the heat flux to the wall calculated. A coolant-side heat-transfer coefficient is then obtained by iteration, such that the desired wall temperature is attained. This procedure is carried out at local positions along the nozzle. Unfortunately, methods of achieving reliable predictions of the gas-side heat flux are not yet available; a status report on methods now used will be given.

REACTOR CORE

The final design of a reactor involves an iteration among the results obtained from nuclear, temperature, and stress calculations. The nuclear calculations result in several geometries that could be used and that will give the required reactivity. After the temperatures and stresses are calculated for the reactor parts resulting from these geometries, the dimensions of the final reactor parts are chosen.

The reactor core poses the largest problem of heat removal and existing high temperatures during operation. This problem may be illustrated by a comparison of heat-release rates of modern-day steam boilers with those of proposed reactors for nuclear rockets. A boiler has a typical heat-release rate of 40,000 Btu per hour per cubic foot, while a nuclear-rocket reactor could have a typical heat-release rate of 400,000,000 Btu per hour per cubic foot, a 10,000-fold increase.

In addition to these problems during full operation, another type of problem exists for the period of reactor cool down. The require-

ment of a nuclear rocket for a given space mission would most likely be a startup, full operation, shutdown, coast, and then a restart. During the coast period after shutdown, removal of the reactor afterheat would be necessary. During this cool-down phase, the flow rate is gradually decreased, and in the process of diminishing this flow rate there arises the problem of flow excursion, which will be explained in greater detail in one of the following sections.

Thermal-Stress Considerations

The order of magnitude of thermal stress is, in general, given by

$$\sigma_{th} \sim \frac{E\alpha\Delta T}{1-\nu} \tag{1}$$

where ΔT is considered to be the maximum temperature difference existing between any two points in the material. (All symbols are defined in the appendix.) The entire integrity of the core is coupled to the maximum temperature existing within the material and to the temperature gradient across a given member. Two determining factors involved with these parameters are power density and distance between points of maximum temperature difference. The dependence on these factors is shown, for simplicity, in the steady-state temperature equation for uniform power generation in a slab:

$$T_{max} - T_w = \frac{Q_v \delta^2}{2k} \tag{2}$$

Both T_{max} and $T_{max} - T_w$ must be controlled to within allowable limits. Obviously, T_{max} must be less than the melting point of the material and $T_{max} - T_w$ must be compatible with allowable thermal stresses. These thermal stresses are a function of heat generation, which determines the temperature gradient, and of material properties.

Equation (1) as shown merely indicates the basic parameters involved with thermal stresses; it is not a complete representation. The geometry of a reactor is usually reduced to a simplified representative part, for which thermal-stress equations can be derived. The adequacies of these equations as applied to the entire structure can be verified only by actual operation.

The types of stress usually calculated are elastic stresses, although in the high-temperature range of operation plastic flow undoubtedly will occur. Designing for this plastic flow is acceptable, but existing loads on members must be accurately known. The other items that must be known are stress-rupture data and the required material properties at high temperatures. At present, these high-temperature data are relatively scarce.

Effect of Geometry on Temperature

For nuclear rockets, the maintenance of as small a size as possible is desirable; that is, for a given reactor power, the value of power density will usually be the maximum allowable from a size determination. Equation (2) shows that for a fixed value of Q, the temperature difference could still be reduced by a factor of 4 by reducing the distance δ by a factor of 2. The maximum temperature is also reduced by the amount of the decrease of the temperature difference.

For a given reactor size of high-power rating, maximum temperatures and thermal stresses can thus be controlled by a choice of reactor geometries consisting of a fine structure; that is, all distances δ are kept to a minimum. A reactor consisting of concentric rings of both fuel elements and moderator, for example, could be made to operate in a safe region of thermal stress by splitting these rings into as small a thickness as could be fabricated.

Some typical reactor geometry configurations are shown in figure 44–1. Figures 44–1(a) and (b) show typical fine-structure geometries with possible methods of arranging the coolant passages. By assuming symmetry and uniform heating, the temperature distribution in each shaded segment can be calculated as explained in reference 1. Figures 44–1(c) and (d) show other arrangements of fuel and moderator where again symmetry may be assumed and relaxation methods may be used to calculate internal temperatures. The concentric ring type of arrangement that was mentioned previously is shown in figure 44–1(e).

Of the various geometries shown in figure 44–1, the first two are of the most importance

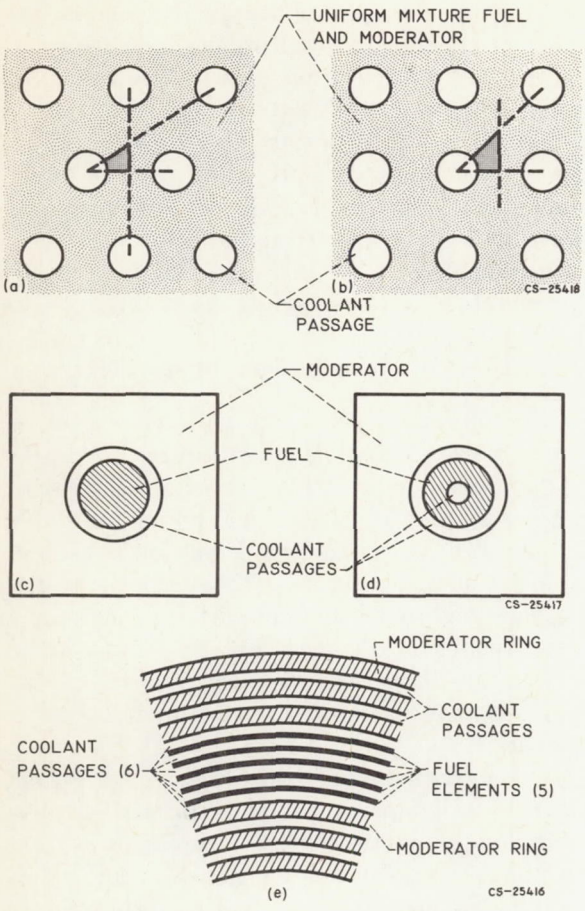

(a) Triangular cooling arrangement.
(b) Square cooling arrangement.
(c) Solid fuel rod with separate moderator.
(d) Tubular fuel rod with separate moderator.
(e) "Flat plate" type fuel elements with concentric split-ring moderator segments.

FIGURE 44–1.—Typical reactor geometry configurations.

herein. This homogeneous type of structure is now readily amenable to adjustment of hole size and spacing to arrive at optimum temperatures. The temperature distribution and the conduction heat-transfer characteristics of the material will depend upon the ratio of the spacing between passage centers to the passage diameter. Equations that give the temperature at every point in the material for both the triangular and the square arrays are presented in reference 1.

The surface temperature of the cooling passage is assumed to be constant around the circumference. Results of reference 1 show that for very large spacings the heat removal is essentially uniform around the periphery, which indicates little influence of the presence of neighboring cooling passages. As these spacings get closer, nonuniformities of heat removal appear, and the temperature distribution around a passage is influenced by neighboring passages more in a square array than in a triangular array. The most important difference between the two arrays, however, is that the hot-spot temperature for a square array will always exceed that for a triangular array for fixed values of heating rate, spacing, and passage diameter.

The actual effect of varying coolant-passage size on maximum temperature and on temperature gradient is shown in figure 44–2. The temperatures were calculated for a typical reactor with graphite assumed to be the predominant material with a geometrical arrangement the same as the triangular array of figure 44–1(a). The core void fraction was kept constant and a cosine distribution was assumed for the heat generation in the axial direction. The fact that reactor power and therefore coolant-flow rate were the same for each geometry resulted in the same coolant temperatures. This procedure makes possible a direct comparison on a geometrical basis alone.

The finer geometry resulting from smaller hole sizes producted a dramatic difference in maximum temperatures and temperature gradients. The maximum temperature of approximately 6400° R for the 0.15-inch-diameter hole geometry was reduced to about 5200° R

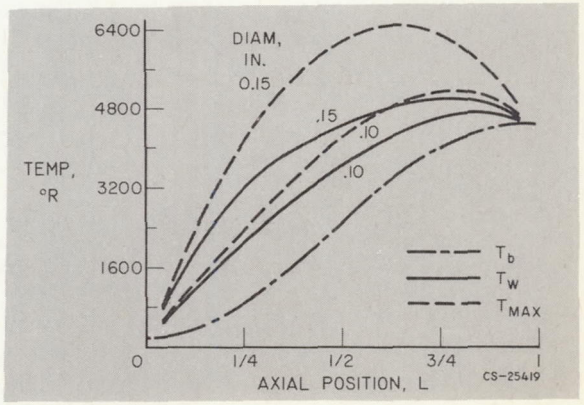

FIGURE 44–2.—Effect of coolant-passage diameter on temperature gradient and maximum temperature (20 percent void).

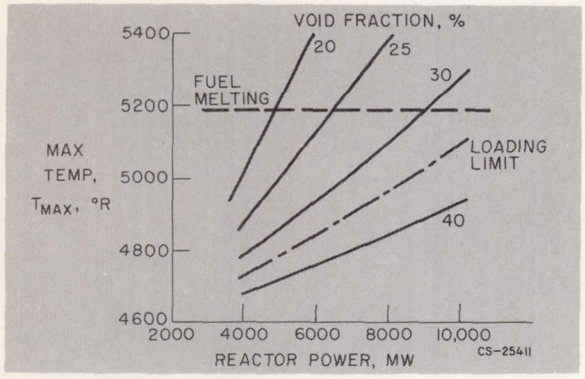

FIGURE 44–3.—Effect of void fraction on maximum temperature. Inlet bulk gas temperature, 200° R; outlet bulk gas temperature, 4500° R; diameter, 0.1 inch.

by using 0.10-inch-diameter holes. Maximum temperature differences were reduced from about 1600° to about 600° R in going to the smaller passages.

As stated in the discussion, these calculations were for a fixed core void fraction and two different hole sizes. The result of varying void fraction for a fixed hole size is shown in figure 44–3. For a reactor power of 6000 megawatts, for example, the maximum temperature is reduced by 500° R in going from a 20- to a 30-percent void. For even higher powers, a 30-percent void results in possible allowable temperatures, whereas a 20-percent void obviously would not even permit the attainment of these higher powers.

Using the results of such curves as those in figures 44–2 and 44–3 allows the calculation of thermal stresses if formulas are available. A maximum allowable stress therefore establishes the geometry sizing required. The introduction of nuclear considerations such as maximum allowable void fraction for criticality (dash-dot line) and of limitations on possible fuel melting (dashed line) then results in a final core choice that is compatible with all factors concerned. Each of these limitation lines is merely representative and may actually be located elsewhere for the core geometry investigated.

In addition to using fine geometrical configurations to reduce maximum temperatures, fuel loading may be distributed so as to reduce hot spots by reducing the power density in certain locations while increasing it in others. When acceptable temperatures have been achieved, nucleonic, mechanical, and volume aspects must be reconsidered. This redistribution of fuel will have some definite limit presented by each of these factors.

Status of Knowledge of Heat Transfer

As the gaseous hydrogen flows through the reactor, its temperature increases from several hundred degrees to about 4500° R or more. Over this wide range of temperatures, the calculation of heat-transfer coefficients becomes questionable. Many investigators have studied gaseous-hydrogen heat transfer, but the individual experiments have usually been limited to wall temperatures below 2600° R; some helium tests have been run at higher wall temperatures (5000° R), but use of such results would not include effects of hydrogen dissociation and variation in fluid properties. Furthermore, most existing correlations are for overall average values rather than local values. Apparently, gaseous-hydrogen heat-transfer data must be augmented for conditions like those prevailing in a reactor core before any conclusive assurance on hydrogen heat-transfer calculation procedures applicable to the core becomes possible.

Flow Excursions

Several effects should be considered in an evaluation of the flow distribution and stability through the core during the cool-down phase of operation. Although the effects of characteristics are somewhat interrelated, they are listed as follows for purposes of discussion:

(1) Distribution of core radial temperature
(2) Variation in velocity head of coolant approaching core passages
(3) Probability of operation in transition region from turbulent to laminar flow during cool-down phase
(4) Prediction by pressure-drop equations that at a given pressure drop a passage may have either of two flow rates with a constant heat input

The core radial temperature profile predicted for design-point operation will not be valid dur-

ing the cool-down phase of operation, and the profile will be exaggerated by the actual flow characteristics. The pressure drop in the hotter passages will tend to be greater, and as the pressure drop is set by the pressure in the inlet and the outlet plenums, the pressure drop can be satisfied only by lower flow rates in the hot passages, which aggravates the condition.

As lower flow rates are considered during the cool down, the second effect becomes more prominent. As the flow rate decreases, the effectiveness of flow-distributing baffles or screens decreases, which could permit a variation in the velocity of the coolant approaching the various core passages and result in additional temperature variation across the core.

The reduced flow rates of cool down would also produce the third effect. The frictional pressure drop through a passage is a function of Reynolds number and depending on the magnitude of the number is expressed in one of two ways. The transition region of values of Reynolds number ranges from 2000 to 10,000 and in this region either the laminar-flow or the turbulent-flow friction factor could be applied. In considering a group of parallel passages, a prediction of whether the flow will be laminar or turbulent in the various passages is nearly impossible if the pressure drop and inlet conditions are such as to establish flow in the transition region. This case will lead to flow maldistribution and to flow oscillations if conditions are such as to permit random tubes to alternate between laminar and turbulent flow. The change in temperature of the coolant as it passes through the passage further compounds this effect by making it possible for flow to enter the passage at a Reynolds number safely in the turbulent range and to leave safely in the laminar range.

The fourth effect is illustrated in figure 44–4. The equation of pressure drop in a uniformly heated tube was written and analyzed. For a given pressure drop, two flow values were possible. A digital-computer program was written at Lewis to evaluate this equation over a range of values. Figure 44–4 presents a series of lines representing the variation of pressure drop with flow rate, each with a constant heat input along the length of the passage. The lower series of curves represents the corresponding

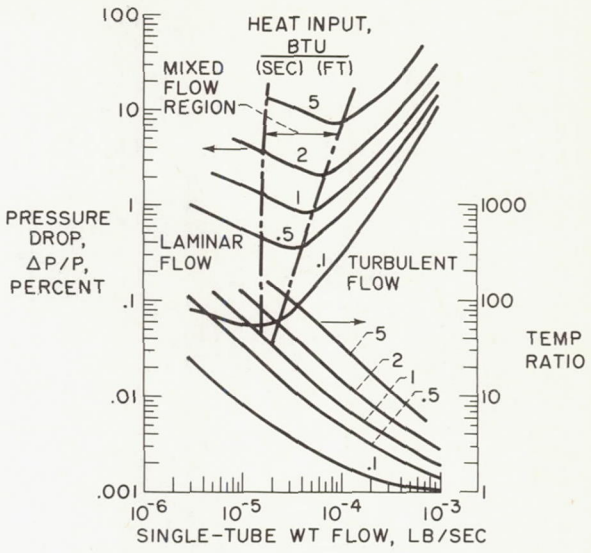

FIGURE 44–4.—Core flow stability.

outlet- to inlet-temperature ratios for the various heat inputs. These computed data have a common inlet pressure and temperature. The transition region between all-laminar and all-turbulent flow is indicated between the dash-dot lines. Figure 44–4 indicates, for example, at 2-percent pressure drop and a heating rate of 1 Btu per second per foot that a flow excursion could occur from 6.2×10^{-6} to 1.45×10^{-4} pound per second, which is an increase in flow by a factor of 23. The corresponding temperature ratios for these flows, as indicated by the lower curves in figure 44–4, are 100 and 6, respectively. If the core-inlet temperature were 150° R, the corresponding core-outlet temperatures would be 15,000° and 900° R at the low and the high flow rates, respectively. This relation can indeed predict serious problems in flow distribution and the related problems of thermal stresses and material failure. In addition, flow excursions could occur in a given passage as the flow cycled back and forth between the two possible flow rates. A similar relation for flow in a capillary tube is presented in reference 2, in which it is indicated that the low flow case is unstable and that the high flow case is stable.

In summarizing the cool-down problem, it must be concluded that current considerations indicate a serious problem and that further analysis and experiments are required; possibly intermittent bursts of coolant at relatively high flow rates should also be considered.

REFLECTOR

A knowledge of the hydrogen state as a function of time is essential in the startup transient. One such typical history is shown in figure 44–5

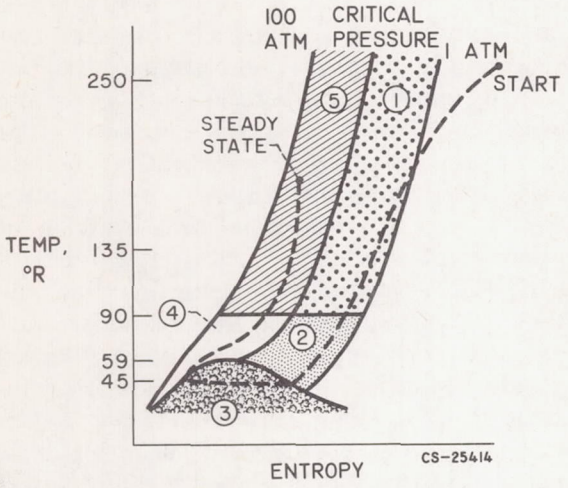

FIGURE 44–5.—Hydrogen state at reflector inlet during startup.

for the reflector inlet, in which time increases in the direction from the starting point to the steady-state full-power point. At startup, the hydrogen enters the reflector in a gaseous state (region 1) and at subcritical pressure. As time increases and the hydrogen temperature at the reflector inlet is reduced to about 90° R, a transition region (region 2) extending to the saturation line is encountered. Then the entering condition reaches the two-phase state and remains in this region (region 3) until the other leg of the saturation curve is met. Region 4, which is supercritical, is then encountered; this region near the saturation line is another transition region. The supercritical gaseous phase begins at about 90° R (region 5). Steady-state operation takes place in region 5. Hence, transition or pseudo-two-phase and two-phase heat transfer are all encountered at the reflector inlet, depending upon time after startup.

Stable Flow

Two-phase hydrogen flow and heat transfer.—The presence of two-phase hydrogen flow through the reflector at some time during startup is indicated in figure 44–5. As the hydrogen entering the reflector in the two-phase state moves along the reflector passages, it picks up additional heat and an increase in quality results. Even after 100-percent quality is attained, the hydrogen may not yet be in the gaseous state, but in the pseudo-two-phase state. Both two-phase and pseudo-two-phase heat transfer and flow will be discussed in this section.

Many investigations of two-phase or boiling fluids, especially in the nucleate boiling range, have been conducted. Data for hydrogen in the film boiling region, however, are limited. Some are presented in reference 3. In the reflector, the magnitude of the difference between the wall and the bulk temperatures is such that film boiling takes place. Film boiling is therefore of prime interest in reflector studies.

The following paragraphs give the status of knowledge of heat-transfer and fluid-flow correlation equations, the need for more data for reactor design and study, and experimental work in progress at the Lewis Research Center related to this subject.

Status of knowledge: According to reference 4, reliable methods for predicting two-phase heat-transfer coefficients are unavailable, because several different kinds of boiling region exist, heat transfer in these regions is affected in different ways by a variety of variables, and flow patterns in two-phase mixtures are not yet established. Some correlations have been proposed for restricted ranges of variables, but to date their limits of applicability are unknown. Moreover, the importance of local conditions is becoming more pronounced. The problem is reviewed in reference 5.

A study of isothermal pressure drop for two-phase flow in a horizontal tube showed that turbulent-flow data for a number of fluids could be correlated on the basis of a dimensionless parameter (ref. 6):

$$\chi_{tt}=\left(\frac{1-x}{x}\right)^{0.9}\left(\frac{\rho_g}{\rho_l}\right)^{0.5}\left(\frac{\mu_l}{\mu_g}\right)^{0.1} \qquad (3)$$

The Martinelli parameter χ_{tt} represents the ratio of shearing forces in the two fluid phases; since only isothermal pressure drops were considered, no momentum pressure drop was included. This parameter, as will be discussed

later, has been used in several proposed heat-transfer correlations for two-phase flow. These correlations, according to reference 4, are formulated in terms of single-phase heat-transfer coefficients for the liquid and thereby imply that the liquid is in contact with the surface. Consequently, there is no assurance that such a correlation would be applicable for cases in which the gas phase is in contact with the surface. Reference 4 also states that χ_{tt} depends on vapor density, which in turn is a function of two-phase pressure drop; since two-phase pressure drop depends on the local density of the mixture, an iteration process is required to obtain χ_{tt} and the two-phase heat-transfer coefficient.

The parameter χ_{tt} was used in reference 7 to correlate two-phase heat-transfer data for water flowing through a vertical tube. Local heat-transfer coefficients were obtained for the nucleate boiling region during circulation vaporization in a long vertical copper tube. The heat flux contributed by nucleate boiling was apparently additive to the convection heat flux. Although this information was not used in the correlation procedure in reference 7, it has been suggested as an alternative method of correlating nucleate boiling data (see ref. 8). Other suggested correlations are discussed in reference 9.

Nucleate boiling heat transfer for five organic liquids flowing by natural circulation through a vertical single tube was correlated with the aid of χ_{tt} (ref. 10). Separation of the effects of convection and nucleate boiling by calculating a convection coefficient in terms of a liquid coefficient and χ_{tt} and applying a nucleate boiling correction factor to the convection coefficient to obtain the two-phase heat-transfer coefficient was attempted in reference 10. The correction factor used varied with the radius of the minimum-size stable bubble and the laminar film thickness.

Reference 3 reports heat-transfer and pressure-drop data for hydrogen flowing under forced convection through a vertical heated tube. In these experiments, the fluid model consisted of a liquid core and a gaseous annulus in contact with the wall. These conditions are opposite to those observed in reference 6; reference 3, however, shows that a two-phase heat correlation can be obtained by use of the χ_{tt} parameter. The parameter χ_{tt} was originally used to correlate pressure-drop data for isothermal conditions and for the nucleate boiling region; it correlated heat-transfer two-phase hydrogen data in the film boiling region for a nonisothermal case. Data were also obtained for hydrogen at supercritical pressure just above and below critical temperature.

In reference 11 are defined five regions into which hydrogen is arbitrarily divided in order to investigate its cooling capabilities. One of these is the two-phase region (region 3 in fig. 44–5), in which the correlation equation of reference 12 was used. The part of region 4 (fig. 44–5) between the saturation line and about 90° F and between the critical pressure line and the 100-atmosphere line is a so-called pseudo-two-phase region, and heat-transfer data for this region are correlated by means of a modified or pseudo χ_{tt}. The 90° F limit attached to this region is used because it is at about this temperature that the specific heat of hydrogen attains its maximum value; this value corresponds to the temperature above which the transport and specific-heat properties of hydrogen appear to be unaffected by the critical temperature condition (see ref. 11). Reference 12 gives a good discussion of boiling and near-critical heat transfer.

Local heat-transfer data are presented in reference 13 for bulk boiling of water in vertically upward forced flow. These data were correlated by means of χ_{tt} and a boiling (or Sterman) number Bo. For low values of the boiling number, the local heat-transfer coefficient is a function of χ_{tt} alone; for large values of the boiling number, the local heat-transfer coefficient becomes independent of χ_{tt} (ref. 13).

In reference 14, the use of a two-phase Reynolds number for correlating two-phase heat-transfer data is proposed. One such number is found from

$$Re_{TP}=Re_{SP,\,l}\left(1-x+x\,\frac{\mu_l}{\mu_g}\right)$$

where

$$Re_{SP,\,l}=\frac{\rho_l u_{l,\,in} D}{\mu_l}$$

The model contained a gaseous core and a liquid annulus; for a liquid core and a gaseous

annulus, $Re_{SP,g}$ may be required. A plot of Nu_g against Re_{TP} correlates film boiling hydrogen heat-transfer data very well.

Data for the heat transfer to hydrogen in the liquid, nucleate and film boiling, and gaseous regions under forced convection have been obtained in electrically heated stainless-steel tubes (ref. 15). These data covered velocities from 25 to 55 feet per second, inlet bulk temperatures from 40° to 57° R, outlet bulk temperatures from 40° to 147° R, inlet pressures from 28 to 213 pounds per square inch absolute, heat fluxes from 0.01 to 6 Btu per second per square inch, and wall temperatures from 51° to 1505° R. The two-phase data were correlated at Los Alamos Scientific Laboratory by use of Re_f, Pr_f, ρ_f/ρ, and T_w/T; the resulting correlation equation is unpublished, to the best of the authors' knowledge. The absence of subscripts on ρ and T appearing in the denominators of the two fractions leaves doubt as to what the basis for these terms should be. Since the correlation is for two-phase flow, these quantities might conceivably be based on mean fluid conditions and hence include quality.

The static-pressure drop for two-phase flow in a horizontal pipe for isothermal conditions led Martinelli to the discovery of the parameter χ_{tt} (ref. 6). The final correlation equation given in reference 6 predicts the static-pressure drop per unit length for two-phase flow in terms of that for gaseous flow and χ_{tt}; in the limiting case, as the gas-flow rate approaches 0, the equation reduces to that for liquid flowing alone. In reference 3, for hydrogen flow through a heated tube, it was found that the viscous shear forces at the wall could be neglected and that the two-phase pressure drop could be determined from the one-dimensional pressure drop due to momentum change alone.

According to reference 11, most of the pressure drop in the pseudo-two-phase region reported was due to change in momentum; however, some frictional drop also existed. It was concluded that both pressure losses should be calculated for the pseudo-two-phase region, but that sufficient information was not yet available for the appropriate selection on the nonisothermal friction factors. Such factors, however, are expected to be appreciably smaller than the isothermal values; the friction data of reference 16 verify this expectation.

Experimental investigations at subcritical pressure: Few experimental data for the pseudo-two-phase region are available. Some data for the two-phase region were presented in reference 3; these data were determined for heated vertical tubes with inside diameters of 0.495 and 0.313 inch and for steady-state conditions. Since both these two diameters are considerably larger than a typical reflector passage, and since it had not yet been ascertained as to what effect diameter might have on two-phase and pseudo-two-phase heat-transfer correlations, a test program was initiated at the Lewis Research Center to consider tubes of 0.188-inch diameter and 52-inch length; this size approximates a typical reflector passage.

The test program was set up to include both transient and steady-state investigations; according to figure 44–5, the reflector operates in both ranges. One of the objectives of the program was to determine whether the same correlation or different correlations are required for steady-state and transient data.

Both unheated and heated tubes were included. Tube-inlet pressures from 22 to 46 pounds per square inch absolute and weight-flow rates from 0.002 to 0.022 pound per second were considered. The heated tubes were supplied with up to 6 kilowatts of electrical power. Wall temperatures varied from 100° to 500° R.

Apparatus and test procedure: A schematic diagram of the liquid-hydrogen heat-transfer facility is shown in figure 44–6. A hydrogen-supply Dewar is shown on the right of the fig-

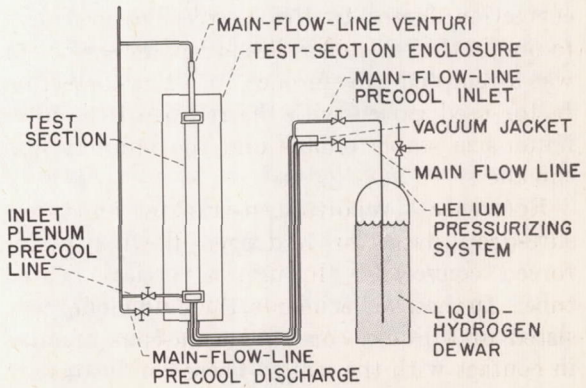

FIGURE 44–6.—Schematic diagram of liquid-hydrogen heat-transfer facility.

ure. The main hydrogen flow line connecting the Dewar to the test section is surrounded by two annuli; the inner annulus precools the main flow line and the outer annulus, maintained at a high vacuum, minimizes external heat leaks. The test sections, complete with inlet and outlet plenums, were contained in a large test-section enclosure that could be evacuated to prevent external heat leaks. A Venturi was located in the vent pipe for flow-measurement purposes. The locations of the various valves are also indicated in figure 44–6.

A photograph of the single-tube test section with three equally spaced electric heaters installed for steady-state runs is presented in figure 44–7. Insulation was wrapped around the

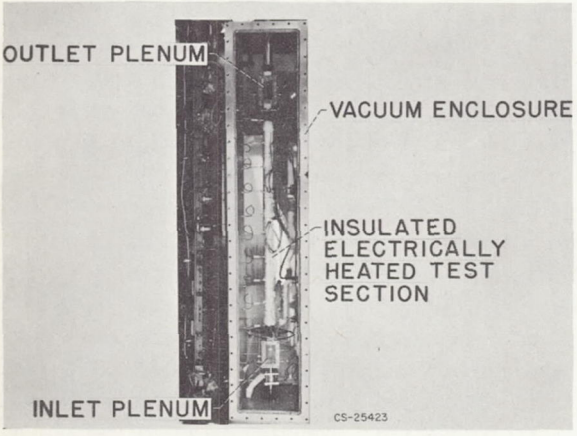

FIGURE 44–7.—Heated test section installed in heat-transfer facility.

assembly to reduce external heat leaks. Figure 44–8 is a closeup view of the inlet plenum of the test section in which the transparent window and instrumentation techniques can be more clearly seen. The unheated-tube installation is the same as that for the heated tube except that no heaters or power supply lines were used.

Aluminum was chosen as a material because its thermal diffusivity is similar to that of material, such as beryllium, generally used in reactor reflectors. The tube size (0.75-in. outer diameter and 0.188-in. inner diameter) was chosen to simulate the ratio of material volume to flow area typical of reflector geometries.

Facility instrumentation consisted of supply Dewar pressure (pressurized with helium gas),

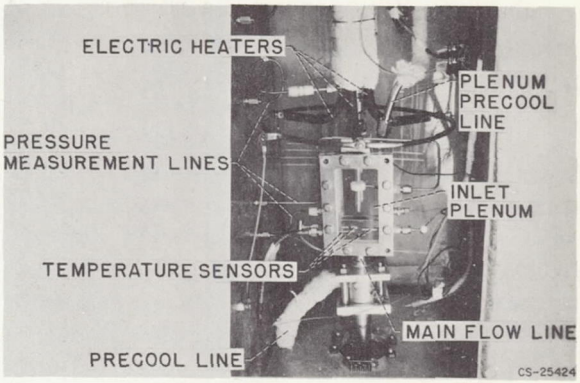

FIGURE 44–8.—Inlet plenum, heated test section, and associated equipment.

precool line temperature, liquid-level indicators in the Dewar, Venturi flow measurement at the exit end of the test section, and electric power when used for the heated test section. The inlet and the outlet plenums of the test sections were monitored by high-speed cameras, so that the quality of the hydrogen entering and leaving the test section could be appraised.

A schematic diagram of the test-section instrumentation used for single-tube experiments, typical for both heated and unheated tubes, is shown in figure 44–9. The pressure and the temperature of the hydrogen were measured in the inlet and the outlet plenums. The tube wall temperature was measured at four radial positions at each of 10 stations along the 52-inch length of the tube. The local pressure of the hydrogen was also measured at the 10 stations.

The output signals from the temperature sen-

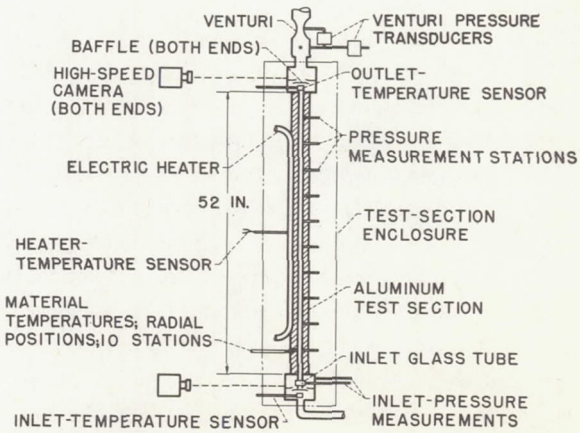

FIGURE 44–9.—Schematic diagram of instrumentation on heated test section.

sors and pressure transducers used for sensing the test variables were passed through appropriate signal-conditioning electronic equipment and readout was on direct-writing recording oscillographs or on magnetic tape that was then automatically processed to obtain the data.

Details of typical pressure- and temperature-instrumentation installation methods are presented in figure 44–10. Considerable difficulty

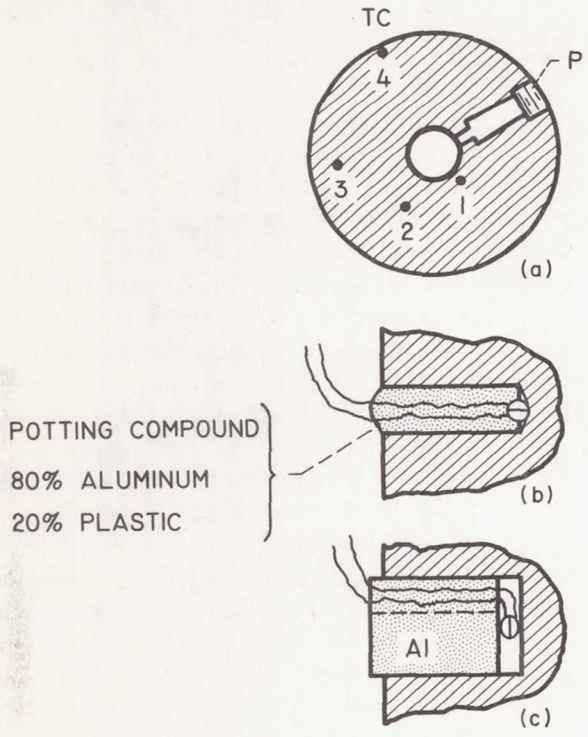

(a) Pressure- and temperature-measurement locations.
(b) Potted thermocouple.
(c) Plugged thermocouple.

FIGURE 44–10.—Typical pressure- and temperature-instrumentation installation on test sections.

was encountered in obtaining accurate temperature measurements of the test-section material. Calculated radial-temperature profiles from a transient-conduction heat-transfer digital-computer program indicated a maximum radial gradient of about 10° R from the inner to the outer wall of the test section.

Comparison of individual experimental thermocouple measurements indicated that each thermocouple measurement could vary by as much as ±15° (average deviations about ±5°), which resulted in an erratic measurement of radial gradient. This variation is a result of differences in contact thermal resistance between the thermocouple bead and the test section and the influence of the material that holds the thermocouple in place. Two thermocouple-installation methods that were used are shown in figure 44–10. Neither one, however, was satisfactory for precise measurements of radial profiles. For transient tests, in which the test section was cooling down with time, the slope of indicated temperature with time was consistent and the heat-flow rate based on this method was accurate within ±5 percent.

The procedure for test operation is given in the following discussion: The hydrogen-supply Dewar was filled with liquid hydrogen (99+ percent para-hydrogen) from large transportable delivery Dewars through a transfer system incorporated in the test stand. Prior to a run, the flow line connecting the supply Dewar to the test section was precooled by flowing liquid hydrogen in an annulus surrounding the main flow line under control by the precool valves shown in figure 44–6. The test-section-inlet plenum chamber, which supplies hydrogen to the test section, was also precooled by flowing hydrogen through the main line and out the plenum precooling valve. The test section was kept warm during the precooling process by a reverse purge of warm helium gas through the test section that was also vented from the system through the plenum precooling valve. The flow from both precooling systems and the test-section flow were all vented through a common vent stack to the atmosphere.

During a run, an automatic timer controlled the valves, valve positions, data recorders, and camera over preselected time periods.

The operating procedures for both the heated and the unheated tubes were generally the same, except that recording instruments were turned on before test-section flow started for the unheated-tube runs and after flow and power were stabilized for the heated-tube steady-state runs.

Description of data-reduction methods: A brief summary of the calculations made in correlating the two-phase-flow data for the unheated tube follows: (This study is for transient heat transfer.) The flow rate $\dot{w}$ was determined at the vent Venturi located down-

stream of the test section proper. The standard Venturi equation and the data recorded at the Venturi were used; an iteration on the Venturi discharge coefficient was performed until calculated and calibrated values agreed to within 0.2 percent. The test-section inlet quality of the fluid was obtained with the aid of motion-picture photographs taken of the inlet glass tube. From the photographs, a value of the inlet velocity of the mixture was determined. This value, together with the glass-tube passage area and the calculated flow rate, yielded an inlet mixture density. This density, together with measured inlet pressure, permitted the reading of inlet quality from a chart in reference 17.

The heat input to the hydrogen from a section of the tube of axial length Δl was obtained from

$$Q_{\Delta l}=W_m c_{p_m} \frac{\Delta T_m}{\Delta t}$$

where

$$W_m=\frac{\pi}{4} \rho_m \Delta l (D_o^2-D_i^2)$$

The term c_{p_m} was evaluated at the third radial temperature measured at the station at the midpoint of the section of length Δl, and $\Delta T_m/\Delta t$ was taken as the temperature gradient at this position. A typical plot of T_m against time of the type that was used to determine the gradients is shown in figure 44–11. The third radial

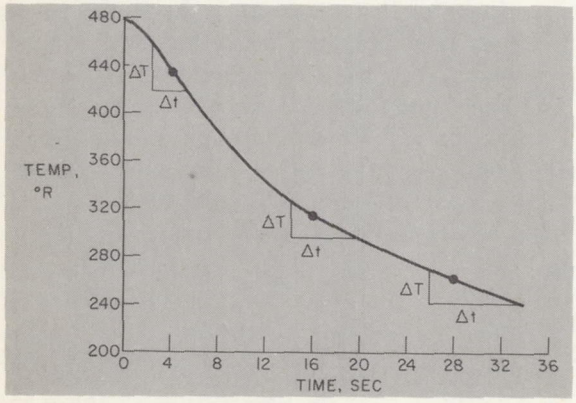

FIGURE 44–11.—Typical variation of tube-wall temperature with time in single unheated tubes.

position corresponds closely to the center of mass. The value of the local experimental heat-transfer coefficient was found from

$$h_{\text{exp}}=\frac{Q_{\Delta l}}{A_s(T_w-T_b)}$$

where

$$A_s=\pi D_i \Delta l$$

and T_w is the inner wall temperature.

The local fluid quality was evaluated from

$$x=x_i+\sum \Delta x$$

where

$$\Delta x=\frac{Q_{\Delta l}}{\dot{w}\lambda}$$

The heat of vaporization λ was determined at the local pressure with the aid of reference 17.

The initial attempt at correlating two-phase heat-transfer data was to follow the procedure in reference 3; other attempts will be made in the future. Since the tube diameter of reference 3 differed from that for which the data herein were obtained, calculation of the parameters required for the chosen correlation method was necessary because the correlation equation of reference 3 may not apply to other tube diameters. In fact, other investigators have already made use of the boiling or Sterman parameter to account for diameter changes. In addition, the data of reference 3 were for steady-state heat flow; hence, the correlation of $Nu_{\text{exp}}/Nu_{\text{calc}}$ against χ_{tt} is used herein. The parameter χ_{tt} has already been defined by equation (3); values of χ_{tt} were obtained by use of this equation. The values of Nu_{exp} were obtained from

$$Nu_{\text{exp}}=\frac{h_{\text{exp}} D_i}{k_f}$$

and h_{exp} has already been discussed. The value of Nu_{calc} was obtained from the equation used in reference 3:

$$Nu_{\text{calc}}=0.023(Pr_f)^{0.4}(Re_{TP})^{0.8}$$

The value of Re_{TP}, as in reference 3, was found from

$$Re_{TP}=\frac{\dot{w}}{A_i} \frac{D_i}{\mu_f} \frac{\rho_{fm}}{\rho_b}$$

and the densities required for this evaluation from

$$\rho_{fm}=\frac{1}{\frac{x}{\rho_{vg,f}}+\frac{1-x}{\rho_{l,\text{sat}}}}$$

and

$$\rho_b = \frac{1}{\frac{x}{\rho_{g,\,sat}} + \frac{1-x}{\rho_{l,\,sat}}}$$

The two-phase Reynolds number was defined, according to reference 11, to account for film-density changes incurred over a large range of qualities from the near-gaseous to the near-liquid values. As the fluid approaches the gaseous phase, the Reynolds number becomes the same as the usual gaseous Reynolds number.

For the pseudo-two-phase region, the procedure suggested in reference 11 for supercritical conditions might be applicable for subcritical conditions. The procedure employs the use of a light and a heavy species and bases property values for the heavy species on the melting temperature of the fluid and for the light species on the bulk temperature. The correlation is of the form Nu_{exp}/Nu'_{calc} against χ'_{tt}, where

$$\chi'_{tt} = \left(\frac{1-x'}{x'}\right)^{0.9} \left(\frac{\mu_{melt}}{\mu_{pg,\,f}}\right)^{0.1} \left(\frac{\rho_{pg,\,f}}{\rho_{melt}}\right)^{0.5}$$

$$Nu'_{calc} = 0.023 (Pr_f)^{0.4} (Re'_{TP})^{0.8}$$

$$Re'_{TP} = \frac{\dot{w}}{A_i} \frac{D_i}{\mu_f} \frac{\rho'_{fm}}{\rho'_b}$$

$$\rho'_b = \frac{1}{\frac{x'}{\rho_{pg,\,b}} + \frac{1-x'}{\rho_{melt}}}$$

$$\rho'_{fm} = \frac{1}{\frac{x'}{\rho_{pg,\,f}} + \frac{1-x'}{\rho_{melt}}}$$

The value of χ'_{tt} may be determined as follows: The equation for ρ'_b may be solved for x'. In order to determine the numerical value of x', the values of $\rho_{pg,b}$ and ρ_{melt} can be found from tabulated or graphical hydrogen data and the value of ρ'_b can be determined by use of Goodwin's iteration. This iteration requires the assumption of a value of specific volume and calculation until an output specific volume agrees with the input specific volume.

In order to apply this procedure to the subcritical cases, properties for the light species might be evaluated at the wall or the film temperature and for the heavy species, at the saturation temperature for either gas or liquid. To date, these attempts have not been made for a sufficient amount of data to permit any further comment.

Steady-state heat transfer was investigated by use of heated tubes. A brief description of the method of correlation for these tests follows. Steady-state conditions were obtained by manipulating flow rate and electric power to the heaters until thermocouples imbedded in the test section gave a steady reading. About 20 seconds after a stable condition was visually determined, the 15-second recording of run conditions was made.

All the steady-state tests were made with subcooled hydrogen entering the test section. The inlet flow lines and inlet plenum were precooled, and the supply Dewar was vented to the atmosphere. After stabilization, the Dewar was pressurized to obtain the desired flow conditions. Subcooling from 1.6° to 7.5° R was achieved; these values were obtained by taking the difference between the measured and the saturated temperatures for the measured fluid pressure.

The heat input to the hydrogen was determined from

$$Q_T = \dot{w} \Delta H$$

The flow rate was obtained in the same way as that for the unheated tube, and the change in enthalpy was determined from measured inlet and outlet pressures and temperatures. Since the heaters were shorter than the test section, calculations of the heat entering the hydrogen from these unheated sections were made by use of the conduction equation:

$$Q = kA \frac{\Delta T}{\Delta l'}$$

where ΔT was the difference in measured temperatures in the heated and the unheated lengths and $\Delta l'$ was the distance between the end of the heater and the temperature sense point in the unheated section. The rate of heat addition to the hydrogen along the heated section of the tube was determined by subtracting the two conduction rates from Q_T. This heat addition was then assumed to be distributed uniformly along the heated tube length. Incremental lengths along the heated tube were taken be-

tween instrumentation points. The lengths required to bring the hydrogen from the subcooled state to a saturated liquid and from a saturated liquid to a saturated gas were calculated by use of inlet enthalpy, flow rate, and heat rate per unit length.

The experimental heat-transfer coefficients were obtained from

$$h_{exp}=\frac{Q_{\Delta l}}{A_i(T_w-T_b)}$$

where T_w was taken as the average value between the measured end points of the incremental length Δl. The remainder of the calculations were made in the same way as those for the unheated tube.

Both momentum and friction pressure drops were included to calculate pressure drop for these two regions. The momentum pressure drop, for each incremental length, was obtained from

$$\Delta p_{mom}=\frac{G^2}{g}\left(\frac{1}{\rho_{out}}-\frac{1}{\rho_{in}}\right)$$

where $G=w/A_i$ and ρ_{in} and ρ_{out} are evaluated for each incremental length from the entering enthalpy, the pressure, and reference 17. The frictional pressure drop was determined from

$$\Delta p_{frict}=\frac{0.184}{\left(\frac{GD_iT_b}{\mu_fT_f}\right)^{0.2}}\left(\frac{T_b}{T_f}\right)\left(\frac{l}{D}\right)\left(\frac{G^2}{2g\rho_{av}}\right)$$

Here

$$\rho_{av}=\frac{\rho_{in}+\rho_{out}}{2}$$

for the respective increment.

Results: Figure 44–12 shows a plot of Q/A_s against T_w-T_b for the unheated tests. Since published hydrogen data show the peak nucleate boiling point at a value of $T_w-T_b\approx4°$ and the data on figure 44–12 indicate a value of T_w-T_b ranging from 100° to 400°, the statement that film boiling predominates in the reflector passages is confirmed.

The two-phase heat-transfer data for both the heated and the unheated tubes are shown in figure 44–13. The ordinate consists of the ratio of the experimental Nusselt number to the calculated Nusselt number times the boiling number to the −0.4 power; the abscissa is the Martinelli parameter. The exponent on the boiling number was determined empirically from the experimental data. Superimposed on the slide are some steady-state data from reference 3. The correlation curve was determined for the unheated-tube data and the data of reference 3; the heated-tube data fall into the same general pattern, but slightly higher; this difference may be attributed to the uncertainty in the determination of heat input into the tube. Only the total heat to the tube was measured, and the assumption was used that this heat was uniformly distributed.

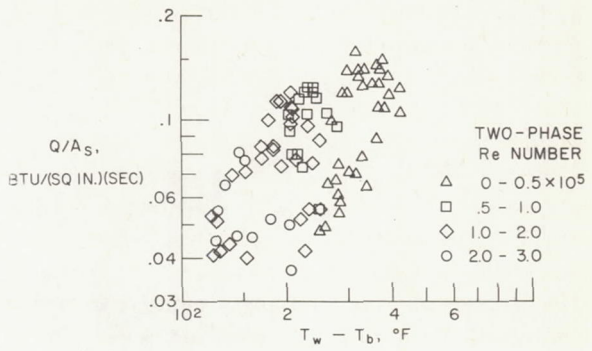

FIGURE 44–12.—Typical hydrogen convective-film-boiling heat-transfer data.

A plot of the ratio of experimental Nusselt number to a calculated Nusselt number against χ_{tt} is presented in reference 3. When the data of the current experiments were plotted on this basis, the data separated into groups according to the boiling number in a manner similar to that presented in reference 13. The heat-transfer rate was more dependent on χ_{tt} at low values of boiling number than at high ones (ref. 13). The use of the boiling number in the correlation should thus improve the two-phase heat-transfer correlation.

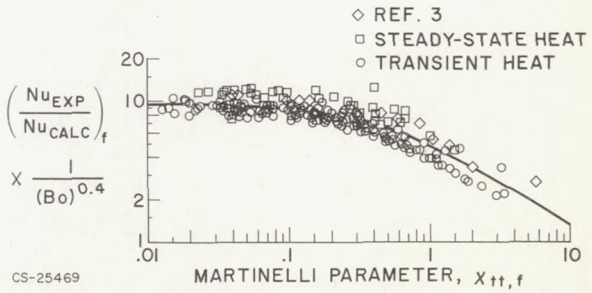

FIGURE 44–13.—Two-phase hydrogen-flow heat-transfer correlation.

A first attempt to apply the boiling number to the data in a simple manner resulted in the correlation presented in figure 44–13. Although this correlation appears satisfactory because it reduced an original ±60-percent spread to a ±25-percent maximum spread for two different sets of data, it should be considered as only the beginning of the investigation. The study of liquid- and gaseous-interface geometries and the degree of wall wetting during two-phase flow with heat addition, together with the establishment of an improved model based on visual observations, might yield more information on this subject. The theory developed in reference 13, for example, is based on a wetted wall with bulk boiling in forced flows; the wall- to bulk-temperature ratios in the current experiments (fig. 44–12), however, indicate film boiling.

A plot of experimental against calculated two-phase pressure data is shown in figure 44–14; data from several runs with the unheated tube are shown. A sample run is marked with an arrow that indicates the direction from the tube inlet. The calculated absolute pressures at the tube entrance are matched with the experimental values for the calculations. As the flow proceeds up the tube, the calculated pressures become larger than the measured pressures; in other words, the calculated pressure drops are lower than the experimental pressure drops. The shearing forces between the liquid and the gaseous layers were not included in the calculations. Martinelli (ref. 6) correlated isothermal pressure-drop data for a gaseous core and a liquid annulus by including shearing forces between the liquid and the gaseous phases. If this procedure applies to the present model (liquid core and gaseous annulus), the pressure drop caused by these shearing forces should be included, and the absolute value of the calculated pressure would be reduced. This should give better agreement between calculated and experimental pressures along the tube length.

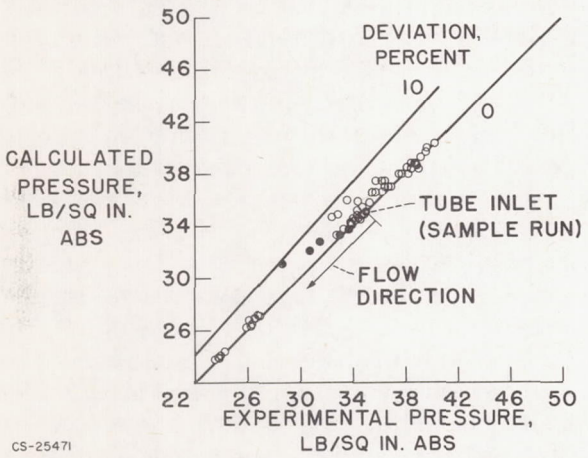

FIGURE 44–14.—Transient two-phase hydrogen-flow pressure drop.

Gaseous-hydrogen flow and heat transfer.—During the initial phases of startup, gaseous hydrogen is present in the reflector at subcritical pressure, as shown in figure 44–5. Steady-state operation in the gaseous region at supercritical pressure is also shown in this figure. In fact, even if two-phase hydrogen enters the reflector, somewhere along the reflector passage the hydrogen enters the gaseous phase. The following discussion reviews the current status of knowledge for gaseous flow and heat transfer and describes current Lewis tests involving gaseous-hydrogen flow and heat transfer.

Status of knowledge: Reference 11 presents a list of correlation equations, with pertinent limits, presented by various investigators for gaseous-phase hydrogen (and, in certain cases, helium). These equations were taken from references 16, 18, 19, and 20. Most of them are for an average heat-transfer coefficient for the entire test section and of the general form

$$Nu = C(Re)^{a}_{ref}(Pr)^{b}_{ref}\left(\frac{l}{D}\right)^{c}$$

The coefficients and exponents vary from investigation to investigation; some of the proposed correlations contain a wall- to bulk-temperature ratio raised to different powers. A comparison of data from references 16, 18, 19, and 20 is presented in reference 11; the data were extrapolated over a range of values of T_w/T_b from less than 10 up to 100. The data of reference 18, extrapolated, show a different trend with T_w/T_b from those of references 16, 19, and 20; this difference might result from the fact that the original data of reference 18 covered temperature ratios from 1.5 to 2.8 and the extrapolation to a value of 100 may not be ac-

curate. The other three sets of data indicate fairly good agreement in their trends with T_w/T_b. The respective curves are close, although not perfectly correlated.

Reference 11 also proposes that local coefficients may be correlated by use of the equation

$$Nu_f=0.021Re_f^{0.8}Pr_f^{0.4}$$

This equation was applied to hydrogen data and worked well for the test section except for regions near the entrance and the exit. For entrance and exit regions, some alterations are required.

Local heat fluxes are plotted against T_w-T_b in reference 21 for hydrogen flowing through a 0.194-inch-diameter heated tube for hydrogen at pressures from 680 to 1344 pounds per square inch absolute and at values of T_w/T_b from 1.36 to 16.5. At a value of T_w-T_b of about 500° R, an abrupt change in the slope of the line through the data occurred; two distinct correlation equations were therefore obtained, one for $T_w-T_b<500°$ R and one for $T_w-T_b>500°$ R, with property values based on bulk temperature. These results appear in the form

$$Nu=CRe_b^{0.8}Pr_b^{0.4}\left(\frac{T_w}{T_b}\right)^d$$

where C and d differ for the two regions. The explanation for the existence of these two correlations for this set of data is given in reference 21 and is repeated herein. At low heat fluxes, the unit heat flux is proportional to a fractional power of the temperature driving force ($Q/A<1$ Btu/(sec)(sq. in) and $T_w-T_b<500°$ R). At higher heat fluxes, the unit heat flux is proportional to the first power of the temperature driving force. A relation seems to exist between the first correlation (for low heat fluxes) and a transition region, according to reference 21.

In reference 18, hydrogen data is compared with the helium data of reference 20 by means of the correlation

$$Nu=0.027Re^{0.8}Pr^{0.4}$$

where all properties are based on wall temperature. These sets of data were for comparable conditions: For H_2, $l/D=42.6$ and 67 and $T_w/T_b=1.5$ to 2.8; for He, $l/D=60$ and $T_w/T_b=1.8$ to 3.9. This correlation was satisfactory, since the same data did not correlate when plotted in reference 11 against T_w/T_b, but correlated well in reference 18. The statement made previously relative to the extrapolation of the data of reference 18 is confirmed.

The preceding discussion indicates that at least two correlations for local gaseous-hydrogen heat-transfer data have been successful. Both are of the form

$$Nu=CRe^{0.8}Pr^{0.4}$$

where in one case $C=0.021$ and fluid properties are based on film temperatures and in the other case $C=0.027$ and fluid properties are based on wall temperatures.

The pressure drop in the gaseous region must include both momentum and frictional losses. The general pipe equation useful for this determination is available in almost any advanced fluid-mechanics textbook.

Experimental investigations at subcritical pressure: It was previously stated that even when two-phase hydrogen enters the test section, the gaseous phase will be attained at some point farther up the tube. Hence, data for the gaseous region were obtained from the same tests that supplied the two-phase data. Consequently, the test program and the ranges in variables are the same as those discussed for the two-phase state.

Description of data-reduction methods: The method used for obtaining the heat input to the hydrogen for the gaseous data is the same as that used for the two-phase-flow data for both the transient and the steady-state experiments. The temperature and the other properties of the hydrogen required for correlations, however, had to be obtained from accumulated total enthalpy gain of the hydrogen from the tube entrance (which was supplied with liquid hydrogen), local measured pressures, and available hydrogen-property tabulations. Data reduction was accomplished by means of a digital-computer code including a subroutine containing the hydrogen properties for the transient experiments and by hand calculations for the heated-tube steady-state experiments. Values of density, Reynolds number, Prandtl num-

ber, and experimental Nusselt number were all calculated three times on the basis of bulk, film, and wall temperatures of the hydrogen. With this information, the data could be plotted according to the various heat-transfer correlations available. Friction, momentum, and total-pressure drops were also computed by the digital code.

Results: Local heat-transfer data for gaseous-hydrogen points above 90° R were plotted as $Nu_{exp}/Pr^{0.4}$ against Re for bulk, film, and wall conditions, but the results indicated considerable scatter. The next attempt to correlate the data used equations from the literature (summarized in ref. 11), which were successful for the case of supercritical pressures and temperatures greater than 90° R, which is region 5 in figure 44–5. Most of these equations include wall- to bulk-temperature ratios and an l/D term and use overall bulk or average temperature for fluid-property evaluation. Defining the l in the equation posed a problem since liquid hydrogen entered the test section. The following model was assumed: As hydrogen flows up the tube, the liquid is converted to gas in the two-phase region. When all liquid is evaporated and warmed to 90° R, the gas region is assumed to begin and l is the distance from this point to the end of the tube. Uniform velocity distribution is also assumed at this point.

With these assumptions, the best correlation to date, shown in figure 44–15, uses the equation of reference 16. Data for both the steady-state (heated-tube) and transient runs are shown, as well as the line representing the equation of reference 16. The data points show

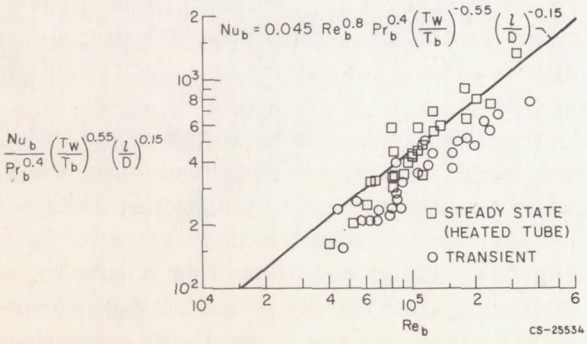

FIGURE 44–15.—Heat-transfer correlation for gaseous hydrogen. Bulk gas temperatures, >90° R; pressure, 1 to 3 atmospheres.

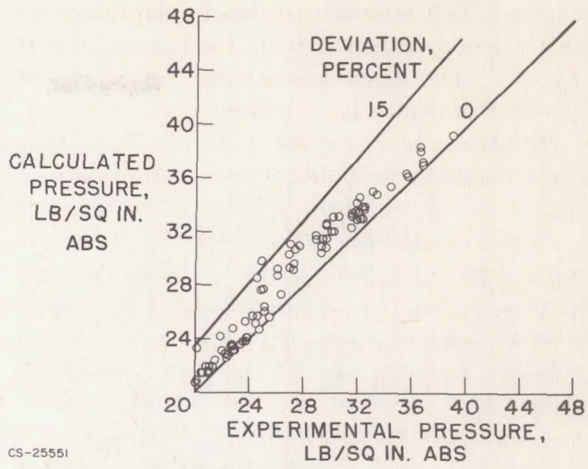

FIGURE 44–16.—Transient gaseous-hydrogen-flow pressure drop.

that the heated-tube results are again somewhat higher than the transient points, such as was the case in the two-phase-flow heat-transfer data.

Calculated pressure is plotted against experimental pressure for the gaseous region in figure 44–16. Calculated pressures are shown to be larger than experimental pressures. Investigation revealed that the experimental friction factors were larger than those calculated in the usual way by use of the von Kármán equation. This difference in friction factor apparently accounts for the discrepancy in the pressure data. A more careful study of friction factors may be in order, especially since low friction pressure losses exist with hydrogen and two-phase flow precedes the gaseous region in the tube.

Oscillatory Flow

It has previously been stated that during reactor startup two-phase flow occurs somewhere in the rocket flow system. For safe operation of the rocket, stable flow conditions must prevail. Consequently, an investigation of possible two-phase-flow oscillations in the system is necessary to find methods for determining whether stable or unstable flows will exist in a system. From such knowledge, stable systems can be designed.

Pressure oscillations are generated by the boiling process during two-phase flow. Particles of liquid vaporize and cause pressure surges; the vapor is condensed when cooled by

surrounding liquid and this condensation causes pressure decreases. These processes occur at random rates, and a spectrum of frequencies of pressure perturbations results.

In recent years, many attempts have been made to predict circumstances leading to parallel channel instabilities. In 1938, unstable operation was reported whenever the steady-state pressure-drop–flow curve exhibited a negative slope (ref. 22). More recently, pronounced flow oscillations were observed in a series of parallel channels in which the steady-state pressure-drop–flow curve exhibited a positive slope (ref. 23). In reference 23, the criteria for flow instabilities were attained in terms of initial fluid conditions, channel geometry, and heat-flux distribution. Other investigators have also been active in this field.

Flow oscillations have recently been observed at the Lewis Research Center in some of the two-phase hydrogen heat-transfer tests conducted for single tubes. Some gross effects observed in these tests will be presented later. Existing methods for determining characteristics of the oscillations, such as amplitude, for example, are available and will be used to compare theoretical results with the experimental data being obtained. A brief résumé of some of these approaches is given subsequently.

Status of knowledge.—According to unpublished information from Los Alamos Scientific Laboratory, a simple spring-mass model that included a dashpot and a forcing function resulted in the successful simulation of the amplitudes of pressure oscillations obtained during an experimental run. The damping coefficient and hence the amplitude of the pressure oscillations varied with the cube of the passage diameter. The use, of course, of a spring model for determining oscillations depends upon the degree of nonlinearity of the system.

Flow oscillations were analyzed in reference 23 by considering the four basic transient equations for two-phase flow in a heated channel: energy, continuity, state, and momentum. Perturbations were applied to the variables and the resulting equations were integrated in the flow direction. The channel enthalpy profile was assumed to be of the same shape (but not necessarily the same level) as if steady-state operation existed. A second-order transfer function relating heat flux and inlet flow perturbations was obtained; from this transfer function, the criteria of flow instabilities in terms of initial fluid conditions, channel geometry, and heat flux distribution were determined. Comparison with data showed that this analysis could predict coolant conditions at the inception of flow oscillations and the frequency of the oscillations.

Another type of analysis was used in reference 24 to study a two-phase natural-circulation system. An exact solution of equations expressing mass and energy conservation for a channel subjected to a cyclic variation was obtained by use of a Lagrangian coordinate model. Channel pressure drop was predicted by numerical integration; from a Nyquist diagram, channel stability was investigated. No slip flow or uniform-heat-flux profile is required for this method.

Another method of analysis was presented in reference 25. Differential equations for the transient conservation laws in the fluid and metal and heat-transfer conditions at the fluid metal interface were used to obtain difference equations (without perturbations). These equations permitted determination of fluid conditions and metal temperatures at a discrete number of points in the channel and a discrete number of times during a transient. The equations were solved on a digital computer to determine fluid conditions in response to arbitrary time variations in heat-generation rate, plenum to plenum pressure drop, and inlet enthalpy. Channel oscillatory tendencies could then be predicted by determining flow as a function of time after a small step increase in heat generation. Advantages of this approach over those of references 23 and 24 are also given in reference 25.

A number of responses to step inputs were calculated at different heat fluxes near those where oscillations occurred in the heated channel experiments with boiling water. At heat fluxes slightly less than the flux required for oscillating flow, the calculated response to the step change (1 percent of steady-state heat flux) showed a slightly overdamped response. When the heat flux was equal to the experi-

mental condition, the response was slightly underdamped, but the oscillations converged rapidly to the new steady-state operating condition. When a larger heat flux was used in the calculations (e.g., a flux of 1.15 times the experimental flux), the system oscillated with continually increasing amplitude. The oscillating mass velocity (flow) curves had the appearance of sine waves until large amplitudes were reached, when the shape of the curves was distorted because of the increasing significance of nonlinear effects. The equations, however, in no case predict a sustained oscillation of constant amplitude, which is often encountered in two-phase-flow experiments (refs. 23 and 25).

A certain amount of flow or pressure variation with time or "noise" is always present in two-phase-flow systems. If the damping ratio is small (low friction), the existing noise will be greatly amplified when the frequency of the "noise" approaches the natural frequency of the system. This phenomenon is probably occurring in many of the experimental observations.

The need for more theoretical work is required in the study of these flow oscillations in order to predict when they will occur and their magnitude in complex systems. Experimental data with hydrogen should then be obtained and analyzed to confirm the calculations.

Flow stability during experiments.—Flow oscillations have been recorded during the single-tube experiments. A typical pressure trace of one type of oscillation measured at one of the static-pressure locations along the test section during a transient run is presented in figure 44–17. At the beginning of the run (time, 0), high-amplitude oscillations existed; these oscillations persisted during the run until about 16.3 seconds later (fig. 44–17), at which point the amplitude was quickly damped; evidence of the frequency, however, still persisted. The resonant frequencies, in general, decreased during the transient runs. The flow rate at the test-section exit for the run shown in figure 44–17 oscillated ±25 percent about the mean value at the beginning of the transient, and the inlet liquid hydrogen had three degrees of subcooling.

Some of the instabilities were traced to oscillation sources in the flow system and means

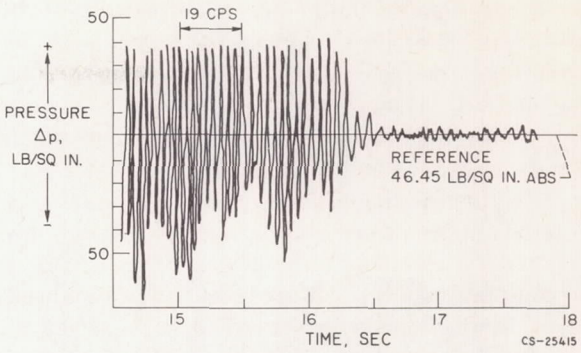

FIGURE 44–17.—Pressure-data trace of oscillating-flow transient run.

were found to eliminate them. An initial criterion based on the frequency of the flow oscillations has been established for conditions that will produce oscillations greater or less than a selected value of frequency. The criterion for grouping the runs according to frequency will be discussed first, and then a model representative of the flow oscillation sources in the system will be described and discussed.

The trend that developed during the heated-tube experiments is illustrated in figure 44–18. The dashed line separates the data into regions having higher (unstable) or lower (stable) frequencies than 2 cycles per second. If the liquid entering the test section is subcooled less than 2° to 2½° R and if there is sufficient heat input to attain an outlet- to inlet-velocity ratio in excess of 350, low-frequency runs will be attained. Conversely, when the entering fluid is more subcooled and the heat rate is insufficient to attain the high velocity ratios, the flow rate oscillates at higher frequencies.

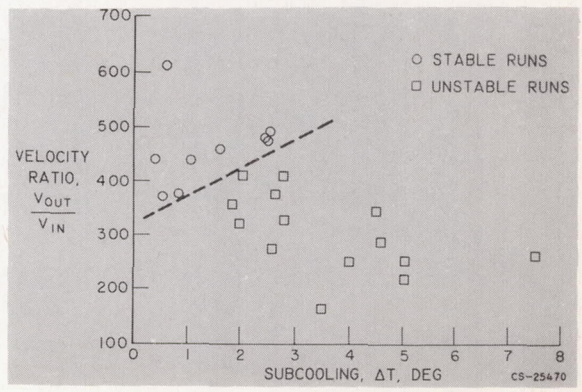

FIGURE 44–18.—Variation of subcooling with velocity ratio.

It was operationally possible during heated-tube experiments to decrease the frequency of the flow oscillations either by decreasing the amount of subcooling in the inlet plenum or by increasing the test-section heat input, which increased the velocity ratio.

This information should be considered as a status report on experiments and analysis now being performed and is presented primarily to cultivate interest in a recurring and unexplained phenomenon. The terms velocity ratio and subcooling will probably be replaced by more pertinent parameters, and amplitude will probably be used as a criterion instead of frequency.

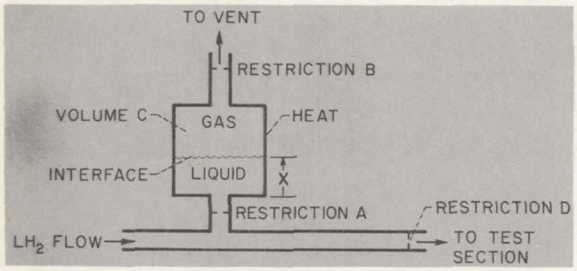

FIGURE 44–19.—Model of oscillator in system.

Sources of oscillation in the system can be described by the model shown in figure 44–19. As the pressure rises in the liquid-hydrogen flow line, liquid flows through restriction A into volume C. The liquid is vaporized in the volume because of heat addition. The phase change in the volume results in an increase in pressure; first liquid and then gas are forced back into the liquid flow line through the restriction A. When the pressure in the volume approaches the line pressure, liquid may again enter volume C. Initially, the remaining gas in the volume will be cooled, with a further decrease in pressure, which will allow more liquid to enter the volume. When the evaporation rate and the resulting increase in pressure balance the line pressure, the flow through the restriction reverses and the cycle continues.

This phenomenon is cyclical (i.e., the distance X to the interface is periodic with time) and affects the mass-flow rate in the main flow line by alternately bleeding off liquid to volume C and then returning liquid and then gas to the flow line. The flow variations are then reflected as system pressure oscillations if there is a restriction downstream of the flow oscillator, such as restriction D.

A mathematical model that assumes that the evaporation rate is proportional to the liquid column height X has been shown to be unstable.

Two points in the Lewis flow system were similar to the model. One was a T in the trans-

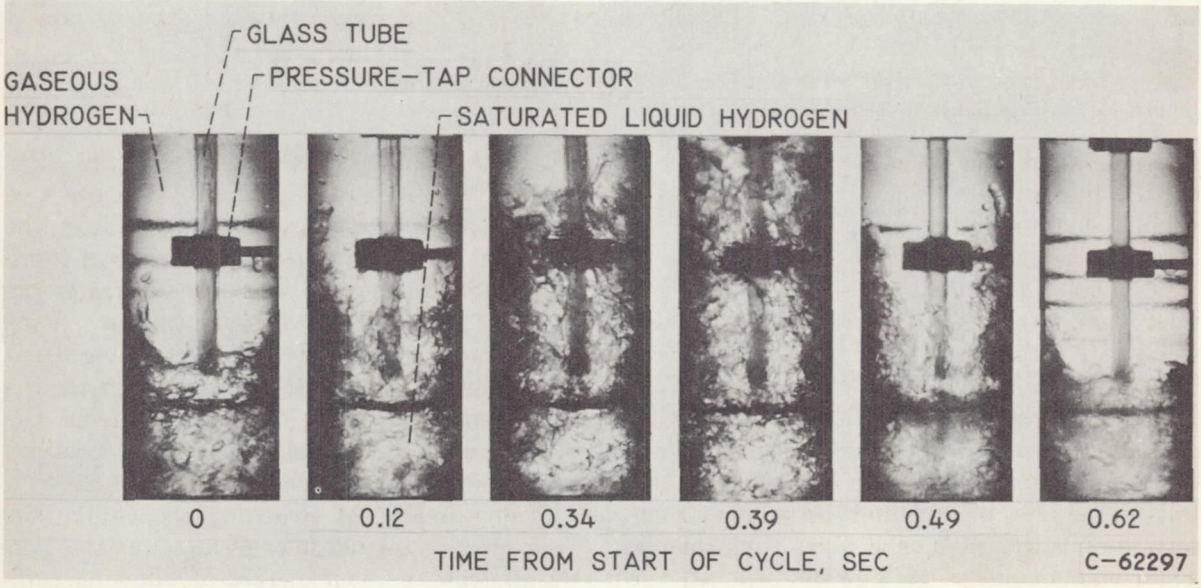

(a) Inlet-plenum oscillation.

FIGURE 44–20.—Enlargement of frames from high-speed motion pictures of oscillating hydrogen flow.

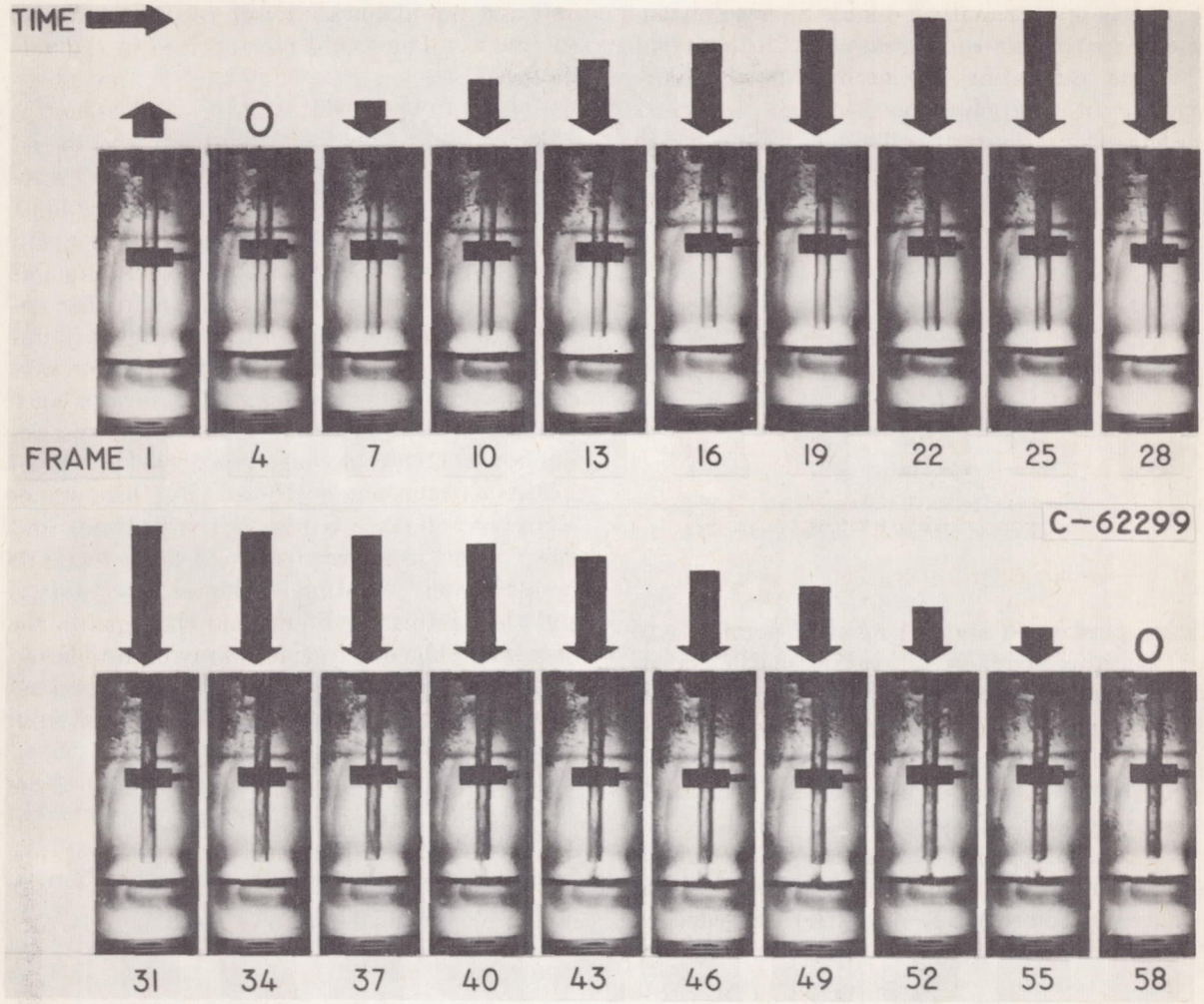

(b) Test-section oscillation. Arrows indicate relative flow velocity.

FIGURE 44–20 (Concluded).—Enlargement of frames from high-speed motion pictures of oscillating hydrogen flow.

fer line, where the hydrogen was diverted to the precooling annulus, and the other was the volume surrounding the glass tube at the entrance to the test section.

High-speed motion pictures were taken of the inlet plenum that supplied hydrogen to the test section. At least two forms of oscillation were identified. Enlargements of photographs taken during two runs showing the two oscillating modes are presented in figure 44–20. In figure 44–20(a), the saturated liquid level rises and falls in the inlet plenum and the volume of gas surrounding the glass tube varys with time in a periodic manner. In figure 44–20(b), the inlet plenum is full of subcooled liquid hydrogen and the flow in the glass tube varys in such a periodic manner (19 cps) that the flow actually reverses during part of the cycle as shown. Static-pressure measurements along the tube for this type of oscillation showed high-amplitude variations such as illustrated in figure 44–17. Also observed in the photographs were a few small bubbles that originated from a small amount of nucleate boiling in the upper part of the chamber and from the "breathing" of the instrumentation pressure lines connected to the chamber (fig. 44–20(b)).

The technique of removing the oscillations from the test-section inlet plenum and the T in the system consisted merely of allowing sufficient flow through restriction B (fig. 44–19) that no meniscus could form or that if it did

form the gas generated would be vented out at a rate that held the meniscus fixed with time.

When this model has been thoroughly analyzed mathematically and verified by experimental data, the approach can be applied to other parts of the flow system. During the experiments, only the test section, not the rest of the flow system, has been instrumented. In particular, a question arises as to whether the pressure-tap lines in the lower plenum and along the test section are acting as oscillators and generating the flow oscillations.

Maldistribution of Flow

One of the most important problems encountered in reactor design is the prevention of maldistribution of flow. Since both the reactor reflector and the reactor core contain numerous different-size parallel coolant passages, and since the power generation throughout a typical reactor is nonuniform, the maldistribution problem becomes even more severe. The different-size passages (with different surface areas) receive various amounts of heat from different volume elements, and hence the flow rates in the passages must be different in order to maintain the same outlet pressure for each passage. Since most methods of reactor control tend to change the pattern of heat generation, an extra difficulty is encountered. According to reference 26, the designer must therefore be prepared to sacrifice potentially achievable coolant-outlet temperatures by allowing for substantial differences between the maximum (design) and the average coolant-outlet temperature or to incorporate such devices as orifices to counteract flow maldistribution and thus increase the average coolant-outlet temperature at the expense of increased pressure drop. The following sections will give some indication of the Lewis effort in this vital area of flow maldistribution.

Description of typical reflector.—A typical reflector might consist of several annular segments of a selected reflector material with coolant passages between the sectors and between the outermost sector and the pressure shell. Numerous coolant holes would also probably be required in the annular regions. In many reactors, the control devices are located in the reflector. Additional holes and annular flow passages in the control devices will be required for such cases since the control devices would also have to be cooled. A typical reflector will thus contain numerous coolant passages of different diameters and annuli of different sizes; adequate flow distribution among these many passages must be maintained.

Power distribution in the reflector.—According to reference 27, about 5 percent of the total heat release in the reactor takes place in the reflector and the pressure shell. The sources of this reflector heat are neutron leakage from the core and gamma radiation. These heat sources decrease in importance as the distance penetrated in the reflector from the core increases; that is, the greater the distance from the core within the reflector, the smaller is the neutron and gamma attenuation. In a typical reflector consisting of two annular rings and a pressure shell, it was estimated that about 3 percent of the total reactor heat release occurred in the inner reflector annulus, about 2 percent in the outer reflector annulus, and about 1 percent in the pressure shell. These are average values, and because of the change in energy attenuation through these pieces, passages in the individual pieces do not all receive the same amount of heat. In fact, even for two similar passages, the one receiving the greater heat input will undergo a greater change in momentum pressure drop, and hence the two passages will have different temperatures and flow rates, which leads to the flow-maldistribution problem.

Theoretical background.—When an appreciable change in density occurs in the coolant as it flows through a reactor, the distribution of fluid among parallel passages may be affected by a number of things. An analytical study of the variations in outlet fluid temperatures and maximum tube-wall temperatures resulting from nonuniformity of heat flux, mass-flow rate, tube shape, or tube dimensions among the members of a group of flow passages is presented in reference 26. All these factors are interrelated and dependent upon the physical properties of the coolant. Analytical expressions for partial derivatives that measure flow variations are determined for a number of situations and are applied to the study of water

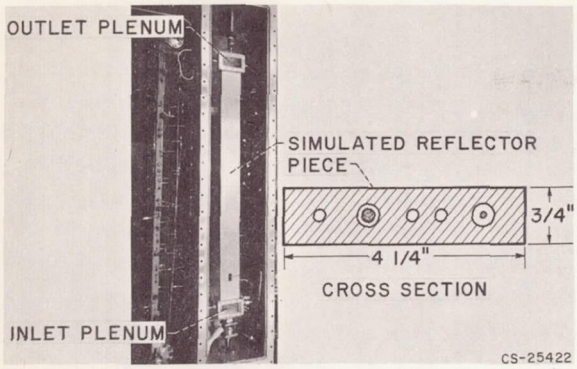

FIGURE 44–21.—Simulated reflector piece for maldistribution studies.

flowing through a system at supercritical pressure. In the example, if one tube should receive 1 percent more heat than its neighbors, the fluid outlet temperature would be 67° F hotter, the wall temperature would be increased 80° F, and the flow rate reduced 3.75 percent.

Experimental apparatus.—In order to study reflector heat transfer and flow maldistribution during reactor startup, a simulated aluminum reflector segment was used. A photograph of the test section installed in the test facility and a sketch of the cross section, including the hydrogen passages (circular and annular), are shown in figure 44–21.

Contemplated instrumentation for a typical passage will include that for inlet and outlet plenum temperatures and pressures, static pressures along the tube, and tube-exit pressure. From the exit total and static pressures, the relative flow rates can be determined. Metal temperatures at several planar locations will also be obtained. Cameras will be provided to photograph the inlet and outlet plenums.

Calculation of reflector design parameters.—One of the objectives of the test program is to compare experimental parameters, such as individual passage flow rates, bulk temperatures, heat-transfer coefficients, pressure drops, and metal temperatures with purely analytical calculated values. The design of workable reactors for nuclear rockets requires the ability to predict these parameters accurately.

The largest contributor to the difficulty of making these predictions is the interdependence of metal temperatures and coolant temperatures. As previously mentioned, for flow systems with multipassages, variations in heat flux into the fluid produce maldistribution of flow in the passages. The calculation of this heat flux under both transient and steady-state conditions is dependent upon the metal temperatures, which in turn are dependent upon the boundary conditions (fluid temperature and heat-transfer coefficient) existing at a given axial location.

For one passage and the material surrounding it, iteration techniques are thus required to obtain material and coolant temperatures that are compatible, in terms of heat flux, out of the material and into the coolant. If this situation is compounded with several passages that must be handled simultaneously, a very complex mathematical procedure is definitely required.

The procedure that would be required for a part of a possible reflector design will be described so that this complexity may be illustrated more clearly. The reflector segment being considered, which for cooling and fabrication purposes could conceivably be divided into an inner and an outer reflector section surrounded by the pressure vessel, is represented in figure 44–22. A cooled control rod is considered as being located in the outer reflector section.

If the control rods are assumed to be evenly spaced, symmetry can then be used to reduce the complication of calculations. Figure 44–23 shows this symmetrical section and indicates how this section can be further broken down into individual symmetrical parts. These parts are still related through the same boundary conditions at adjoining coolant passages. For temperature solutions, each symmetrical part can be divided into nodal points, and calcula-

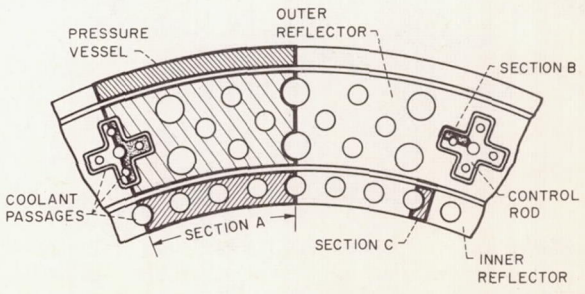

FIGURE 44–22.—Typical reflector segment showing symmetric arrangement of individual parts.

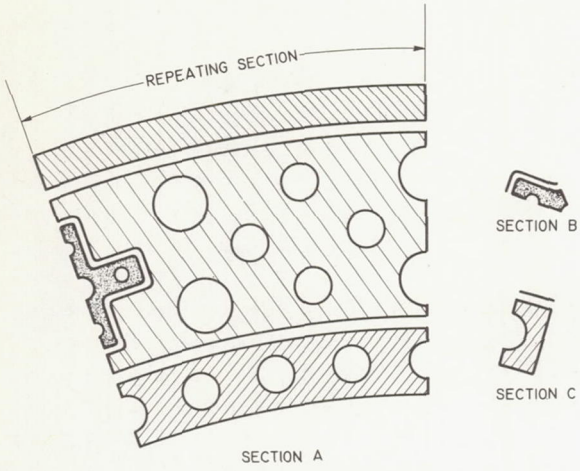

FIGURE 44–23.—Individual symmetric parts within symmetric system.

tions can be made that utilize the appropriate equation listed in figure 44–24.

High - speed - electronic - computer programs can be and have been set up to solve these heat-transfer equations for a three-dimensional body. As discussed in the preceding paragraphs, however, necessary input to this type of program is the boundary conditions (coolant temperature and heat-transfer coefficient). Other programs can be written to calculate these values, but part of the required input for these programs is heat flux into the coolant. Iteration between these two types of programs could result in final numbers. Ideally, both programs would be combined into one large overall program. Either approach results in the previously mentioned complex mathematical procedure. Even with the use of high-speed computers, the time to perform these calculations becomes rather lengthy and correspondingly expensive. This calculation procedure, however, will be used until an improved method becomes available.

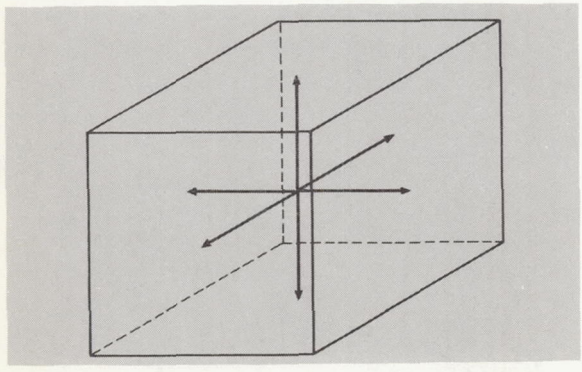

FIGURE 44–24.—Typical nodal point. Applicable equations for calculating metal temperatures are as follows: transient, $\nabla^2 T = \frac{1}{\alpha}\frac{dT}{d\tau}$; steady state, $\nabla^2 T = 0$.

Experimental results from reflector segments.—A few preliminary experimental transient runs with the simulated reflector segment shown in figure 44–21 have been made with liquid nitrogen and liquid hydrogen as the fluid. These experiments demonstrate a problem in multiple-parallel-passage geometries that was not mentioned in the preceding paragraphs.

In an actual system, the flow passes through the nozzle cooling passages before it enters the reflector, and often there are abrupt changes in flow direction at such interface locations as the connection between the nozzle and the reflector. During the startup transient, gas and then liquid enter the reflector (see fig. 44–5) from the nozzle coolant-passage discharge.

The experiments were run with the fluid, first gas and then liquid, entering the inlet plenum at a position 90° to the flow direction in the test section; a structure that approximately simulated a mechanical support structure found in an actual system was included.

Enlargements of high-speed motion pictures showing views of the test-section inlet are shown in figure 44–25. The photographs show liquid nitrogen entering the inlet plenum, impinging on the diagonal structural member, flowing around the end of it, and then into the upper half of the chamber in which the nitrogen entered the five cooling passages. Near the beginning of the transient, gross maldistribution occurred because of the presence of the structural member, which threw most of the liquid into test-section passages at the right side of the photographs. Much of this maldistribution could be avoided by more careful engineering design; the phenomenon, however, indicates another fundamental problem. Any passage that happens to have more liquid flowing through it initially than through any other passage during the start transient (when the reflector material is cooling down) will tend to continue to have more liquid flowing through it because that part of the reflector system will be colder than the

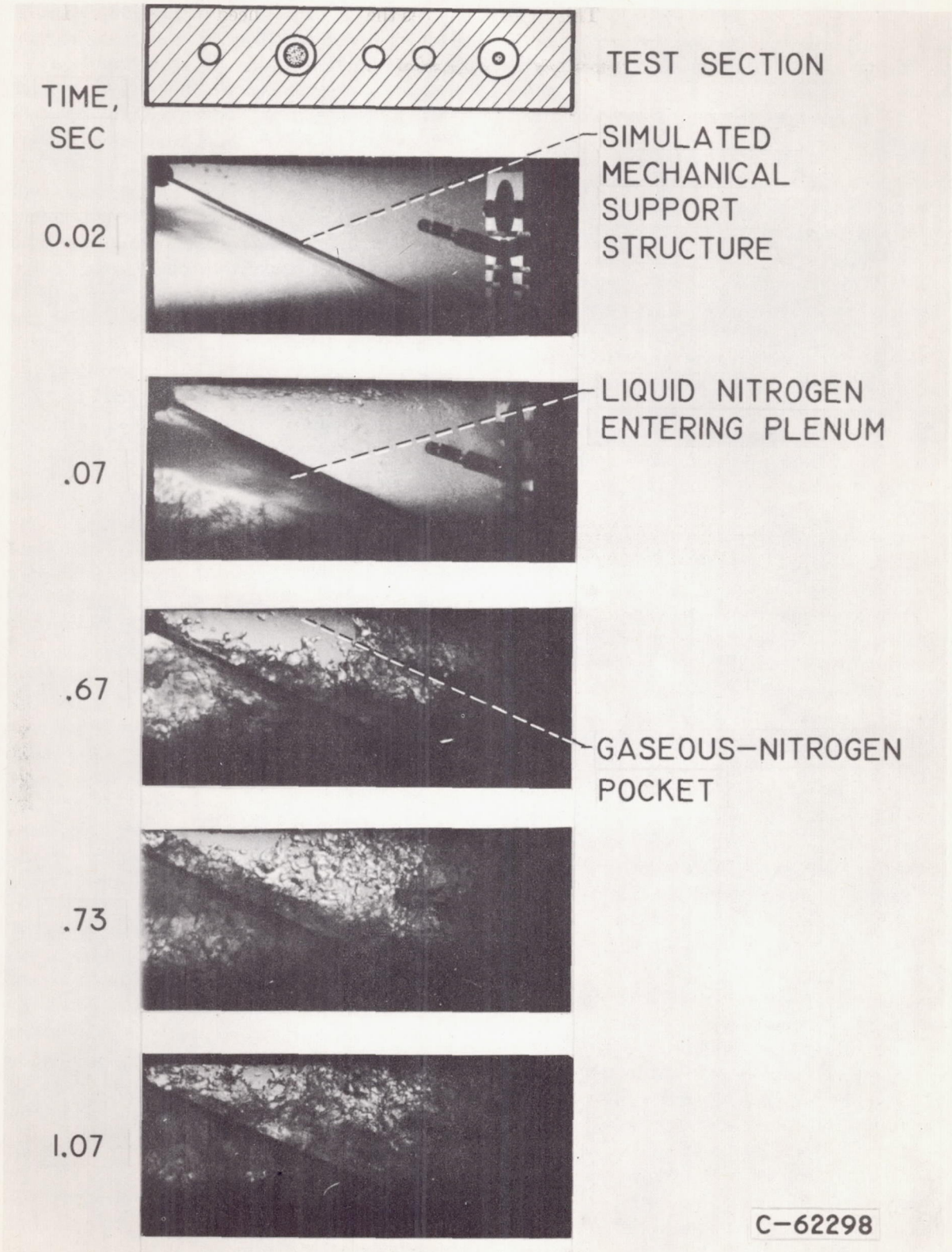

FIGURE 44–25.—Enlargements of high-speed motion pictures of inlet plenum of simulated reflector piece showing flow phenomena during startup transient.

other parts. This factor complicates the calculations of reflector geometries and requires knowledge of the initial flow distribution in the system.

Force or Gravity Effects

The use of the nuclear rocket is proposed for deep-space probes and interplanetary travel. For such missions, a rocket capable of several restarts is necessary. Since the initial rocket startup will probably take place in an Earth orbit and subsequent starts will occur in space, knowing what effects a low- or zero-gravity condition will have on the rocket flow system, especially during startup, is essential. This, of course, involves a knowledge of boiling heat transfer under low-gravity conditions.

Numerous investigations into low-gravity effects have been and are being made. According to reference 3, nucleation and the rate of bubble growth are not affected by a reduction in the gravitational force field; the rate of vapor removal, however, depends upon the nature of the force field. In forced convection flow, the velocity gradients are highest near the solid surface. Bubbles in this region are subjected to lift forces and tend to travel toward the tube center. The vapor, concentrated in the high-velocity region, moves at a faster rate than it would under a uniform distribution. The result is that the mean velocity of the vapor is larger than that of the liquid. The ratio of these mean velocities is the slip velocity u_g/u_l. Reference 3 further states that in the bubble-flow region, the slip velocity exceeds the value of 1, which is the slug-flow-region value for this factor in a low-gravity field.

Under force fall, a definite decrease in heat flux occurs in all boiling regions except perhaps the nucleate boiling region (ref. 28). This conclusion was based on short-time force-fall tests of boiling heat transfer to liquid nitrogen at atmospheric pressure from a 1-inch-diameter copper sphere. One possible explanation for the fairly large heat fluxes obtained in these short-time tests has been offered: The momentum of the liquid set up by the action of vapor departing from the sphere during 1–g conditions may continue to sweep vapor from the vicinity of the sphere under the zero-gravity conditions. This situation would be most pronounced in film boiling. In addition, this well-defined maximum heat flux in saturated liquid nitrogen under zero-gravity conditions may be linked to the dynamics of bubble formation and growth; that is, the hydrodynamic forces of bubble growth far overpower the buoyant forces.

Many other zero-gravity investigations of nucleate and pool boiling, with various fluids, have been made. Many have been limited to the study of the flow phenomena of fluids contained within a sphere or Dewar. The problem of concern in the nuclear rocket, however, deals with a flowing system. One such investigation for a water system was reported in reference 29. A forced-flow water heat-transfer apparatus using a resistance-heated tube was flown in an airplane for a 15-second near-zero-gravity test. The test was conducted to determine whether a zero-gravity environment influenced the nature of two-phase-flow patterns; such changes would be observed in the heat-transfer results. An instability, initiated by a momentary interruption of flow, forced the transition from a highly subcooled bubbly flow to a slug-type phenomenon that resulted in a 16-percent increase in local heat-transfer coefficients.

Not only must the effects of low gravity on flow and heat transfer be known, but the effects of high-gravity fields are also of interest, since the nuclear rocket will pass through such environments in its proposed missions. Not many investigations in this area have been made. Pool boiling of distilled water at approximately atmospheric conditions up to 21 g's has been tested (ref. 30). The influence of acceleration was greatest in heat fluxes up to 50,000 Btu per hour, where a transition in the convective mechanism apparently took place. The acceleration decreases the value of $T_w - T_{sat}$ required for a given flux. Above this heat flux, a reversal of the effect of acceleration on $T_w - T_{sat}$ was observed. Data of reference 31 agree with those of reference 30.

As noted previously, the nuclear-rocket low-gravity problem deals with a flowing system. Reference was made to one such investigation using water. An experiment is currently being planned at Lewis that will involve a hydrogen

flowing system. The multiple-passage reflector simulation shown in figure 44–21 is being prepared for insertion into a so-called drop package. This package will be dropped from a drop tower, and a force fall of about 2 seconds will be attained. Recorded data and motion pictures taken during this test will be compared with similar data obtained for the same test section in a 1–g experiment.

One phenomenon that might be expected is that the initial flow distribution into a multiple-passage test section might be different in a zero-gravity environment than in other gravity fields. Maldistribution of flow in the passages as previously discussed may therefore be different.

NOZZLE

The design of a regeneratively cooled rocket nozzle is based on calculation of a balance between the heat flux from the hot gas to the nozzle wall and from the nozzle wall to the coolant. Such calculations require accurate estimates of heat-transfer coefficients on both the hot gas and the coolant sides of the nozzle. In addition, accurate estimates of coolant pressure drop are also necessary. An excellent review of the nozzle-design problem and the shortcomings of current nozzle-design methods is given in reference 12.

A nozzle design is usually determined for full-power operating conditions. Startup times for nuclear rockets, however, are much longer than those for chemical rockets, and the serious problem of possible choking in the cooling passages at the nozzle throat during startup must not be overlooked. The tapered cooling passages have minimum cross-sectional area at the throat. A nozzle intended for use on a nuclear rocket should therefore be designed for full-power operating conditions and then for possible choking at startup. A redesign may then be required.

Current design methods are dependent upon the hot-gas-side heat flux, and to date adequate methods for estimating this flux are not available. Two methods are currently being used, but each has discrepancies. The first uses a turbulent-flow heat-transfer correlation that assumes a constant coefficient for the entire nozzle and uses the local diameter; this method is an adaptation of the correlation originally determined for a constant-diameter pipe in which there are no appreciable axial pressure gradients. The determination of the Reynolds number for use in the correlation equation, moreover, involves a term $\rho_s V_s$ that may be calculated in two ways, a one-dimensional or a three-dimensional determination of $\rho_s V_s$ at the wall. Reference 12 explains discrepancies encountered in these calculations and how they differ for conical or bell-shaped nozzles. The

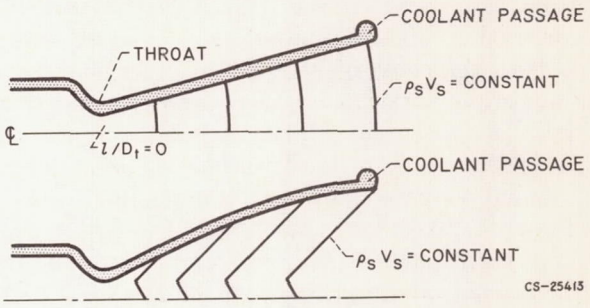

FIGURE 44–26.—Surfaces of constant $\rho_s V_s$ for typical conical and bell nozzles.

lines of constant $\rho_s V_s$ for typical conical and bell-shaped nozzles are shown in figure 44–26, taken from reference 12. No essential difference exists between a one-dimensional calculation (a point on the centerline) and a three-dimensional calculation (a point at the wall) for the conical nozzle. On the other hand, for the bell-shaped nozzle, a considerable difference in the one- and the three-dimensional calculated values of $\rho_s V_s$ will exist. The three-dimensional procedure has been recommended for bell-shaped nozzles.

The second approach to gas-side heat-flux calculations involves boundary-layer solutions. For turbulent flow, only approximate boundary-layer solutions exist. Two distinct approaches to this type of solution are also currently employed. The first case assumes that the boundary-layer thickness is zero at the core end of the nozzle; the second case assumes that there is a finite boundary-layer thickness at this point.

A comparison of calculated and experimental values of heat-transfer coefficient for the bell-shaped nozzle is presented in figure 3 of reference 12 and is summarized for several locations along the nozzle as follows:

Location along nozzle, l/D_t	Comparison of calculated with experimental heat-transfer coefficients			
	Turbulent-flow solution		Boundary-layer solution	
	One-dimensional determination	Three-dimensional determination	Case 1	Case 2
−1.9	40 percent low	40 percent low	30 percent low	45 percent low
0	Good	Good	35 percent high	16 percent high
>.5	50 percent low	23 percent low	35 percent high	16 percent high

The degree of accuracy varies with distance from the nozzle throat. The turbulent-flow correlation underestimates experimental data in both the convergent and the divergent sections of the nozzle and agrees with experimental data at the throat. The largest discrepancy (50 percent) is in the divergent section. The boundary-layer solutions underestimate experimental data by as much as 45 percent in the convergent part of the nozzle and overestimate the experimental data by as much as 35 percent in the divergent part of the nozzle. Experimental data are required in order to determine the type of variation that the coefficient in the turbulent-flow correlation should follow.

The preceding discussion illustrates inadequacies in nozzle design heat-transfer relations. For nuclear rockets, in which nozzle-throat heat fluxes may be twice those for chemical rockets, and in which nozzle wall temperatures may be limited to 1600° or 1800° F and temperature differences greater than 2000° F are required between the nozzle wall and the hot gas, the nozzle cooling and design problem become more severe. Hot-gas-side nozzle heat transfer must be more thoroughly investigated.

Coolant-side heat transfer is similar in both nozzle and reflector, and the latter has been discussed in some detail in a preceding section.

CONCLUDING REMARKS

Core, reflector, and nozzle heat-transfer and flow problems that require solutions before adequate nuclear rockets can be designed are presented. Core problems, such as maintaining allowable temperatures and calculating thermal stresses, are included. Core flow-stability problems are also discussed. Reflector two-phase- and gaseous-hydrogen heat-transfer and pressure-drop correlations are illustrated with experimental data. Examples of oscillations and maldistributions in the reflector and discussion of gravitational effects on flow and heat transfer are included. Limitations of nozzle-design methods are reviewed.

A careful investigation of the aforementioned problems revealed that adequate knowledge is not yet available for the determination of satisfactory solutions. More intensive research in such areas as oscillatory flow, maldistribution of flow, two-phase flow, nozzle heat transfer, stress-calculation methods, etc. is urgently needed before improved nuclear rockets can be designed.

APPENDIX—SYMBOLS

A	area
a	constant
Bo	boiling number, $(Q/A_s)/(\lambda\dot{w}/A_i)$
b	constant
C	constant
c	constant
c_p	specific heat
D	diameter
d	constant
E	Young's modulus
f	frequency
G	mass-flow rate, $\dot{w}/A_i$
g	gravitational constant
H	enthalpy
h	heat-transfer coefficient
k	thermal conductivity
l	length
$\Delta l'$	distance between end of heater and temperature sense point in unheated section
Nu	Nusselt number, hD_i/k
Pr	Prandtl number
p	pressure
Q	heat-flow rate
Re	Reynolds number
T	temperature
t	time
u	velocity
V_s	nozzle stream velocity
W	weight
$\dot{w}$	flow rate
X	distance to interface
x	quality
α	coefficient of linear expansion
δ	distance between T_{max} and T_w
λ	heat of vaporization
μ	viscosity
ν	Poisson's ratio
ρ	density
ρ_s	nozzle stream density
σ_{th}	thermal stress
χ_{tt}	Martinelli parameter

Subscripts:

av	average
b	bulk
calc	calculated
exp	experimental
f	film
fm	film mean (for two phase)
frict	friction
g	gas
i	inner
in	in
l	liquid
Δl	incremental length
m	metal
max	maximum
melt	melting point
mom	momentum
o	outer
out	out
pg	perfect gas
ref	reference
SP	single phase
s	surface
sat	saturated
T	total
t	nozzle throat
TP	two phase
v	per unit volume
w	wall

Superscript:

$'$	pseudo-two-phase quantities

REFERENCES

1. Sparrow, E. M.: Temperature Distribution in an Internally-Cooled Heat-Generating Solid. Jour. Heat Transfer, ser. C, vol. 82, Nov. 1960, pp. 389–393.
2. Bussard, R. W., and DeLauer, R. D.: Nuclear Rocket Propulsion. McGraw-Hill Book Co., Inc., 1958.
3. Hendricks, R. C., Graham, R. W., Hsu, Y. Y., and Friedman, R.: Experimental Heat Transfer and Pressure Drop of Liquid Hydrogen Flowing through a Heated Tube. NASA TN D–765, 1961.
4. Zuber, Novak, and Fried, Erwin: Two-Phase Flow and Boiling Heat Transfer to Cryogenic Liquids. ARS Jour., vol. 32, no. 9, Sept. 1962, pp. 1332–1341.
5. Collier, J. G.: A Review of Two-Phase Heat Transfer. CE/R–2496, British AERE, 1958.
6. Martinelli, R. C., et al.: Isothermal Pressure Drop for Two-Phase Two-Component Flow in a Horizontal Pipe. Trans. ASME, vol. 66, no. 2, Feb. 1944, pp. 139–151.
7. Dengler, C. E., and Addoms, J. N.: Heat Transfer Mechanism for Vaporization of Water in a Vertical Tube. Heat Transfer Symposium, Louisville (Ky.), vol. 52, no. 18, 1956, p. 95.
8. Kreith, Frank: Principles of Heat Transfer. International Textbook Co., 1961.
9. Timmerhaus, K. D., Drayer, D. E., and Dean, J. W.: An Experimental Investigation of Over-All Heat Transfer Coefficient for Condensing and Boiling Hydrogen Films. Paper presented at Int. Heat Transfer Conf., Boulder (Colo.), Aug. 28–Sept. 1, 1961.

10. GUERRIERI, S. A., and TALTY, R. D.: A Study of Heat Transfer to Organic Liquids in Single-Tube Natural-Circulation Vertical-Tube Boilers. Heat Transfer Symposium, Louisville (Ky.), vol. 52, no. 18, 1956, p. 69.
11. HENDRICKS, R. C., GRAHAM, R. W., HSU, Y. Y., and MEDEIROS, A. A.: Correlation of Hydrogen Heat Transfer in Boiling and Supercritical Pressure States. ARS Jour., vol. 32, no. 2, Feb. 1962, pp. 244–251.
12. BENSER, W. A., and GRAHAM, R. W.: Hydrogen Convection Cooling of Rocket Nozzles. Preprint 62–AV–22, ASME, 1962.
13. SCHROCK, V. E., and GROSSMAN, L. M.: Forced Convection Boiling in Tubes. Nuclear Sci. Eng., vol. 12, 1962, pp. 474–481.
14. GROOTHUIS, H., and HENDAL, W. P.: Heat Transfer in Two-Phase Flow. Chem. Eng. Sci., vol. 2, 1959, p. 212.
15. CORE, T. C., HARKEE, J. F., MISRA, B., and SATO, K.: Heat Transfer Studies. Aerojet-General Corp., Sept. 1959.
16. WOLF, H., and MCCARTHY, J. R.: Heat Transfer to Hydrogen and Helium with Wall to Fluid Temperature Ratios to 11.09. Abs. 100, Presented at AIChE Meeting, (Wash., D.C.), Dec. 4–7, 1960.
17. RODER, HANS M., and GOODWIN, ROBERT D.: Provisional Thermodynamic Functions for Para-Hydrogen. TN 130, NBS, Dec. 1961.
18. MCCARTHY, J. R., and WOLF, H.: Forced Convection Heat Transfer to Gaseous Hydrogen at High Heat Flux and High Pressure in a Smooth Round, Electrically Heated Tube. ARS Jour., vol. 30, Apr. 1960, pp. 423–425.
19. WRIGHT, C. C., and WALTERS, H. H.: Single Tube Heat Transfer Tests, Gaseous and Liquid Hydrogen. TR 59–423, WADC, Aug. 1959.
20. TAYLOR, MAYNARD F., and KIRCHGESSNER, THOMAS, A.: Measurements of Heat Transfer and Friction Coefficients for Helium Flowing in a Tube at Surface Temperatures up to 5900° R. NASA TN D–133, 1959.
21. THOMPSON, W. R., and GEERY, E. L.: Heat Transfer to Cryogenic Hydrogen at Supercritical Pressures. Vol. 7 of Advances in Cryogenic Eng., 1962, pp. 391–400.
22. LEDINEGG, M.: Instability of Flow During Natural and Forced Circulation. Die Warme, vol. 61, 1938, pp. 891–898.
23. QUANDT, E. R.: Analysis and Measurement of Flow Oscillations. Preprint 27, AIChE–ASME, 1960.
24. WALLIS, G. B., and HEASLEY, J. H.: Oscillations in Two-Phase Flow Systems. Trans. ASME, ser. C, Jour. Heat Transfer, vol. 83, 1961, pp. 363–369.
25. MEYER, J. E., and ROSE, R. P.: Application of a Momentum Integral Model to the Study of Parallel Channel Boiling Flow Oscillations. Trans. ASME, ser. C, Jour. Heat Transfer.
26. GRUBER, ALAN R., and HYMAN, SEYMOUR C.: Flow Distribution Among Parallel Heated Channels. AIChE Jour., vol. 2, no. 2, 1956, pp. 199–205.
27. GLASSTONE, SAMUEL: Principles of Nuclear Reactor Engineering. D. Van Nostrand Co., Inc., 1955.
28. MERTE, H., and CLARK, J. A.: Boiling Heat Transfer Data for Liquid Nitrogen at Standard and Near Zero-Gravity. Paper presented at Cryogenic Eng. Conf., Ann Arbor (Mich.), Aug. 1961.
29. PAPELL, S. STEPHEN: An Instability Effect on Two-Phase Heat Transfer for Subcooled Water Flowing under Conditions of Zero Gravity. Paper Presented at Am. Rocket Soc., Inc. Space Power Systems Conf., Santa Monica (Calif.), Sept. 1962.
30. MERTE, HERMAN, Jr., and CLARK, J. A.: Pool Boiling in an Accelerating System. Trans. ASME, ser. C, Jour. Heat Transfer, vol. 83, no. 3, 1961, pp. 233–241.
31. COSTELLO, C. P., and TUTHILL, W. E.: Effects of Acceleration on Nucleate Pool Boiling. Paper Presented at AIChE–IMIQ Meeting, Mexico City, June 1960.

Problems in Dynamics and Control of Nuclear Rockets

By John C. Sanders, Herbert J. Heppler, Jr., and Clint E. Hart

JOHN C. SANDERS *is Technical Consultant for Development in the Advanced Development and Evaluation Division of the NASA Lewis Research Center. Currently concerned with nuclear rocket research, he has specialized in research on aircraft and nuclear powerplants and propulsion systems with particular emphasis on application of controls to these systems. He attended Virginia Polytechnic Institute, receiving B.S. and M.S. degrees in Mechanical Engineering in 1936 and 1937, respectively. He is a member of the American Society of Mechanical Engineers and the Institute of the Aerospace Sciences.*

HERBERT J. HEPPLER, JR., *is Head of the Nuclear Rockets and Control Section of the NASA Lewis Research Center. He is currently working on nuclear rocket engines for NERVA and other advanced concepts, particularly in the field of controls and applications of propulsion devices and systems analysis. Mr. Heppler is a graduate of the University of Detroit where he received a B.S. degree in Electrical Engineering in 1951.*

CLINT E. HART, *Aerospace Scientist in the Nuclear Rocket Dynamics and Controls section at the Lewis Research Center, has performed experimental work on the dynamics and control of turbojet engines and analytical studies on the dynamics and control of chemical and nuclear rocket systems and components. He received his B.S. degree in Electrical Engineering from the University of Michigan in 1948.*

The problems and the behavior of a complete nuclear rocket, and, in particular, problems in control, are considered herein. Topics covered are damage limits, performance, stability dynamics, startup, and control selection. Listing of fields where further research and development would be helpful is presented.

NUCLEAR-ROCKET FLOW SYSTEM

One possible nuclear-rocket flow system is shown in figure 45–1 together with an indication of the control problems. This system is called the hot bleed cycle because the power to drive the pump is derived from hot gas extracted at high pressure from the reactor outlet region.

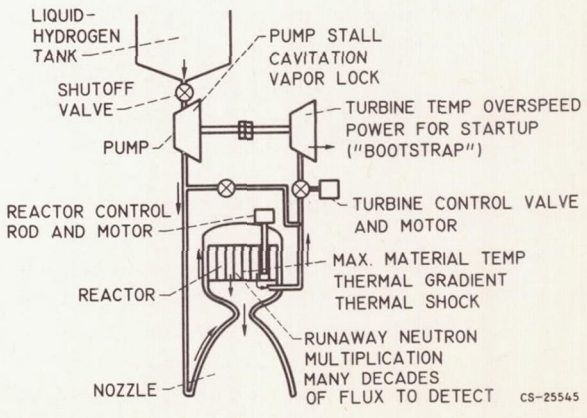

FIGURE 45–1.—Control problem areas and operational limits.

One of the most important operational limits the control must observe is the rate of neutron multiplication; this rate should be slow enough that the control can always move quickly enough to avoid a runaway multiplication. This control function is most stringently demanded in the startup maneuver. Reference 1 presents a good exposition of some of the problems of reactor control for the maneuver of raising the neutron flux from source level to a level that produces significant heat in the reactor.

A second control requirement is that the maximum gas temperature be obtained without damage to the material of the reactor. This control function is most important because the specific impulse is proportional to the square root of the gas temperature, and, consequently, the highest temperature that will not damage the reactor is desired.

Within the core are additional limitations on engine operation. Thermal gradients induce high stresses or may result in hot spots at higher temperature than the material can stand. Similarly, quick changes in temperature can induce high thermal shock stresses.

Another control problem associated with the core is the wide range of neutron flux (10 decades) that must be sensed for safe control.

In regard to the other parts of the system, the pump is limited in operating condition to avoid stall and possible damage during startup. Cavitation within the pump can cause erosion and damage and perhaps lead to a "vapor lock," which is the presence of a large enough quantity of gas in the liquid to impair the pumping capability of the pump. Such a condition can arise in starting if the pump and the lines have not been chilled down. Also, it can occur near the end of powered flight when the propellant that has picked up heat in the tank enters the pump.

A CONTROL SYSTEM

One possible control system would utilize measurement of reactor outlet gas temperature, reactor outlet pressure, and neutron flux to manipulate turbine valve and control rod. Figure 45–2 is a block diagram of this control scheme. Such a control would fulfill most of the required functions, provided a dependable temperature sensor was available. Also, the flux sensor must provide a good enough signal to permit rapid calculation of the rate of change of flux, particularly during startup.

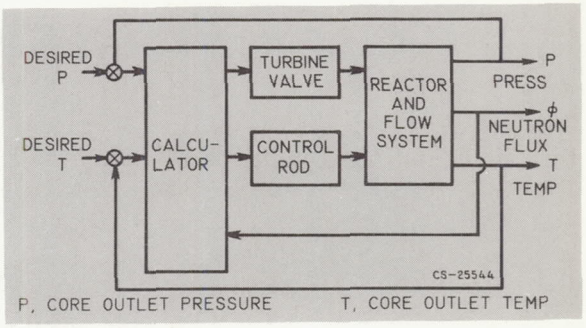

FIGURE 45–2.—A control for maximum power operation of a nuclear rocket.

Selection of the computer functions for dispatching commands to the valve and control rod is aided by a knowledge of the dynamical behavior of the components of the system.

DYNAMICS OF REACTOR AND FLOW SYSTEM

For control stability purposes (accurate, fast controls may suffer from instability), the dynamical relations among the manipulated and output variables may be expressed in terms of steady-state gain and frequency response. The gains are derived from a steady-state calibration, such as shown in figure 45–3. Here the

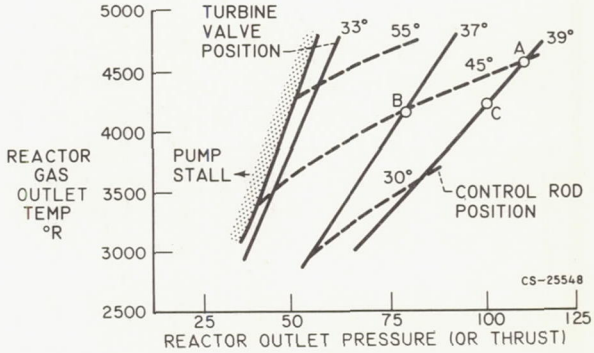

FIGURE 45–3.—Control parameters near maximum power for a nuclear rocket.

steady-state settings of turbine valve and control rod to generated selected value of gas temperature and reactor pressure are shown. The gains about point A in the map are as follows:

	Valve	Rod
$\partial P/\partial\theta$, percent/percent	1.1	0.7
$\partial T/\partial\theta$, °R/percent	14	21

Incidentally, figure 45–3 gives a view of some damage limits and their relation to controls. Directly observable are the maximum temperature limit and the conditions of pump stall. Derivable from this data is a function of thermal gradient; this gradient increases with pressure at a selected temperature.

An alternate map, replacing temperature with reactor neutron flux, could be prepared for use in the event that sensing of neutron flux proves to be more reliable than temperature sensing.

Of great interest to the control designer is the strong effect of the flow system on the reactor power. For illustration, if the turbine valve is closed from 39° to 37° while the reactor control rod is held fixed at 45°, the pressure and temperature are reduced (when an increase in temperature might be expected). This strong reverse effect almost equals the effectiveness of the control rods and is explained by the large effect of hydrogen in the reactor on its reactivity. Here, then, is a significant difference between this reactor system and others commonly studied. The effect of hydrogen in the core is to make the system less stable (runaway rather than oscillatory) than a reactor in which the coolant does not influence the nucleonic processes.

The time-varying portion of the dynamic relations among control variables is shown in figure 45–4. The information is in the convenient frequency-response form. This frequency-response information is combined with the steady-state gains to give a complete dynamic description through the following relation:

$$\frac{\theta_{\text{out}}}{\theta_{\text{in}}}=KG$$

where

G frequency (or time) variant portion of the description

K steady-state gain

θ_{out} change in output function being observed

θ_{in} change in input function being disturbed

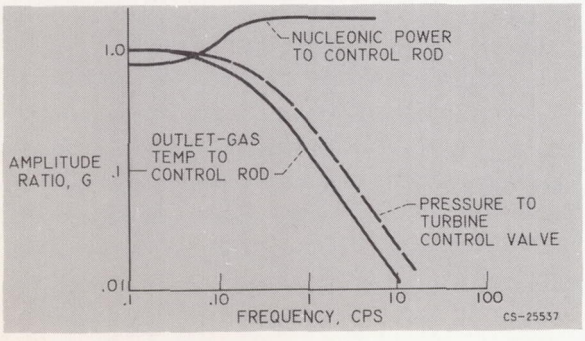

FIGURE 45–4.—Frequency responses among control variables for a nuclear rocket.

The response of nucleonic power to control rod position, shown in figure 45–4, is not unlike published reactor behavior, such as shown by Schultz in reference 1. The high-frequency dynamics, above 10 cycles per second, are governed by the mean neutron lifetime between generations and are, therefore, related to the degree to which the reactor is moderated. At low frequency, below 1 cycle per second, the behavior of the nucleonic power differs somewhat from the published literature because the interaction of the hydrogen with the nucleonic process is significant.

Of considerable interest is the fact that, although the system is quite complex, including pump, turbine, heat exchangers, and so forth, the responses of pressure and temperature are reasonably described by a single time constant. Phase measurements show a similar result.

The time constants of the flow system vary approximately inversely as the flow rate. Thus, it is possible to estimate the dynamics at other than maximum power. This approximation is not good for extension down to startup; also, some of the high-frequency dynamics of the reactor are not closely related to the flow system.

DYNAMICS IN STARTUP REGIME

In the startup transient, several dynamical properties not observable at high power must be considered. Some of these properties arise from the phase change of hydrogen from gas

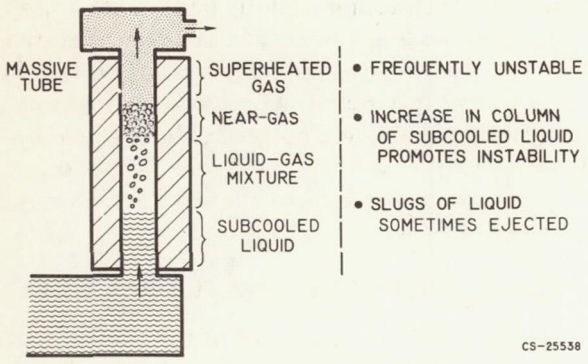

FIGURE 45–5.—Dynamic model of evaporation in cooling jacket.

to liquid at low pressure. The boiling of hydrogen while flowing through a tube has been observed to be quite oscillatory in many instances. This problem is illustrated in figure 45–5. The change from all liquid to a mixture of a liquid and vapor and thence to some sort of gas is accompanied by momentum pressure drop that is a function of the flow, which is, in turn, a function of pressure drop. Several modes of severe oscillation are possible and have been observed. Oscillations violent enough to cause ejection of slugs of liquid from the exit even when the steady-state heat balance would indicate superheated gas have been observed.

Flow instability due to inadvertent stall of the pump is an occurrence that can be introduced by inadequate control of flow and power during startup. Attempt to start flow before the pump is adequately cooled is also a source of unstable flow.

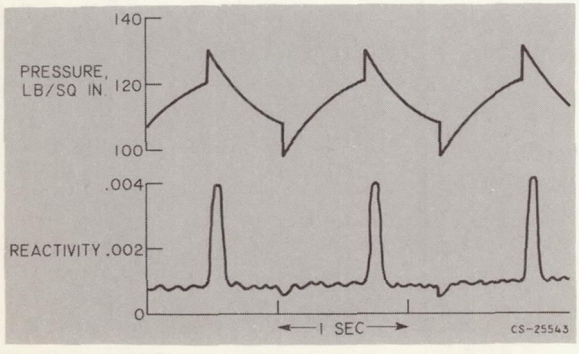

FIGURE 45–6.—An estimated flow oscillation and reactivity excursion.

The dynamics of unstable flow are of great concern because the periodic ingestion of large amounts of hydrogen into the reactor could cause severe and perhaps runaway transients in reactivity. A rough estimate has been made to show the effect on reactor period of a severe oscillation in flow such as might be induced by pump stall. The results are shown in figure 45–6. In this instance sharp spikes in period occur, reaching the dangerously short period of 1 second. Only slight more reactivity would produce periods of milliseconds and possible destruction.

CONTROL DURING STARTUP

One control scheme for conducting the engine from a condition where hydrogen has been admitted to the core to a terminal condition of full

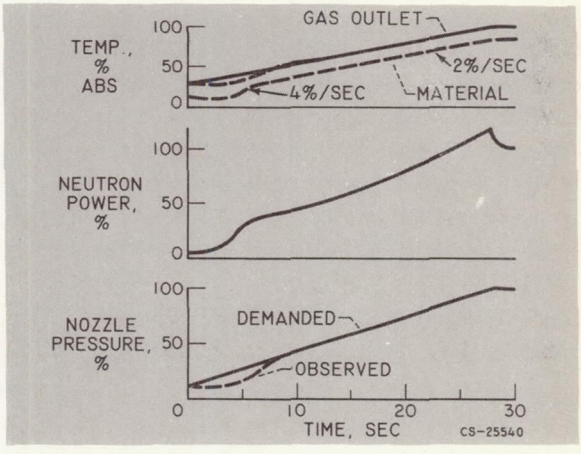

FIGURE 45–7.—Example startup transient.

power would be to use the control of figure 45–2, imposing thereon demanded pressure and temperature scheduled with time. (This system is not necessarily the best or recommended.) The program calls for a linear rise in temperature to maximum temperature in 28 seconds; the linearity is desired to minimize thermal shock. A schedule in pressure to avoid stall and to reach full thrust in 28 seconds is also used. These schedules of demanded pressure and temperature and the calculated behavior of the system are shown in figure 45–7.

The resultant performance shows inadequacy of the control at the start and gives a very rapid

rise in flux corresponding to a dangerously short period and subsequent rapid rate of rise of material temperature, more than twice the desired rate. Similar results have been published for a somewhat different nuclear rocket system by Mohler and Perry (ref. 2).

Thus, the results shown here illustrate that careful selection of the control is needed to avoid trouble in the early part of the startup. Modern control theory appears to be quite adequate at high power near maximum thrust.

Another thought induced by the foregoing results is the possible consequence of simultaneously imposed flow instability and improper control. Such a combination could produce more severe reactor and pump excursions than shown.

SENSOR PROPERTIES THAT INFLUENCE CHOICE OF CONTROL

The control system of figure 45–2 depends upon a temperature sensor that is dependable and accurate in a severe environment of up to 5000° R, intense nuclear radiation, and high flow velocities. A temperature sensor meeting these requirements may not be developed for a long time, and other means of control will be sought.

One alternative might be to use the neutron flux sensor to measure the nucleonic power, and, since nozzle pressure is measured, the mean gas temperature can be inferred. This system is particularly attractive since the neutron detector is used to measure nucleonic power and to control the reactor from source level up to a power level where the temperature sensor gives a readable and accurate signal.

The primary difficulty in using the neutron detector to control at maximum power is that it is not accurate enough. This inaccuracy is due not as much to the inaccuracies in the instrument itself as to the nonuniformity of the neutron flux field in regions where the detector might be located. Presence of volumes of hydrogen, changes in control rod position, and many other disturbing factors cause considerable uncertainty in the relation between the flux at a selected point and the reactor nucleonic power. Furthermore, the reactor that is used in a space vehicle will never have been operated at high power before flight; thus calibration is made very uncertain. If a good temperature sensor is not created, however, the neutron detector system could be used, but reduction of maximum temperature to allow for error would be necessary.

SOME PROBLEMS NEEDING FURTHER WORK

As may be seen, treatment of the problems of dynamics and controls in the nuclear rocket is in an embryonic state, and much progress is yet needed. Most of the problems are of a general nature, applicable to a variety of possible designs of nuclear rockets. Some of these problems that could be explored further by independent investigation are mentioned in the following paragraphs.

A reliable temperature sensor capable of surviving in hydrogen at 4000° to 5000° R for 1 hour is urgently needed. Fast response time, less than 1-second time constant, would simplify the control system using the sensor.

A neutron flux detector that could be calibrated accurately to 1 percent could be used in a control system that does not need the temperature sensor. The source of error here seems to be the spatial variability of the neutron flux field in the vicinity of the detector. The calibration difficulty is compounded by the fact that the particular reactor used in a space mission will never have been operated at power prior to the mission.

A statement of the dynamic properties of hydrogen boiling while flowing through an evaporator tube is needed. Progress is being made, but considerably more work is needed, both in experimental observation and in theory.

The mathematical tools used to select optimum control functions should be extended to fit a particular class of large-scale disturbances in nonlinear systems. The particular case is for a dynamical system having square-law relations among some of its parameters (i.e., flow to pressure drop). Current linear techniques seems to be satisfactory for transients around maximum flow.

REFERENCES

1. SCHULTZ, M. A.: Control of Nuclear Reactors and Power Plants. McGraw Hill Book Co., Inc., 1955.
2. MOHLER, RONALD R., and PERRY, JOSEPH E., JR.: Nuclear Rocket Engine Control. Nucleonics, vol. 19, no. 4, April, 1961, pp. 80–84.

U.S. GOVERNMENT PRINTING OFFICE : 1963 O—672065

Publ. No.	Title	Price
SP–13	Geophysics and Astronomy in Space Exploration	.35
SP–14	Lunar and Planetary Sciences in Space Exploration	.55
SP–15	Celestial Mechanics and Space Flight Analysis	.35
SP–16	Data Acquisition from Spacecraft	.40
SP–17	Control, Guidance, and Navigation of Spacecraft	.40
SP–18	Bioastronautics	.30
SP–19	Chemical Rocket Propulsion	.40
SP–20	Nuclear Rocket Propulsion	.45
SP–21	Power for Spacecraft	.25
SP–22	Electric Propulsion for Spacecraft	.35
SP–23	Aerodynamics of Space Vehicles	.40
SP–24	Gas Dynamics in Space Exploration	.40
SP–25	Plasma Physics and Magnetohydrodynamics in Space Exploration	.50
SP–26	Laboratory Techniques in Space Environment Research	.40
SP–27	Materials for Space Operations	.35
SP–28	Structures for Space Operations	.35